

MASTER OF SCIENCE THESIS

Environmental Optimization of Helical Approaches

S. El Kasri

December 13, 2015

Faculty of Aerospace Engineering · Delft University of Technology



Environmental Optimization of Helical Approaches

MASTER OF SCIENCE THESIS

For obtaining the degree of Master of Science in Aerospace Engineering
at Delft University of Technology

S. El Kasri

December 13, 2015



Delft University of Technology

Copyright © S. El Kasri
All rights reserved.

DELFT UNIVERSITY OF TECHNOLOGY
DEPARTMENT OF
AIR TRANSPORT OPERATIONS OF CONTROL AND SIMULATION

The undersigned hereby certify that they have read and recommend to the Faculty of Aerospace Engineering for acceptance a thesis entitled “**Environmental Optimization of Helical Approaches**” by **S. El Kasri** in partial fulfillment of the requirements for the degree of **Master of Science**.

Dated: December 13, 2015

Chairman:

Dr.ir. H.G. Visser

Supervisor:

Dr.ir. S. Hartjes

Summary

Air traffic has been growing rapidly for the past few decades and will continue to do so. Airports need to be able to cope with this increase, and thus increase their own capacity. However, due to the landing and departure operations, which take place at low altitudes, high noise levels are generated and affect the neighboring communities. This in turn limits the growth of airports that are located near inhabited areas, due to the restrictions on noise levels set by governments for airports.

In order to reduce the aircraft noise, a number of solutions have been developed. Some of these solutions are on the aircraft level while the others are on the airport level. A number of solutions implemented on the aircraft level are for example, noise efficient engines and noise reducing fairings. The airport level knows the development of noise abatement operational procedures, such as the CDA. However, there are downsides to such a procedure, like the limitations that it only allows vertical optimization or flight at night.

Therefore, a new noise abatement procedure has been developed called HeNAP, which stands for Helical Noise Abatement Procedure. As the name suggests it is a procedure where the descent approach is performed by means of a spiral. This allows the aircraft to perform a flyover the inhabited areas at a higher altitude and perform a descent near the airport by means of a spiral. This would reduce the noise levels perceived by the inhabitants.

Earlier research showed a decrease in noise levels but an increase in fuel consumption and time; however, it was never optimized with respect to these factors and at closely inhabited airports. Therefore:

The aim of this project is to develop noise-optimal HeNAP approach trajectories using methods from optimal control theory. The noise benefits of the optimal HeNAP trajectories need to be assessed through comparison with conventional noise abatement procedures. In addition, an analysis needs to be made of the operational consequences of introducing HeNAP procedures.

For this purpose, a GPOPS-based environmental optimization framework for HeNAPs was created. By performing the research on the HeNAP and validating it at the same time, a set of research goals are investigated during this thesis:

- Develop a code for optimizing the HeNAP trajectories within GPOPS .
- Assess the influence of changing multiple variables such as the altitude, the helical radius and number of spirals performed before landing on the environmental optimization of HeNAP's with respect to noise impact, fuel usage and time.

The framework that is created in GPOPS for the HeNAPs combines a number of models in order to generate noise, namely, a noise model and an aircraft model. This combination results in noise generation of the trajectory flown, and is processed further in a model that calculates the impact of the noise on inhabited areas. By means of sleep disturbance dose-response relationship, the impact is converted into the number of awakenings. All of the models interconnect such that a gradient-based optimization is performed to optimize the HeNAP procedure.

With the usage of Optimal Control Theory, the cost function, consisting of a weighted noise factor and fuel contribution, is minimized by means of a dynamic process in order to find the optimal controls of the problem. With the help of the Radau pseudospectral method, the dynamics of the problem is accurately approximated. This allows the continuous problem to be discretized to change the infinite-dimensional problem into a finite-dimensional nonlinear programming problem. This can be solved with a numerical solver and results in optimal controls and states that form the HeNAP trajectory.

To assess the different changes in altitude, radius and number of spirals and impact of the resulting solutions on the environment, for the majority of the time a single-phase optimization is used. However, in order to assess sections of the HeNAP trajectory, multi-phase optimization is sometimes used as well. The help of these optimizations simulates different HeNAP routes until the most favorable one is found.

A case study is performed in a highly inhabited area around Amsterdam Airport Schiphol. During this case study, a number of routes are simulated and investigated. Different altitudes, radii and number of spirals are compared while adhering to the different airspace regulations.

Over 300 simulations have been performed, as this was an intensive trial and error process, eventually resulting in a number of cases over four different optimization problems. These problems are defined as followed, *minimum time optimization problem*, *minimum fuel optimization problem*, *minimum time and noise abatement optimization problem* and finally *minimum fuel and noise abatement optimization problem*. The cases that are solved for these problems are as followed:

- Case 1: is a CDA procedure that is performed at an altitude of 7000 ft and minimum ILS approach distance of 6.2 NM.
- Case 2: is the first HeNAP simulation and is run with an altitude of 7,000 ft and one spiral.
- Case 3 the altitude is changed from 7000 ft to 10,000 ft.
- Case 4 the altitude of case 3 is still in effect and the number spirals is changed from 1 to 2.

The results of these cases are all comparable throughout the different optimization problems. All of them reveal that the CDA procedure is the most favorable procedure as it has the least number of awakenings, fuel consumed and time needed to land.

However, when relocating the population around the airport to the first part of the trajectory it yields better results. Case 3 is then the most favorable case, with promising results.

The changes in altitude for the HeNAP showed that by having a higher initial altitude the number of inhabitant awakened is reduced, however when the number of spirals is increased this effect is dismissed.

The following recommendations might help improve/show more of the HeNAP possibilities.

The first recommendation that can be given, is to use the results that are found within this thesis and use them as a basis for the same research but within another area that might be less inhabited than the area around AAS and where the night-curfew is also in effect.

Another recommendation that can be made is to add the wind and weather conditions to the GPOPS tool in order to get results that are more realistic and increase the reliability of the results and feasibility of the trajectories performed.

A final recommendation is to introduce better methods to avoid local minima within the GPOPS tool, this result in unnecessary delays.

Nevertheless, the HeNAP procedure has great future possibilities only not within the Netherlands.

Acknowledgment

This report is the result of a master's thesis study performed at the chair of Air Transport Operations of Control and Operations of the faculty of Aerospace Engineering, Delft University of Technology.

First, I would like to acknowledge and thank my supervisors for all the guidance and help they provided me:

- Dr.ir. H.G. Visser; associate professor at the chair of Air Transport Operations
- Dr.ir. S. Hartjes; assistant professor in the field of airline operations at the chair of Air Transport Operations

Words can hardly describe the gratitude I have towards these two great minds. Sander Hartjes was there when I needed technical advice for all the technical difficulties during this thesis, which were numerous, with his help and guidance I was able to finish this project. Dries Visser gave me the freedom to explore all the possibilities within the scope of this project while keeping me focused on the main goal when I was about to lose it. I thank you both for your patience and for your support during this period.

Delft, The Netherlands
December 13, 2015

S. El Kasri

Contents

Summary	v
Acknowledgment	ix
List of Figures	xvi
List of Tables	xvii
Nomenclature	xix
1 Introduction	1
1.1 Background	1
1.2 Thesis Assignment	2
1.2.1 Research Goals	2
1.3 Report Structure	3
2 Previous Research	5
2.1 Noise	5
2.1.1 Sound Pressure Level	6
2.1.2 Perceived Noise Level	6
2.1.3 A-Weighted Correction	7
2.1.4 Sound Exposure Level	8
2.1.5 Effective Perceived Noise Level	9
2.1.6 The Sleep Disturbance Dose-Response Relationship	9
2.2 Noise Abatement: Aircraft Level	10
2.2.1 Aerodynamic Noises: Landing Gear	10
2.2.2 Aerodynamic Noises: High-Lift Devices	12
2.2.3 Engine Noise	13
2.3 Noise Abatement: Airport Level	14

2.3.1	Short Term Procedures	14
2.3.2	Medium Term Procedures	15
2.4	Noise Abatement Procedures	15
2.4.1	Conventional Approach	15
2.4.2	Two-Segment Approach	16
2.4.3	Three Degree Decelerating Approach	16
2.4.4	Continuous Descent Approach	17
2.4.5	Advanced Continuous Descent Approach	17
2.4.6	Precision Navigation Instrument Departure	18
2.5	Helical Noise Abatement Procedure	19
3	GPOPS Optimization Framework	21
3.1	Optimal Control Theory	21
3.2	NOISHHH Optimization Framework	23
3.3	GPOPS Framework Structure	23
3.4	General Pseudospectral Optimal Control Software	24
3.4.1	Radau Pseudospectral Method	24
3.4.2	Detailed Program Structure of the HeNAP Optimization Tool	25
3.5	Aircraft Model	26
3.5.1	Point Mass Model	27
3.6	Noise Model	31
3.6.1	Integrated Noise Model	31
3.6.2	Implementation of the Noise Contribution	31
3.7	Awakenings Model	33
3.7.1	Geographic Information System	33
3.7.2	Implementation of the Awakenings Cost Parameter	34
3.8	Inequality Path Constraints	35
3.9	Cost Function	37
4	Case Study	39
4.1	Amsterdam Airport Schiphol	39
4.1.1	Runways	41
4.2	Regulations and Guidelines	43
4.2.1	Airspace Domains	43
4.2.2	Lateral Freedom	43
4.2.3	Standard Terminal Arrival Routes	44
4.3	HeNAP Routes Setup	44
4.3.1	Case 1: CDA	45
4.3.2	Case 2: HeNAP	45
4.3.3	Case 3 & Case 4: HeNAP	45
4.4	Case Study Strategy	47

5	Results	49
5.1	Minimum Time Problem Solutions	49
5.2	Minimum Fuel Problem Solutions	52
5.3	Minimum Time & Noise Problem Solutions	55
5.4	Minimum Fuel & Noise Problem Solutions	58
5.5	Trade-Off	61
5.5.1	Adjusted Population	62
5.5.2	Capacity	68
6	Conclusions and Recommendations	71
6.1	Conclusions	71
6.2	Recommendations	72
A	Additional Theorem	73
A.1	Implementation of the Awakenings Gradients	74
A.2	Multi-Phase Optimal Control Problem	77
B	Flight Charts	81
	References	89

List of Figures

2.1	Equal Loudness Contours for Pure Tones [11].	6
2.2	Equal noisiness curves [11].	7
2.3	Frequency weighting characteristics [11].	8
2.4	Recommended Sleep Disturbance Dose-Response Relationship [12].	9
2.5	Examples of Noise Reduction Fairings and Next-Gen Design [3].	11
2.6	Flap side-edge fences and porous-edge replacements for noise reduction [3].	13
2.7	History of commercial aircraft noise levels and progression of engine type and bypass ratio [13].	13
2.8	35Ke Noise contour of Schiphol airport (left) and Rotterdam airport (right) [1, 14].	14
2.9	Conventional Approach [10].	16
2.10	Two-Segment Approach [20].	16
2.11	Three Degree Decelerating Approach [20].	17
2.12	Continuous Descent Approach [10].	17
2.13	Advanced Continuous Descent Approach [14].	19
2.14	Helical Noise Abatement Procedure [28].	20
3.1	GPOPS Tool Structure [9].	23
3.2	Program Structure of the Environmental Optimization Tool [10].	25
3.3	Royal Air Maroc Boeing 737-700.	26
3.4	Forced Ground Track	28
3.5	Force Equilibrium in a Horizontal Steady Turn [32].	30
3.6	Airplane in Symmetric Flight [32].	31
3.7	Population Density Map of the AAS Area [10].	34

4.1	Location of AAS in The Netherlands and Surrounding Cities.	40
4.2	AAS Runways	41
4.3	Runway Usage over a Period of One Month at AAS	42
4.4	CDA (left) in red, HeNAP (right) in green	46
5.1	Trajectories of all the Minimum Time Problem Results Cases	50
5.2	Velocities and Altitudes of all the Minimum Time Problem Results Cases	51
5.3	Trajectories of all the Minimum Fuel Problem Results Cases	53
5.4	Velocities and Altitudes of all the Minimum Fuel Problem Results Cases	54
5.5	Trajectories and Sound Patterns of all the Minimum Time & Noise Problem Results Cases	56
5.6	Velocities and Altitudes of all the Minimum Time & Noise Problem Results Cases	57
5.7	Trajectories and Sound Patterns of all the Minimum Fuel & Noise Problem Results Cases	59
5.8	Velocities and Altitudes of all the Minimum Fuel & Noise Problem Results Cases	60
5.9	Possible Airports For HeNAP Procedure	61
5.10	Trajectories and Sound Patterns of all the Minimum Time & Noise Problem Results Cases for the New Scenario	63
5.11	Velocities and Altitudes of all the Minimum Time & Noise Problem Results Cases for the New Scenario	64
5.12	Trajectories and Sound Patterns of all the Minimum Fuel & Noise Problem Results Cases for the New Scenario	66
5.13	Velocities and Altitudes of all the Minimum Fuel & Noise Problem Results Cases for the New Scenario	67
5.14	Wake Turbulence Related IFR Aircraft Separation Minima [36]	68
5.15	Aircraft Category Per Type Of Aircraft [36]	69
5.16	Adjusted Separation Distance [37]	69
A.1	Possible Linkages for a Multi-phase Optimal Control Problem [38].	79
B.1	Maastricht UAC En-route Communication at or above FL 245 [39].	82
B.2	Amsterdam FIR En-route Communication [39].	83
B.3	Airspace Structure and ATS Airspace Classification [39].	84
B.4	Instrument Approach Chart For Amsterdam Runway 27 [39].	85
B.5	Instrument Approach Chart For Eindhoven Runway 3 [39].	86
B.6	Instrument Approach Chart For Rotterdam Runway 24 [39].	87

List of Tables

3.1	General Boeing 737-300 Characteristics [9].	26
4.1	Beacons, Waypoints and Runway 27 coordinates	45
5.1	Minimum Time Problem Solutions	49
5.2	Minimum Fuel Problem Solutions	52
5.3	Minimum Time & Noise Problem Solutions	55
5.4	Minimum Fuel & Noise Problem Solutions	58
5.5	Minimum Time & Noise Problem Solutions V2.0	62
5.6	Minimum Fuel & Noise Problem Solutions V2.0	65
5.7	Capacity Calculations Homogeneous Mix	70

Nomenclature

Latin Symbols

A	Total number of awakenings of all observer grid points	[-]
$Awakenings$	Number of awakenings in an observer grid point	[-]
C	Algebraic path constraints	[-]
D	Drag force	[N]
f_i	Set of functions	[-]
g_0	Acceleration of gravity at sea-level	$[m/s^2]$
J	Performance index	[-]
$\mathbf{J}_{A,controls}$	Total awakenings Jacobian of the controls	[-]
$\mathbf{J}_{A,states}$	Total awakenings Jacobian of the states	[-]
\mathbf{J}_T	Thrust Jacobian	[-]
k	Weight factor of a cost function objective	[-]
\mathcal{L}	Lagrangian	[-]
L	Lift force	[N]
L	Number of phases to be linked	[-]
LA	Lateral attenuation correction	[dB]
L_A	A-Weighted Sound Level	[dBA]
L_{AE}	Sound Exposure Level	[dBA]
$L_{AE,flt}$	Corrected total SEL of the flight at the observer point	[dBA]
$L_{AE,NPD}$	Interpolated Sound Exposure Level derived from NPD data	[dBA]
$L_{Aeq,T}$	Equivalent A-Weighted Sound Level	[dBA]
L_{EPN}	Effective Perceived Noise Level	[EPNdB]

L_{PN}	Perceived Noise Level	[PNdB]
L_{TPN}	Tone corrected Perceived Noise Level	[TPNdB]
M	Mach number	[-]
m	Mass	[kg]
m_f	Fuel used	[kg]
NF	Noise fraction correction	[dB]
n	Number of inhabited grid points	[-]
n	Total number of functions	[-]
n_{seg}	Number of segments	[-]
P	Total number of phases	[-]
p	Loudness Level	[phon]
p	Phase index	[-]
p_0	Air pressure at sea-level	[N/m ²]
p_e	Effective (sound) pressure	[N/m ²]
p_{e0}	Reference(sound) pressure	[N/m ²]
pop	Number of inhabitants at the observer grid point	[-]
\mathbf{q}	Static parameters	[-]
R	Specific gas constant of air	[m ² /s ² K]
R	Turn radius	[m]
SA	Speed adjustment correction	[dB]
SPL	Sound Pressure Level	[dB]
s	Phase link index	[-]
s	Distance	[m]
\dot{s}	Distance time derivative	[m/s]
s_0	Begin of the ground track	[m]
s_f	End of the ground track	[m]
T	Ambient temperature	[K]
T	Thrust force	[N]
T	Time period	[s]
T_0	Temperature at sea-level	[K]
T_{max}	Maximum thrust	[N]
T_{min}	Minimum thrust	[N]
t	Time	[s]
t_0	Start time	[s]
t_f	Final time	[s]
\mathbf{u}	Control vector	[-]
U	Bounded set of control variables	[-]

u	Control variable	[-]
u_k	Set of control variables	[-]
\mathbf{v}	Vector containing the dependent states and control	[-]
V	True Airspeed	[m/s]
\dot{V}	Speed time derivative	[m/s ²]
W	Weight of the aircraft	[N]
\mathbf{x}_{INM}	State vector sent to INM	[-]
\mathbf{x}	State vector	[-]
x	State variable	[-]
x	x-coordinate of the aircraft	[m]
\dot{x}	First order differential equation of the dynamics	[-]
\dot{x}	x-coordinate time derivative	[m/s]
x_i	Set of state variables	[-]
x_0	Initial x-coordinate of the ground track	[-]
x_1	Initial x-coordinate of the spiral	[-]
x_2	Exit x-coordinate of the spiral	[-]
x_c	x-coordinate of the spirals' center	[-]
x_f	Final x-coordinate of the ground track	[-]
y	y-coordinate of the aircraft	[m]
\dot{y}	y-coordinate time derivative	[m/s]
y_0	Initial y-coordinate of the ground track	[-]
y_1	Initial y-coordinate of the spiral	[-]
y_2	Exit y-coordinate of the spiral	[-]
y_c	y-coordinate of the spirals' center	[-]
y_f	Final y-coordinate of the ground track	[-]
z	Altitude	[m]
\dot{z}	Altitude time derivative	[m]

Greek Symbols

Γ	Normalized throttle setting	[-]
γ	Flight path angle	[rad]
γ	Ratio of the specific heats of air	[-]
δ	Pressure ratio	[-]
θ	Temperature ratio	[-]
λ	Temperature lapse rate	[K/m]
μ	Bank angle	[rad]

ρ	Air density	$[\text{kg}/\text{m}^3]$
ρ_0	Air density at sea-level	$[\text{kg}/\text{m}^3]$
ϕ	Boundary conditions	$[-]$
χ	Heading	$[\text{rad}]$
ω	Angular velocity	$[\text{rad}/\text{s}]$

Subscripts

0	Initial value
0	Sea-level
1	One second reference
\mathcal{L}	Lagrange
AE, NPD	Equivalent A-Weighted from NPD data
<i>Awakenings</i>	Awakenings
<i>flt</i>	Flight
<i>fuel</i>	Fuel
<i>INM</i>	Integrated Noise Model
<i>points</i>	Total number of inhabited observer grid points
<i>seg</i>	Segment
<i>A</i>	Total number of awakenings of all observer grid points
<i>f</i>	Final value
<i>f</i>	Fuel
<i>i</i>	Index
<i>k</i>	Index
<i>l</i>	Left phase number
<i>T</i>	Thrust
<i>u</i>	Right phase number

Superscripts

<i>p</i>	Phase index
<i>s</i>	Phase link index

Abbreviations

AAS	Amsterdam Airport Schiphol
------------	----------------------------

ACC	Area Control Centre
ACDA	Advanced Continuous Descent Approach
AEL	Equivalent A-Weighted Sound Level
AL	A-Weighted Sound Level
ATC	Air Traffic Control
ATM	Air Traffic Management
ATS	Air Traffic Services
CAS	Calibrated Airspeed
CBS	Centraal Bureau voor de Statistiek
CDA	Continuous Descent Approach
CTR	Control Zone
DME	Distant Measuring Equipment
EAL	Equivalent A-Weighted Sound Level
EAS	Equivalent Airspeed
EPNL	Effective Perceived Noise Level
FAA	Federal Aviation Administration
FICAN	Federal Interagency Committee on Aviation Noise
FIR	Flight Information Region
FL	Flight Level
FMS	Flight Management System
GE	General Electric
GIS	Geographic Information System
GPOPS	General Pseudospectral OPTimal Control Software
GPS	Global Positioning System
HeNAP	Helical Noise Abatement Procedure
IFR	Instrument Flight Rules
ILS	Instrument Landing System
ISA	International Standard Atmosphere
NAP	Noise Abatement Procedure
NASA	National Aeronautics and Space Administration
NDB	Non Directional Beacon
NPD	Noise-Power-Distance
PNID	Precision Navigation Instrument Departure
PNL	Perceived Noise Level
RD	Rijksdriehoeks coordinate system
RNAV	Area Navigation
RPM	Radau Pseudospectral Method
SEL	Sound Exposure Level

SER	Sound Exposure Ratio
SID	Standard Instrument Departure
STAR	Standard Terminal Arrival Route
TAS	True Airspeed
TDDA	Three Degree Decelerating Approach
TMA	Terminal Control Area
TOD	Top Of Descent
TPNL	Tone corrected Perceived Noise Level
UAC	Upper Area Control
VOR	VHF Omnidirectional Radio

Chapter 1

Introduction

1.1 Background

Due to the continuous growth of commercial air traffic and the rise of urbanization around airports has led to the increase of environmental impacts on the people. This in turn led to the reduction of capacity for airports [1]. Accordingly, the pressure on reducing the environmental impacts of noise and gaseous emissions on residential areas has grown.

Earlier research has shown that aircraft noise is one of the major concerns for airports when making decisions on operations [2]. This led to many solutions for reducing noise. There are two levels where this is accomplished, one being the aircraft level and the other being the airport level. The aircraft level has led to the development of noise and emissions efficient engines as well as frame/landing gear adjustments that lead to noise reduction [3]. Whilst the developments on the airport level led to (night) curfews, restrictive noise zones, the use of preferential runways and environmental friendly approaches and departure procedures.

The first three measures of the airport level can lead and have led to a reduction in air travel from and to airports [1]. The final measure in combination with navigational systems such as Global Positioning System (GPS), Area Navigation (RNAV) and the on-board Flight Management System (FMS), allow for a 4-D trajectory navigation and optimization. This measure allowed for the development procedures such as Continuous Descent Approach (CDA) and the Helical Noise Abatement Procedure (HeNAP) [4].

Hence, the focus of this thesis project being the HeNAP. The research done here will compare the standard landing approaches and CDA to the HeNAP with respect to feasibility, safety and cost.

1.2 Thesis Assignment

The research objective is to explore the benefits of the HeNAP as a possible source of noise reductions around and at airports by comparing it with standard noise abatement procedures with respect to cost and safety.

Due to a broad research on the subject of trajectory optimization with regard to noise within the Faculty of Aerospace Engineering of Delft University of Technology the software tool NOISHHH was created and used [5–10]. This tool uses the EZOPT collocation-based trajectory optimization algorithm, by using and extending NOISHHH a new tool was developed that is based on open-source General Pseudospectral (OPT)imal Control Software (GPOPS). This new tool is used for optimizing the HeNAP approach and comparing it with standard approaches and CDA.

1.2.1 Research Goals

The aim of this project is to develop noise-optimal HeNAP approach trajectories using methods from optimal control theory. The noise benefits of the optimal HeNAP trajectories need to be assessed through comparison with conventional noise abatement procedures. In addition, an analysis needs to be made of the operational consequences of introducing HeNAP procedures.

To reach this objective the following research goals have been defined:

- Develop a code for optimizing the HeNAP trajectories within GPOPS .
- Assess the influence of changing multiple variables such as the altitude, the helical radius and number of spirals performed before landing on the environmental optimization of HeNAP's with respect to noise impact, fuel usage and time.

This thesis project involves several subjects that are used to achieve the before mentioned research goals. An example of these subjects is the development of a realistic optimization framework for the optimization of HeNAPs. To obtain such a realistic optimization framework an aircraft model using real aircraft characteristics and supplemented with a standard atmosphere model is used. In addition, a fuel, thrust and noise model are included to evaluate the research goals with realistic results. With the noise impact being measured by an awakening model that correlates sleep disturbance to noise via dose-response relationship.

To validate the produced framework a study case is used to measure the effects of changing multiple variables such as the altitude, the helical radius and number of spirals at Amsterdam Airport Schiphol (AAS), while satisfying the constraints that are set by the Air Traffic Control (ATC) for this airport.

Finally, all of these subjects form an optimal control problem that is solved with a gradient-based optimization technique.

1.3 Report Structure

Excluding this introductory chapter, the thesis report comprises the following five chapters:

- Chapter 2: Previous Research
 - This chapter illustrates research done in the past with regards to noise abatement and HeNAPs.
- Chapter 3: GPOPS Optimization Tool
 - This chapter describes the developed GPOPS based optimization tool.
- Chapter 4: Case Study
 - This chapter describes the preformed study case.
- Chapter 5: Results
 - This chapter illustrates the results obtained from the case study.
- Chapter 6: Conclusion & Recommendation
 - This chapter gives a summary of the results of this thesis and provides recommendations for possible future work.

Chapter 2

Previous Research

As mentioned in the previous chapter, due to the growth of commercial flight, noise has become a leading factor in the decision making of airports with regard to operations. This has led to a growing pressure of reducing this effect, which in turn led to a number of researches being done on the subject. In order to create the optimization framework needed for this thesis, a number of these researches were explored in a literature review to serve as a reference for learning about the following topics:

- Noise Abatement
 - Aircraft Level
 - Airport Level
- HeNAP

This chapter will discuss the results from using this literature study as well as the as the definition of noise in order to help understand the work done during this thesis.

2.1 Noise

This section defines noise and describes the metrics used to measure the aircraft sound effect. What type of sound effect does one consider noise?

For instance, a small extreme sound for a short period is not always considered annoying in comparison to a low intense sound that continues over a long period. As there is a difference between the level of sound and the time one is exposed to it, it is assumed that the contribution to noise is not only due to the intensity of sound but also due to the time exposed to it.

Thus when measuring aircraft noise in a specific location both these contributions are accounted for. The coming subsections describe the different noise metrics used to measure aircraft noise.

2.1.1 Sound Pressure Level

Sound Pressure Level or *SPL* for short, is the basic measurement for sound levels and is expressed in decibel (dB). The following equation shows the relation between SPL and effective pressure p_e .

$$SPL = 10 \log \frac{p_e^2}{p_{e0}^2} \quad (2.1)$$

As can be seen from Equation (2.1), the SPL is ten times the log of the ratio between the squared effective pressure p_e and the square of the reference pressure p_{e0} , with p_{e0} being equal to $2 \times 10^{-5} \text{ N/m}^2$.

However, to measure the sound levels for the aircraft noise effectively, some corrections are needed and can be found in the coming subsections.

2.1.2 Perceived Noise Level

As mentioned before, not all sound perceived by the human ear is judged as noise. This is because humans only perceive a range of frequencies that lie between 20 and 20,000 Hz. When comparing pure tones with the same frequency from this audible range, the ear judges the frequency with the higher SPL as *loud*. Based on this and a proliferation of listeners the loudness levels of pure tones have been recorded. Figure 2.1 shows the results.

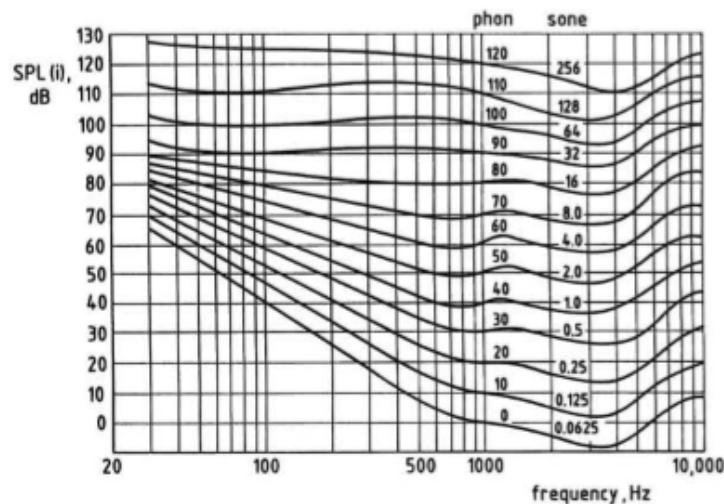


Figure 2.1: Equal Loudness Contours for Pure Tones [11].

Figure 2.1 shows the *loudness level* with the unit *phon* and sign *p* with respect to SPL. However, when considering aircraft flyovers the measure *Perceived Noise Level* (PNL) is commonly used instead of loudness level. The reason behind this is that the humans are prone to be more sensitive to complex sounds with high frequencies than pure tones of high frequencies. Figure 2.2 shows the equal noises curves.

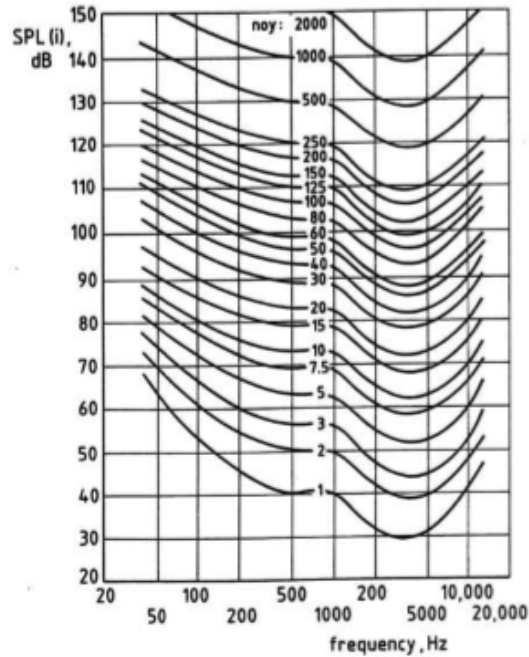


Figure 2.2: Equal noisiness curves [11].

With the help of Figure 2.2 the PNL can be calculated using the following equation:

$$L_{PN} = 40 + 33.3 \log N \quad (2.2)$$

The PNL is represented by L_{PN} and is measured in $PNdB$, N is the overall *noy* value that can be found in Figure 2.2 for specific SPLs and frequencies.

2.1.3 A-Weighted Correction

In order to measure loudness caused by complex sounds, frequency-weighting filters are incorporated in sound level meters. These filters correct for each SPL according to frequency. There are four of these weighing filters labeled A, B, C and D respectively. Figure 2.3 shows these filters.

The most commonly used filter in aviation is the A filter, that is because it works on all levels of loudness comparison. The *A-weighted sound level* (AL) or L_A is expressed in dBA and is the result of this filter, is also found to be equal to the PNL minus a constant 14 dB. The following Equations give a representation of how L_A is calculated.

$$L_A = L_{PN} - 14 \quad (2.3)$$

$$L_A = 10 \log \sum 10^{\frac{L_A(i)}{10}} \quad (2.4)$$

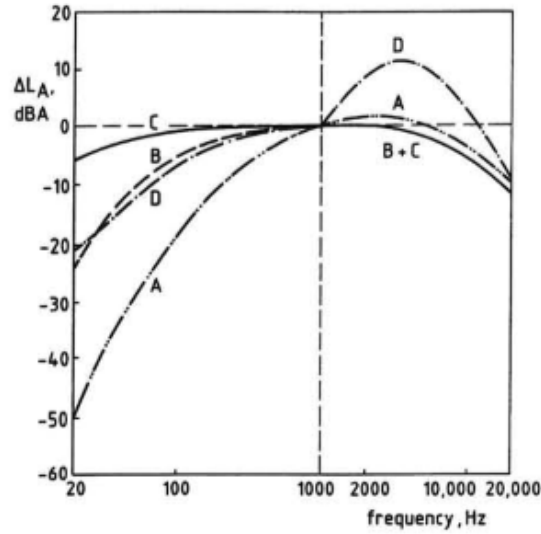


Figure 2.3: Frequency weighting characteristics [11].

$L_A(i) = SPL(i) + \Delta L_A(i)$ is the corrected band level.

2.1.4 Sound Exposure Level

As mentioned in the introduction of this chapter, not only the intensity of the sound but also the duration of is important. Thus, when considering a flyover, the sound observed from the ground strengthens to a maximum and then dies down. In such a case it is useful to integrate the L_A over time. This results in the *Equivalent A-Weighted Sound Level* (EAL) with symbol $L_{Aeq,T}$ and dBA as a measuring unit. The next equation reveals the integration over time T .

$$L_{Aeq,T} = 10 \log \left[\frac{1}{T} \int_0^T 10^{\frac{L_A(t)}{10}} dt \right] \quad (2.5)$$

By eliminating the influence of the magnitude of T , and replacing it by a period of one second T_1 in Equation (2.5), the formula for *Sound Exposure Level*(SEL) is obtained. SEL is thus the EAL over a period of one second, its symbol is L_{AE} and it is expressed in dBA.

$$L_{AE} = 10 \log \left[\frac{1}{T_1} \int_0^T 10^{\frac{L_A(t)}{10}} dt \right] \quad (2.6)$$

With the help of SEL it is now possible to measure the loudness of flyovers over a period of time. The same goes for any other transient sound.

2.1.5 Effective Perceived Noise Level

Another common noise metric for aircraft flyover noise is the *Effective Perceived Noise Level* (EPNL), conveyed in EPNdB units. It is derived from PNL and resembles SEL except for the fact that it also accounts for pure tones. The reason it accounts for pure tones is that increased noisiness of audible discrete frequency components that are found in aircraft flyover noise. Equation (2.7) gives the definition of EPNL (L_{EPN}).

$$L_{EPN} = 10 \log \left[\frac{1}{T_{10}} \int_0^T 10^{\frac{L_{TPN}(t)}{10}} dt \right] \quad (2.7)$$

As can be seen from Equation (2.7) a time period T_{10} of 10 second is used as a normalizing constant, and L_{TPN} is the instantaneous *Tone Corrected Perceived Noise Level* (TPNL) and it is measured in TPNdB.

2.1.6 The Sleep Disturbance Dose-Response Relationship

When judging sound on the merits of being annoying, the duration and intensity of the sound were discussed. However, there is one other factor that can be considered, namely when does the sound occur.

It seems that the noise created by aviation during the day is better endured than at night. People are inclined to ignore it if it happens during the day than at night, even for the same level of loudness. This phenomenon led to a number of studies that examine the physical and psychological effects of aircraft noise on sleeping individuals. The *Federal Interagency Committee on Aviation Noise* (FICAN) collected and assessed the results. This led to the sleep disturbance dose-response relationship for aircraft noise [12]. This is shown in Figure 2.4.

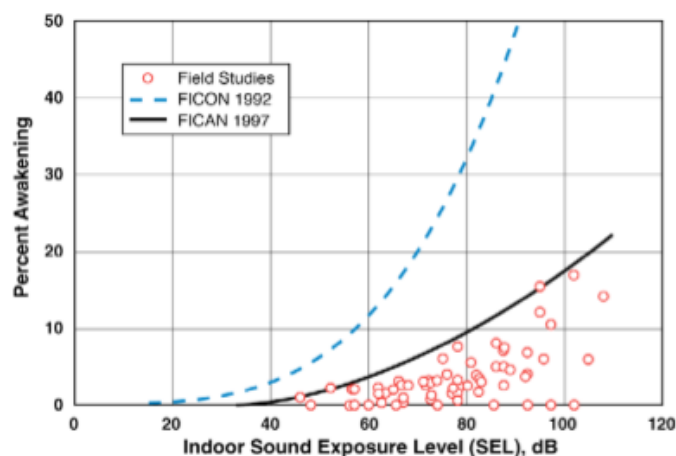


Figure 2.4: Recommended Sleep Disturbance Dose-Response Relationship [12].

This relationship provides the possibility to calculate the maximum percentage of awakened

people by a single flyover as function of SEL, as can be seen in Equation (2.8).

$$\%Awakenings = 0.0087 \times (L_{AE} - 30)^{1.79} \quad (2.8)$$

By implementing this function in the GPOPS tool and combining it with a known population distribution and density, the absolute number of awakened people can be calculated, as can be seen done in these previous researches [5–10].

2.2 Noise Abatement: Aircraft Level

The aircraft knows a number of noise sources during take-off and landing. These are aerodynamic noises, engine and other mechanical noises and noises that come from aircraft systems. The aerodynamic noises are generated from the airflow around the aircraft fuselage and control surfaces. This type of noise increases at low altitudes (landing) due to the air density as well as due to aircraft speed. The major sources of this noise are the landing gears, slats and flap edges.

For example engine noise from jet engines is the main source during take-off and climb, this due to the fact that the engines are working on 90 - 100 per cent capacity during these stages. However, this is not the case during landing where aerodynamic noises are the mayor source.

The noises that come from aircraft systems have no consequence on the exterior of the aircraft (surrounding areas, airports, etc.) but they are a noise source within the cockpit and cabin. However, as they do not affect the outside community, they are not considered for this review.

In the coming subsections, the aerodynamic and engine noise sources will be discussed as well as the solutions that have been found for these sources.

2.2.1 Aerodynamic Noises: Landing Gear

During the 1990s with the availability of large acoustic wind-tunnel facilities it was possible to test full scale landing gears. As a result from the tests performed it was apparent that the noise levels occur around 0.5 to 3 kHz. This range corresponds to the sensitive range of human noise perception [3]. This is due to the fact that the landing gears consist of a vast number of smaller components and these contribute to the high frequency noises. So the landing gear is a cluster of aerodynamic noise sources due to flow separation from the variety of small components with the incoming flow.

The parameters that play a major part in the generation of these noises are the flow turbulence intensity and the local mean flow velocity. As mentioned before the lower this velocity is the higher the sound intensity increases. One of the solutions for this problem is the arrangement of components in line to minimize the noise generation [3].

As to be able to come up with improvements for the landing gear designs, prediction models are used. These models predict the noise levels that are generated by the different type of designs. The first prediction model was based on flight test data and simplified scale model wind-tunnel test data and was developed by Fink [3]. However, this was not an accurate representation

as it considered the landing gear to be one large component. The first model to consider the landing gears as a combination of multiple components is the model of Smith and Chow. However, this model was lacking as well as it only considered the major components (primary structure). Based on the same idea is the Guo model, this model distinguishes between large, medium and small scale elements with corresponding low, medium and high frequency noise contributions. This model is combined with the Fink model and is used by the *National Aviation and Space Administration* (NASA) to improve the prediction accuracy of noise levels.

By using the knowledge gained from wind-tunnel experiments, prediction models and noise reduction concepts aimed at the reduction of the number and complexity of the components that are exposed to the incoming airflow. These resulted in the idea of covering the whole gear structure with streamlined fairings [3], see Figure 2.5. This development allows to a potential reduction of more than 10 dB, however this solution is not practical due to operational and cost constraints.

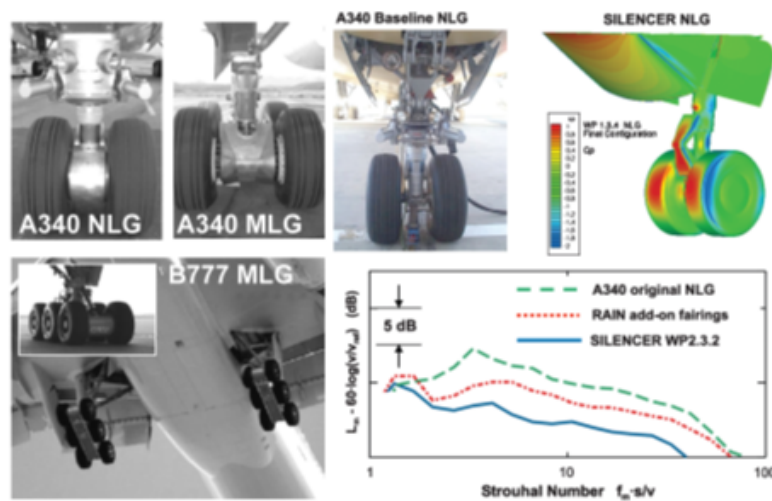


Figure 2.5: Examples of Noise Reduction Fairings and Next-Gen Design [3].

For the current landing gears an add-on fairing is still possible, one that only covers the complex parts. These add-on fairings have been tested and had a potential noise reduction of 3 dB. While for future designs it would be prudent to optimize the designs of all the components of the landing gear for low aerodynamic noise generation. This has led to the design of the Silencer concept, according to full-scale gear mock-ups wind-tunnel testing it could result in a noise reduction of 7 dB.

So for current landing gears there is the possibility of ad-on fairings and the development of Next-Gen designs should lead to a reduction of the noise coming from the landing gears.

2.2.2 Aerodynamic Noises: High-Lift Devices

The next in line in aerodynamic noises sources are the high-lift devices, such as leading edge slats and trailing edge flaps. However, unlike the landing gear systems there are not any acoustic wind tunnels large enough to house a complete wing system. This in turn results in the testing of scale models of the wing that do not fit in the wind tunnels. Yet, this still results in errors due to the fact that some of the components are not scaled properly. Thus the measurement of the noise is a bit difficult.

So, how is this type of noise created? Taking a look at the leading edge slats, a vortex flow develops in the slat cove due to the flow that passes through the slat slot. This results in the development of an unstable shear layer. The impingement of the vortical shear flow on the cove surface and shedding off of the unsteady flow from the slat trailing edge generate the leading edge slat noise. Since the wing leading edge is located in the acoustic near-field of this trailing edge noise source it is assumed that the wing leading edge reacts as a sound source [3].

The second noise source is represented by the flap side edge. The noise from this source is generated by the multiple vortices that evolve during flight. The first vortex is generated by the flap pressure side close to the flap leading edge. The second vortex is then generated from the edge toward the flap suction side. Both vortices merge and separate from the flap suction side surface which results in the flap noise.

As was mentioned before, it is difficult to get accurate noise measurements due to the lack of large acoustic wind tunnels. This makes prediction models of vital importance. The first prediction model was also developed by Fink [3]. It was based on flight test data from multiple aircraft.

To develop new low noise high lift devices a variety of constraints must be considered as well as the mandatory requirement to not degrade the devices aerodynamic performance. The constraints regarding operation are the maintenance of maximum lift and provision of sufficient lift for moderate angles of attack. Regarding safety, the constraints are reliability and handling quality must remain within high standards. Finally, the cost constraints are weight, structural constraints, system complexity and maintenance.

After having taken all the previously mentioned constraints into account the following solutions were found. For the slat noise source, add-on devices were considered such as a slat cove cover to weaken the strength of the vorticity in the free flow between the cove vortex and the slot flow. However, the implementation of a rigid cover was difficult and was only optimal for one selected angle of attack. A similar approach to the cove cover was the extended seal attached to the slat hook. This then triggered the design for a completely filled slat cove through a streamlined body. With all of these ideas/designs the noise was reduced.

The add-on devices were also considered as well as flow transparent edge replacements. However, the latter suffers from the fact that materials such as porous metal foam are not allowed to be used in aviation even though it is very effective for noise reduction. Another potential noise reduction method is the elimination of the edge by the mold-line technology.

The possibilities for high-lift devices allow for significant noise reduction however, there are some restrictions that need to be overcome and a number of researches need to be done.

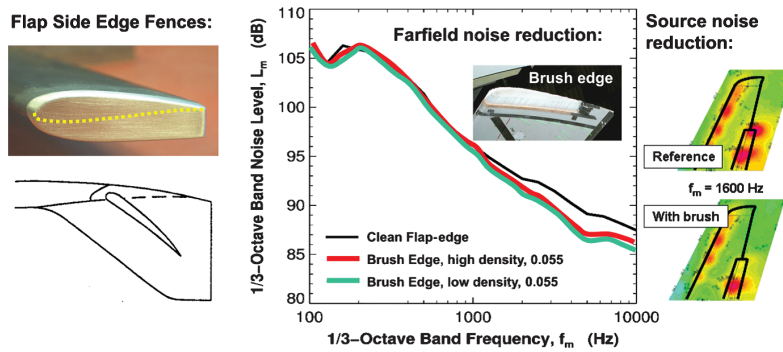


Figure 2.6: Flap side-edge fences and porous-edge replacements for noise reduction [3].

2.2.3 Engine Noise

The 1970s knew the development of the first twin cycle bypass turbofan engines. This advancement triggered the need for reduction of fuel consumption but also had an advantageous side effect on aircraft noise impact as it reduced the jet noise. So the following generations of turbofan engines knew an increase in bypass ratio which allowed for the reduction in noise levels. The reduction in noise levels over the years by means of increasing bypass ratio is shown in Figure 2.7.

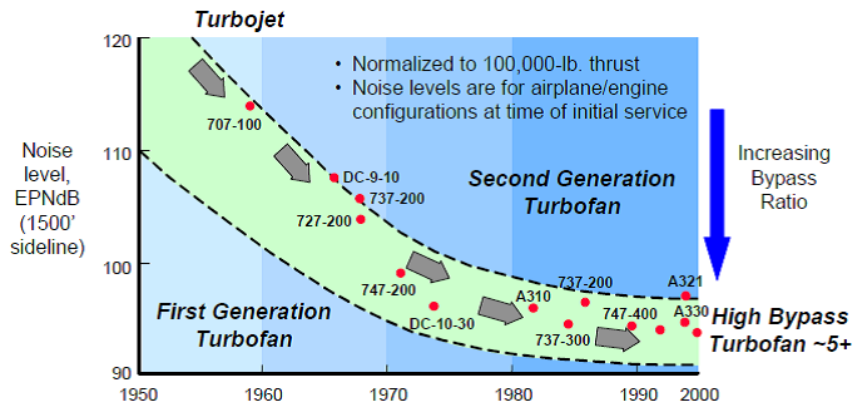


Figure 2.7: History of commercial aircraft noise levels and progression of engine type and bypass ratio [13].

So by reducing the velocity of the jet plume the jet noise is reduced. The increase in bypass ratio in the latest jet engines allows for lower exhaust velocities while maintaining the same thrust levels and thus lower noise levels. However, it is not only the increase in bypass ratio that allowed for a reduction of jet noise levels but also the advancements in quieter fans and turbo machinery designs.

Another development made by *General Electric* (GE) was the creation of the chevron nozzle for separate flow exhaust systems. It reduces jet noise by enhancing mixing of the fan, core and ambient streams faster than the conventional nozzles [13]. It does so by generating stream wise vorticity which enhances the mixing between the streams, reducing the peak velocity and thus the peak noise.

These developments allowed for the engine noise to be reduced to such levels that during landings the aerodynamic noise is as high as the engine noise.

2.3 Noise Abatement: Airport Level

The pressure performed by the governments on airlines and airports to reduce the environmental impact of noise and emissions on residential areas, it has led to an increase in research on noise and emissions abatement measures. As was mentioned before, some of the measures used are on the aircraft level and the ones that are going to be discussed in this section are on the airport operational level.

Some examples of these measures are noise restriction zones around airports which can be observed in Figure 2.8; it shows the cumulative noise contour zone based on 35Ke which is the Dutch noise exposure index. However, this is not the case anymore for AAS but the new measure, consisting of enforcement points, still uses the same pattern shown in Figure 2.8. Another measure is the implementation of curfews that entail flight restrictions between certain periods of time, commonly at night [1]. These measures are both airport based measures.

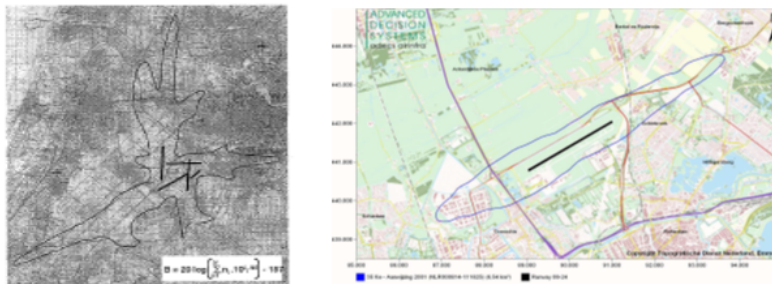


Figure 2.8: 35Ke Noise contour of Schiphol airport (left) and Rotterdam airport (right) [1, 14].

Other measures of interest are operational measures which can be divided into two categories, short and medium term procedures. These categories are going to be discussed in the following subsections.

2.3.1 Short Term Procedures

The short term procedures make use of existing ATC infrastructure and consist of reduced flaps on approach, a slight increase in *Instrument Landing System* (ILS) glide slope and an increase in final approach altitude as well as CDA [14, 15].

The first procedure of this category, the reduced flaps approach, is a procedure where the landing is performed with flap settings that are lower than the maximum landing flaps. The results of this method are mild, however still obvious noise reductions were obtained. This led to the acceptance of this method by pilots and air traffic controllers alike and it has been successfully implemented at Schiphol airport.

The second procedure, the slight increase of ILS glide slope, is a procedure where the ILS glide slope is increased from 3° to 3.2° . The effects were marginal and due to deviation from the standardized approach angle this procedure was abandoned [16].

The third procedure where the final approach altitude is increased is a procedure that requires the final approach altitude to be changed from 2000 ft. to 3000 ft. The effects of this change resulted in noticeable noise level reduction and airport capacity studies showed that such change did not affect the ATC or airport capacity as well as safety, thus implementation of this procedure was pursued [17].

2.3.2 Medium Term Procedures

The medium term procedures may require additional certification and/or modification to existing aircraft avionics in comparison with the short term procedures. These procedures focus on *Advanced Continuous Descent Approach* (ACDA) and *Precision Navigation Instrument Departure* (PNID). ACDA concentrates on the optimization of the current CDA procedure while the PNID focuses on improving the accuracy of tracking aircraft flying *Standard Instrument Departure* (SID) routes [14, 15].

However, implication of these procedures is difficult due to the fact that it demands a lot from the ATC controllers. The fact is that ATC controllers can not separate aircraft that are decelerating at different rates which makes strategic control impossible [18]. A possible solution is the use of an automation infrastructure that incorporates flight operation uncertainties.

All of the previously mentioned procedures as well as others will be discussed in detail in the coming section.

2.4 Noise Abatement Procedures

As mentioned before, this section will describe the different types of *Noise Abatement Procedures* (NAP) as well as the conventional approach that is used by the majority of airports. This approach is not a NAP.

2.4.1 Conventional Approach

This is the approach that is mainly used during landing procedures hence the name conventional approach. During this procedure aircraft are kept separated at specific distances for safety reason, this is handled by the ATC. Due to varied number of arriving aircraft at different velocities it is quite difficult for the ATC to predict the future position of an aircraft and it becomes more complex when handling multiple aircraft at ones. Thus, the ATC needs to maintain the required separation distances; this is achieved by using speed/altitude plateaus [19]. These plateaus have the purpose of allowing for speed reduction and establishing adequate spacing between aircraft. This way the complexity of the workload of the ATC is reduced and the safety is increased. Figure 2.9 depicts this procedure.

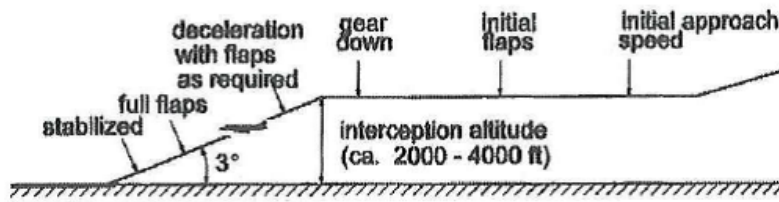


Figure 2.9: Conventional Approach [10].

2.4.2 Two-Segment Approach

This procedure is one of the early methods that were suggested as a NAP. The basis of this method is a steeper descent angle than commonly used. The first part of this procedure started at an altitude of 6000 ft. followed by a descent at an angle of 6° till it reaches an altitude of 1000 ft. where it intercepts the ILS. From this point the second part starts where the aircraft continues the landing at the standard glide slope angle of 3° . As a result of this procedure the noise was reduced. Figure 2.10 shows the inner workings of this method.

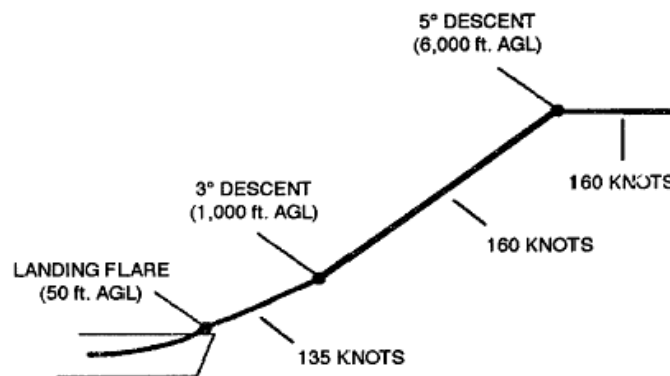


Figure 2.10: Two-Segment Approach [20].

2.4.3 Three Degree Decelerating Approach

This procedure is the predecessor of the CDA. It starts by decelerating with an angle of 3° at an altitude of 6000 ft. and then it intercepts the ILS. During this procedure the engines are set to idle and the aircraft is decelerated by means of drag forces [21]. The results of this procedure are comparable to those of the Two-Segment approach. However, this procedure is much more preferred by pilots than the Two-Segment Approach, due to the fact that no changes need to be done with respect to the glide slope angle. Figure 2.11 demonstrates this procedure.

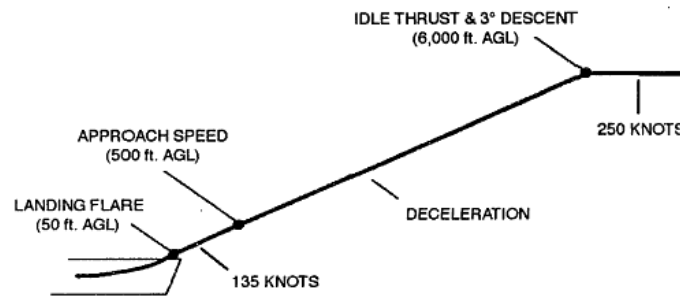


Figure 2.11: Three Degree Decelerating Approach [20].

2.4.4 Continuous Descent Approach

The CDA procedure allows the aircraft to perform the arrival without any flight-level segments, meaning a continuous descent is performed without of the need of leveling off first before descending again, Figure 2.12. The engines are set to idle during this approach, consequently reducing the fuel consumption as well as the noise levels [22]. This procedure is already being tested and applied at major airports such as AAS [15, 23–25].

Nevertheless, there are some downsides to this procedure. The separation interval between approaching aircrafts is increased in congested airspace. This is a direct result of the different features of the approaching aircraft and the accuracy of the FMS. Hence, the only possible application of such a method is during low congested airspace conditions, such as night flights or small airports.

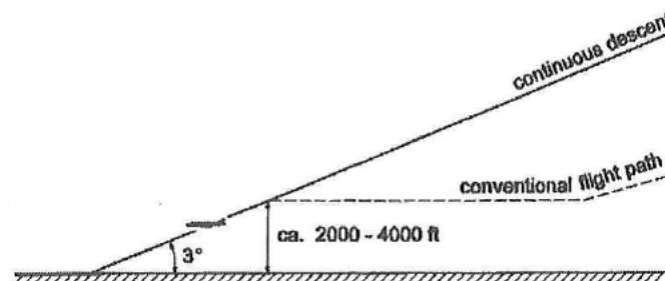


Figure 2.12: Continuous Descent Approach [10].

2.4.5 Advanced Continuous Descent Approach

The idea behind ACDA is the enhancement of the accuracy and predictability of the CDA flight procedure with the intention of restoring the separation distances to a level that applies to the conventional approach procedure. This is being studied on both the cockpit and ATC aspects with the intention of applying this procedure during airport peak hours. Furthermore, noise reduction will be optimized due to the delay of the final stabilization until an altitude of 1000 ft.

The ACDA uses the following technologies/techniques: curved approach, decelerated approach and 4-D RNAV. The curved approach is self-explanatory and has a continuous lateral vertical

guidance while maintaining a constant 3° glide path. This flight is carried out as a decelerated approach which is controlled by an FMS programmed management algorithm. The 4-D RNAV is a prediction of the aircraft trajectory in position and time which is made before the aircraft begins an ACDA procedure. The prediction is based on the aircraft flap/speed schedule and the available information on the wind profile.

With the help of the previously mentioned technologies/techniques it is expected that the obstacle of the reduced landing capacity of the CDA will be overcome. This will allow the application of this procedure during peak hours. However, there are some developments needed to realize this concept. One of these developments is an assistance tool for air traffic controllers. This tool uses the principle called "*ghosting*" that displays the values of the longitudinal separation between aircraft much better. This allows the air traffic controller to assess whether the separation at the fixing point of CDA routes will be acceptable.

Another tool is ACDA in the FMS. This is done by developing an algorithm that enables flying ACDA's [26]. This algorithm ensures that the thrust levers remain in the flight-idle position during the majority of the approach. It is based on two requirements, the first one being the determination of the position along the flight trajectory where the engines are set to idle and where the first flap setting has to be selected. This has to be performed in a manner where the final approach target speed is obtained at a specific distance before the runway.

The second requirement is when deviations from the predicted trajectory due to disturbances occur, the system will adapt the moment of flap selection in such a manner that the target speed at the end of the approach remains unchanged.

With the help of the Monte Carlo simulations, the initial nominal separation is calculated. It uses the case of a Boeing 737 leading a Boeing 747 where the wake vortex separation of 3 nm in the terminal area and 2.5 nm on final approach is maintained throughout the procedure. This initial separation is found to be 9 nm and it would result in a runway capacity of 30 to 52 aircraft per hour given that the approach speed is 140 knots [18].

If the previously mentioned tools are implemented then a significant reduction in the current CDA landing intervals is feasible which will allow an application during airport peak hours. Furthermore, by increasing the length of the flight segment where the engine is in idle state, the noise of the present CDA will be improved even further. The curved approach allows for shorter final segment which in turn allows for flexibility in avoiding urbanized areas around the airport.

2.4.6 Precision Navigation Instrument Departure

The current implantation of SID's by the RNAV makes the flying of an accurate SID trajectory almost impossible, namely during turns. SID's are defined by fly-by and fly-over way-points, which are determined by ground based navigation systems such as *VHF Omnidirectional Radio* (VOR), *Distant Measuring Equipment* (DME) and *Non Directional Beacon* (NDB). Starting from the way point data, the FMS designs a departure track [14].

The PNID concepts are for SID's that are flown as area navigation procedures along a predefined 2-D lateral track. These trajectories consist generally of straight and circular segments. With the usage of satellite navigation system it becomes possible to accurately track the entire departure route. This allows for adaption to local needs, where populated areas can



Figure 2.13: Advanced Continuous Descent Approach [14].

be avoided during take-off. With this maximum flexibility is guaranteed for route definition. Furthermore, the existing noise abatement departure procedures become more effective.

So the expected benefits of PNID are the unambiguous route definition by means of applying of prescribed departure routes along straight and circular segments. SID routes can be adapted to local situations which allows for avoidance of highly populated areas. Furthermore, precise tracking of the prescribed routes increases the efficiency of noise abatement.

2.5 Helical Noise Abatement Procedure

While a number of researchers are focusing on ACDA and/or on PNID [14], there are also the ones that are looking into the possibilities of HeNAP approaches [27–29]. This is the focus of the project and will be compared to the findings of the previously mentioned methods.

As can be seen from Figure 2.14, the HeNAP is a procedure where the aircraft approaches the airport at higher altitudes compared to conventional approaches, which is followed by a spiral descent until interception with ILS where it continues along a 3° glide-slope. This allows the noise that is created during the conventional approach to be redirected from the approach path to the helix, which is in direct vicinity of the airport.

The initial values that were used by Bertsch [28], for the initial altitude where the aircraft approaches the airport is 7500 ft. with a radius of 2000 m and a distance of 3200 m from the center of the helix to the runway and a final altitude where the aircraft exits the helix of 500 ft.. During this test, the aircraft performs three spirals before exiting the helix.

This procedure showed promising results that make further research appealing. It revealed that the HeNAP has a higher noise reduction than the conventional approach. However, this comes at a cost of higher fuel consumption, increase in emissions and flight time.

Volovoi [29] also researched this procedure, however not with regard to noise but with regard to wind effects and the safety concerns that come with such winds. As a result, it was found that during this procedure the aircraft is mostly vulnerable to a combination of cross and

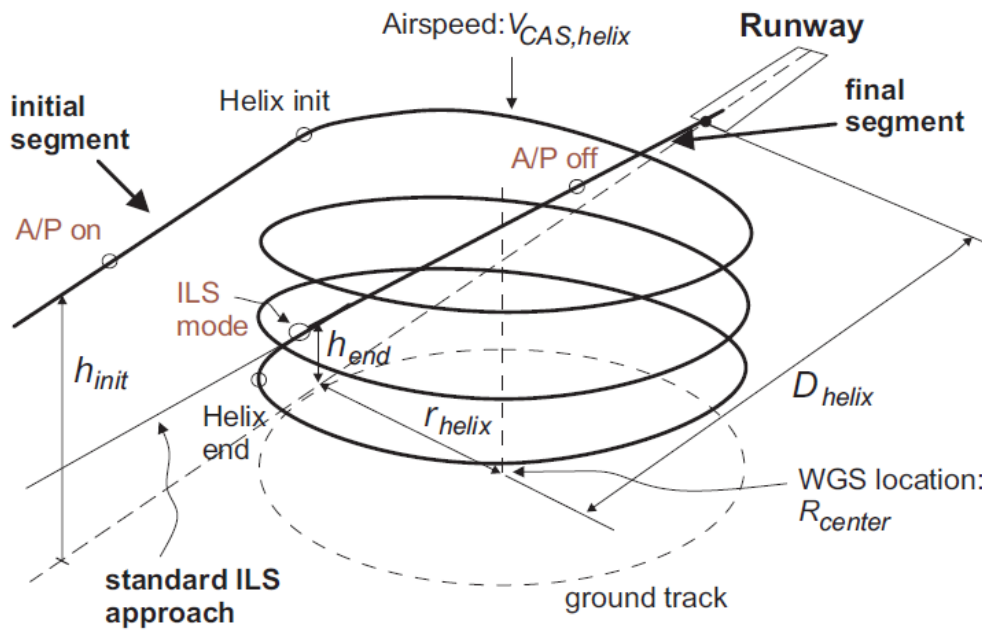


Figure 2.14: Helical Noise Abatement Procedure [28].

head winds where it starts to drift from the initial path and the pilots need to intervene. Thus when such winds occur pilots need to be constantly correcting for these effects, which takes attention from other tasks.

Nevertheless, this procedure has great possibilities, such as the implementation at low capacity airports or during night hours, which would make night curfews obsolete. The later still needs to be researched in terms of how many awakenings occur during the application of this procedure. The same research has been performed with respect to the awakenings due to the CDA [5–8].

GPOPS Optimization Framework

As was explained in Chapter 2, a number of aspects influence the environmental optimization of the HeNAP, such as the number of spirals and the radius of the spiral flown. The constraints of these aspects alter the trajectory of the HeNAP until a balance is found where the HeNAP is both feasible and optimal. This is considered true when the following objectives are optimized within the optimization tool:

- Time
- Fuel
- Number of Awakenings

Ideally, all of these objectives need to be minimized without affecting each other. However, this is not always the case and trade-offs are needed to make a sound assessment. Making this a complex process and the solution needed is obtained by using the so-called multi-objective theory. This theory is often used in process engineering and economics in order to maximize profit and minimize cost. During this thesis work, the multi-objective function will be transformed to a single-objective function in order to obtain an effective optimization.

This chapter explains the developed tool for environmental optimizing of the HeNAP. This is done within the `MATLAB` program and the inner workings and theory of this are explained in the coming sections.

3.1 Optimal Control Theory

An extensive description of the multi-objective optimization theory can be found in [30], and it will be shortly explained in this section.

An aircraft is seen as a dynamic system that travels along a certain path and can be described by a number of parameters called the **state of the system**. This allows to the status of the system to be shown at a particular point in time. The parameters used to describe this are the (state variables) and are indicated as x_i , $i = 1, 2, \dots, n$. Such a dynamic system is not in a steady state but it develops through time. It can also be subjected to **input** with the

so-called **control variables**, which are indicated by u_k , $k = 1, 2, \dots, m$. The state vector \mathbf{x} outlines an n -vector of state variables and the control vector \mathbf{u} outlines an m -vector of control variables. Both these variables can be constrained, and the constraints that are laid may not be violated. This so-called **Optimal control Theory** is used to find the optimal trajectory for dynamic systems and is a modern form of the **Calculus of Variation**. The equation of motion for a typical dynamic system can be described by the following set of first-order differential equations:

$$\dot{\mathbf{x}} = \mathbf{f}[\mathbf{x}(t), \mathbf{u}(t), t] ; \quad t_0 \leq t \leq t_f \quad (3.1)$$

With t_0 and t_f being the initial and final time. By using a **performance index**, the trajectory of a dynamic system can be optimized. In order to find the best values for the performance index, the system of the optimal control problem is determined by the right control variable inputs. The following equation is a typical formulation of the performance index for path optimization.

$$J = \Phi[\mathbf{x}(t_0), t_0, \mathbf{x}(t_f), t_f] + \int_{t_0}^{t_f} \mathcal{L}[\mathbf{x}(t), \mathbf{u}(t), t] dt \quad (3.2)$$

Another name for the performance index is also the *objective function* or the *cost function* of an optimal control problem. The initial part of the cost function J is the **Mayer** part and is denoted by the symbol Φ . This part is calculated at the end of each iteration and added to the total cost function. The final part of the cost function is the **Lagrange** part with the symbol \mathcal{L} and is determined by calculating the time derivatives of the cost parameters and integrating them over time. If the initial or final states of the state vector $\mathbf{x}(t)$ are given, then these are called the boundary conditions. The control variable constraints are defined by stating that \mathbf{u} belongs to a closed bounded set U .

By combining the previous mentioned equations, the general optimal control problem can be stated. The acceptable functions $\mathbf{u}(t)$ minimize the performance index J while the state variables satisfy the **dynamic constraints** \mathbf{f} along with the associated **boundary conditions** ϕ and **algebraic path constraints** \mathbf{C} can all be found in the following equations:

$$\min_{\mathbf{u}(t) \in U} J = \Phi[\mathbf{x}(t_0), t_0, \mathbf{x}(t_f), t_f] + \int_{t_0}^{t_f} \mathcal{L}[\mathbf{x}(t), \mathbf{u}(t), t] dt \quad (3.3)$$

subject to:

$$\dot{\mathbf{x}} = \mathbf{f}[\mathbf{x}(t), \mathbf{u}(t), t] \quad (3.4)$$

$$\phi[\mathbf{x}(t_0), t_0, \mathbf{x}(t_f), t_f] = \mathbf{0} \quad (3.5)$$

$$\mathbf{C}[\mathbf{x}(t), \mathbf{u}(t), t] \leq \mathbf{0} \quad (3.6)$$

For solving modeled optimal control problems, numerical methods are needed and even with these methods, it is still a challenge to solve them. One of the ways that can be used is to simplify the problem and produce near-optimal solutions. For example, this can be done by linearization, segmentation or by neglecting some dynamic effects.

3.2 NOISHHH Optimization Framework

In this section, the old NOISHHH optimization framework is shortly described, because it was the first tool to include the noise abatement into its optimization and the GPOPS tool is based on this concept. The NOISHHH tool optimizes aircraft trajectories with the usage of optimal control theory and gradient-based optimization techniques.

NOISHHH capabilities of generating noise-optimized trajectories are revealed in [5,6]. It combines a noise model with dynamic trajectory optimization algorithms, where it evaluates the fuel consumption, flight time, emissions and noise for single-event abatement procedures.

In 2005, different noise abatement criteria were optimized and compared to a noise performance trade-off [7]. In addition, in 2008, the multi-event optimization tool was added where it shows that it is apt for resolving in-trail separation conflicts in environmental manner [8].

Even though the NOISHHH tool has proved its worth in the past, it had its limitations. The computation times for an optimization run were far too long.

3.3 GPOPS Framework Structure

The structure of the optimization tool is quite simple and is based on the former NOISHHH tool. Figure 3.1 depicts this structure clearly. As can be seen from the figure, an initial guess is needed as an input for the dynamic optimization algorithm. Other than the initial guess, the aircraft model is also needed, which is based on real aircraft characteristics.

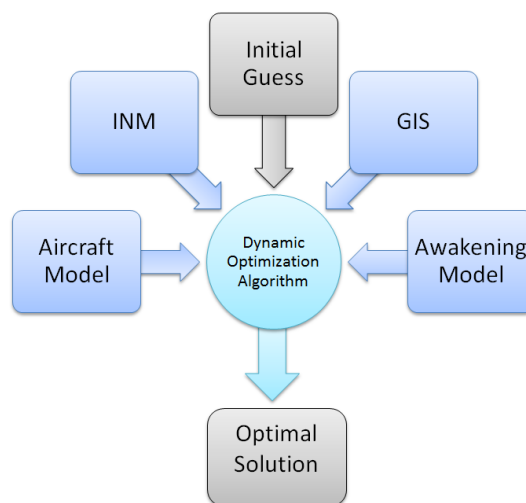


Figure 3.1: GPOPS Tool Structure [9].

A noise model is also needed for the computation of the generated noise during the HeNAP. To calculate the impact of the noise, the noise model is combined with a database that includes information about populated areas. These areas are connected to an awakening model that is based on the sleep disturbance dose-response relationship of Section 2.1.6.

Finally, the combination of all the previously mentioned models and inputting them into the dynamic optimization algorithm, results in the optimal solution of the HeNAP.

3.4 General Pseudospectral Optimal Control Software

As mentioned before, the program that is used to develop the optimization tool for the HeNAP is GPOPS, which as the title of this section suggests stands for General Pseudospectral Optimal Control Software. By combining all the models mentioned in the previous section and running the gradient-based optimization process, it is able to solve optimal control problems that are defined by the user.

First, the problem needs to be defined and used as input for the program. Within this definition the limits, boundary conditions and constraints are specified. Secondly, the user needs to define the path constraints and the cost function needed for the optimization. Having done so, the program is able to solve small problems within seconds, however multi-phase noise optimization can still take a couple of hours.

Some of the key features of GPOPS include:

- A restricted version of a nonlinear programming solver.
- Built-in forward mode automatic differentiation.
- Implementation of an efficient and accurate hp-adaptive algorithm for mesh refinement.
- Sparse finite-differencing of optimal control problem to generate derivative estimates as efficiently as possible.
- The ability to solve general multi-phase optimal control problems.

3.4.1 Radau Pseudospectral Method

As mentioned before, the optimization process is gradient-based and it uses the method that is explained in this section in order to solve the optimal control problem.

If the optimal control problem would be solved analytically, then an exact solution would be found, however this is a difficult and complex process. Therefore, a direct optimization method is needed for this thesis, hence the usage of the Radau Pseudospectral Method RPM [31]. This direct global parameterization method uses Radau quadrature to precisely approximate the dynamics of the problem. Afterwards, orthogonal Legendre polynomials are used to discretize the continuous problem, this way the infinite-dimensional problem is transcribed into a finite-dimensional nonlinear programming problem. The nonlinear problem is then solved with the help of SNOPT¹ numerical solver. For computing the objectives function gradient and constraint Jacobian within GPOPS, INTLAB² is used.

¹http://www.sbsi-sol-optimize.com/asp/sol_product_snopt.htm

²<http://www.ti3.tu-harburg.de/rump/intlab/>

3.4.2 Detailed Program Structure of the HeNAP Optimization Tool

This section reveals a more detailed overview of Figure 3.1 for the HeNAP Optimization tool. As can be seen from Figure 3.2, the iteration process starts with an initial guess where the states and controls as well as the complete limits and linkages setup are sent to GPOPS. Furthermore, the gradients of the objective function and the constraint Jacobian are automatically differentiated by INTLAB. This is followed by the calculation of the awakenings costs and the noise Lagrangian costs, in the form of a noise Jacobian, in the Noise Model. These costs are then combined with the output of INTLAB.

With the RPM method the problem is transformed into a nonlinear problem that is solved with SNOPT. With GPOPS the solutions' feasibility and optimality are checked, by considering if the constraints are satisfied and a certain accuracy level is reached. If this is not the case the whole process is iterated until a solution is found that reaches the desired level of feasibility and optimality. By adding more constraints and making the optimization more complex, it can also be the case that the optimal control problem will be infeasible and consequently no solution is found.

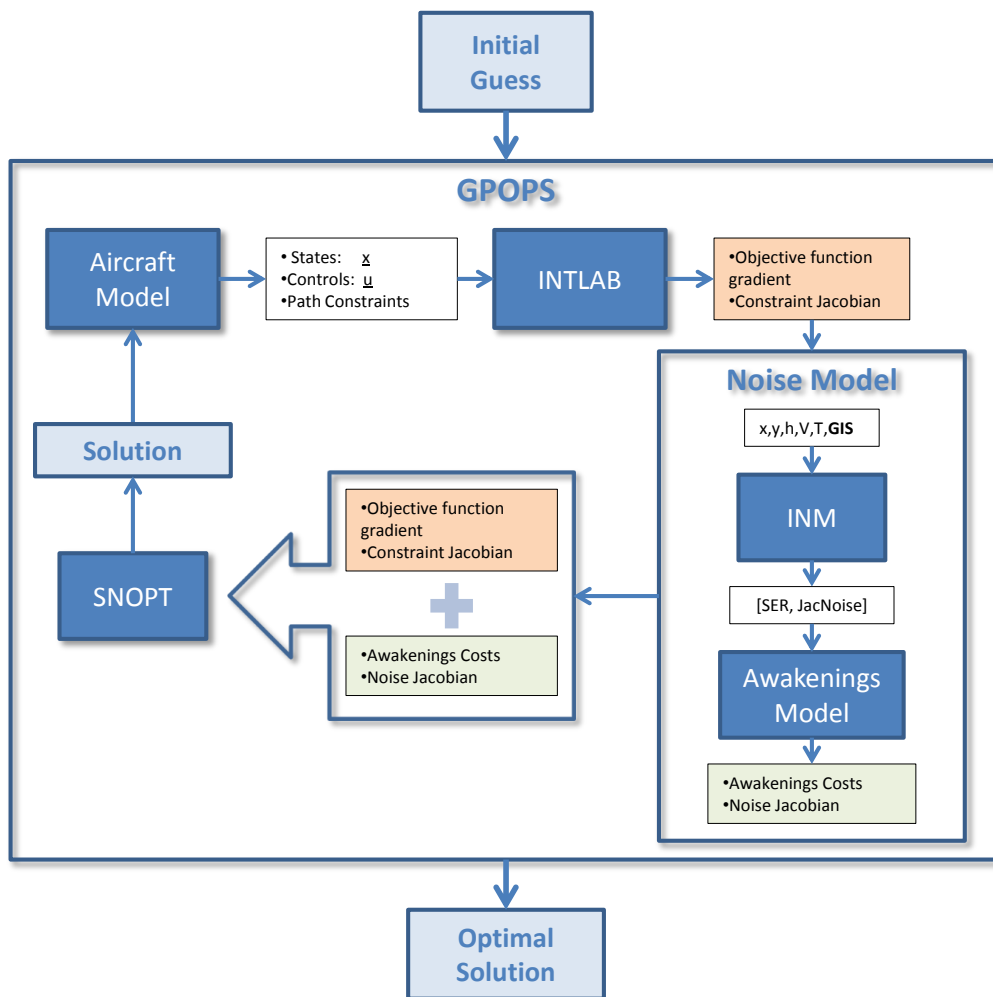


Figure 3.2: Program Structure of the Environmental Optimization Tool [10].

3.5 Aircraft Model

As was mentioned in the previous sections, one of the models used in the GPOPS is the aircraft model. Within the model, all of the states and controls of the optimal control problem are optimized and computed in each iteration. The aircraft model also includes a Point Mass Model and a Standard Atmosphere Model. All of the calculations of this optimization work are performed below the height of 11,000 m, which uses the *International Standard Atmosphere* ISA. This means that seasonal changes for temperature and winds are neglected.

Figure 3.3, shows the type of aircraft used during the simulations. It is a Boeing 737-700 with all of its characteristics given in Table 3.1.

Table 3.1: General Boeing 737-300 Characteristics [9].

Boeing 737-300		
Capacity	Crew	2
	Passengers (typical configuration)	128
Dimensions	Length	33.4 m
	Wing span	28.9 m
	Height	11.1 m
	Wing area	105.4 m ²
Weights	Operating empty weight	31,479 kg
	Maximum Take Off Weight	56,472 kg
Performance	Typical cruise speed	M = 0.76
	Typical range	2,850 nm
	Engines	2 × CFM56-3B1 (20,000 lb SLST)



Figure 3.3: Royal Air Maroc Boeing 737-700.

3.5.1 Point Mass Model

In order to create realistic aircraft trajectories, an intermediate point mass model is used to compute the dynamics of the aircraft. This allows the control variables to be found, which are vital for the optimization to find the optimal controls of the trajectory. Hence, some assumptions are made about this point mass model:

- A flat, non-rotating Earth
- Coordinated flight
- No wind vector

The state vector \mathbf{x} of the optimal control problem is defined as follows and consists originally of 6 states:

$$\mathbf{x} = \begin{bmatrix} x \\ y \\ z \\ V \\ \chi \\ m_f \end{bmatrix}, \quad (3.7)$$

where:

- x and y denote the x and y coordinates of the aircraft both in the “Rijksdriehoeks” (RD)-coordinate system.
- z is the altitude of the aircraft in m.
- V is the True Airspeed (TAS) of the aircraft in m/s.
- χ is the heading of the aircraft in radians defined as the true compass heading with North at 0° and South at 180° .
- m_f is the fuel used in kg.

However, for this thesis work x and y are replaced by s , where s is the along track distance in m. To be exact the ground track is forced by means of s and thus making ($x = x(s)$ and $y = y(s)$) functions of s . See Figure 3.4.

From Figure 3.4, it can be seen that an initial position is needed, represented by (x_0, y_0) , this also the starting point of the track represented by s_0 . The ground track continues to the initial point of the spiral, (x_1, y_1) , and has a length of $L1$ as can be seen from the figure. The spiral is performed by a constant radius R with the center of the circle at (x_c, y_c) . The spiral is then exited at (x_2, y_2) where it continues the approach till the final coordinates (x_f, y_f) for a length of $L2$. The final coordinates also represent the end of the ground track and is given by s_f . The total track is thus represented by the state s with s_0 at the beginning of the track and s_f at the end. All of these points are used within the framework in order to create this ground track.

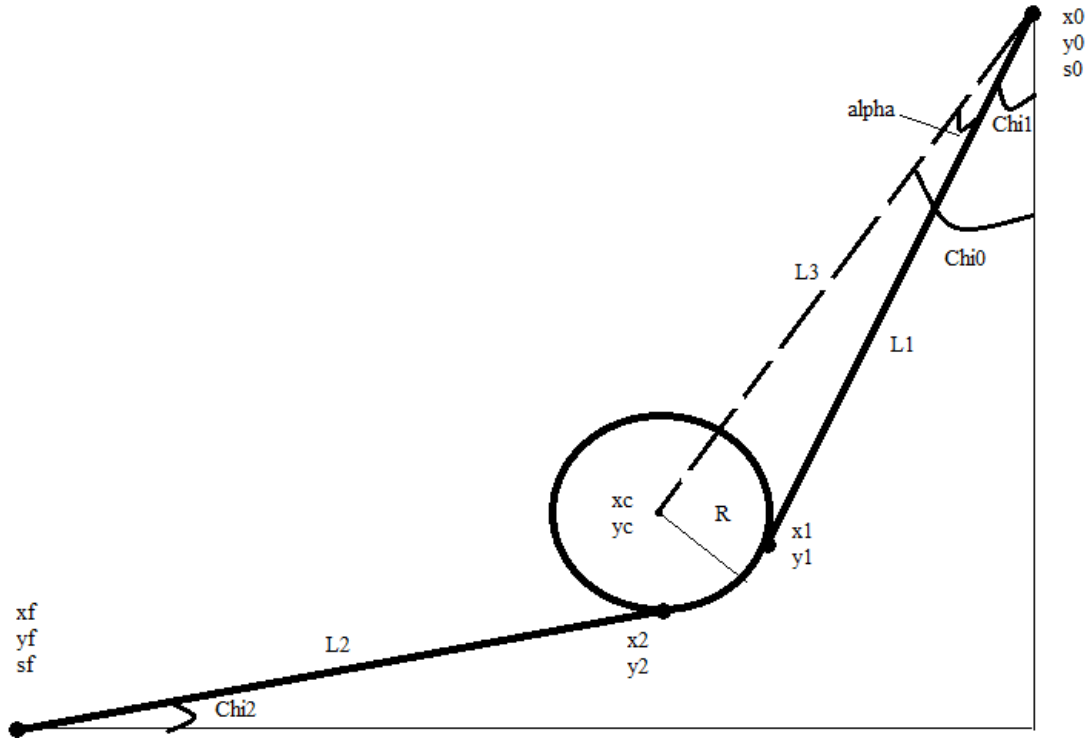


Figure 3.4: Forced Ground Track

The way the coordinated found in Figure 3.4 are used within the tool is as as followed:

- (x_0, y_0) , (x_f, y_f) and χ_2 are known.
- by using (x_f, y_f) , (x_2, y_2) can be calculated
- knowing (x_2, y_2) , (x_c, y_c) is calculated
- by finding (x_c, y_c) , L_3 and χ_0 are then calculated
- this in turn allows L_1 and α to be found
- by finding α , χ_1 can be calculated
- by using the equations the ground track can be optimized within the tool

$$x_2 = x_f - L_2 \sin \chi_2 \quad (3.8)$$

$$y_2 = y_f - L_2 \cos \chi_2 \quad (3.9)$$

$$x_c = x_2 - R \sin \left(\chi_2 - \frac{1}{2} \pi \right) \quad (3.10)$$

$$y_c = y_2 - R \cos \left(\chi_2 - \frac{1}{2} \pi \right) \quad (3.11)$$

$$L_3 = \sqrt{(x_c - x_0)^2 + (y_c - y_0)^2} \quad (3.12)$$

$$L_1 = \sqrt{L_3^2 - R^2} \quad (3.13)$$

$$\alpha = \arcsin\left(\frac{R}{L_3}\right) \quad (3.14)$$

$$\chi_0 = \arctan\left(\frac{x_c - x_0}{y_c - y_0} + \pi\right) \quad (3.15)$$

$$\chi_1 = \chi_0 - \alpha \quad (3.16)$$

Having laid out the ground track by means of the previous equations and thus defined s , the new state vector becomes:

$$\mathbf{x} = \begin{bmatrix} s \\ z \\ V \\ \chi \\ m_f \end{bmatrix} \quad (3.17)$$

For the control vector \mathbf{u} , three controls are used:

$$\mathbf{u} = \begin{bmatrix} \Gamma \\ \gamma \\ \mu \end{bmatrix}, \quad (3.18)$$

where:

- Γ is the normalized throttle setting of the engines with values between 0-1.
- γ is the flight path angle of the aircraft in radians.
- μ is the bank angle of the aircraft in radians. A positive bank angle defines a turn to the right.

The normalized throttle setting control variable Γ ranges from 0 to 1 such that the thrust T is calculated as:

$$T = [T_{max} - T_{min}]\Gamma + T_{min} \quad (3.19)$$

Where T_{max} and T_{min} are the maximum and minimum thrust of the engines.

The time derivatives of the states are defined originally as follows:

$$\dot{x} = V \cos \gamma \sin \chi \quad (3.20)$$

$$\dot{y} = V \cos \gamma \cos \chi \quad (3.21)$$

$$\dot{z} = V \sin \gamma \quad (3.22)$$

However, due to the replacement of x and y by s , the new time derivatives become:

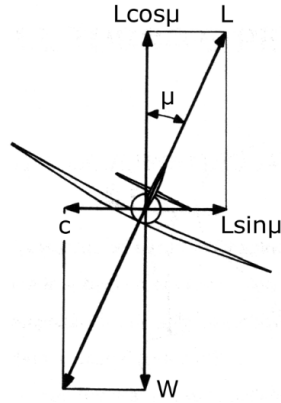


Figure 3.5: Force Equilibrium in a Horizontal Steady Turn [32].

$$\dot{s} = V \cos \gamma \quad (3.23)$$

$$\dot{z} = V \sin \gamma \quad (3.24)$$

In Figure 3.5 the force equilibrium of an aircraft in a horizontal steady turn is shown:

The expression for the time derivatives of χ is obtained from this force equilibrium as follows:

$$W = L \cos \mu \quad (3.25)$$

$$V = \omega R \quad (3.26)$$

$$m \frac{V^2}{R} = L \sin \mu, \quad (3.27)$$

where:

- W is the aircraft's weight in N.
- L is the aircraft's lift force in N.
- ω is the angular velocity in rad/s.
- R is the turn radius in m.
- m is the mass of the aircraft in kg.

From Newton's second law of motion along the axis of the speed vector and Figure 3.6 the time derivative \dot{V} is defined as follows:

$$\dot{V} = \frac{g_0}{W} [T - D - W \sin \gamma] \quad (3.28)$$

D is the drag force in Equation (3.27).

With this, all off the states and time derivatives, except \dot{m}_f , are symbolized. The reason for not showing \dot{m}_f is because of its extensiveness.

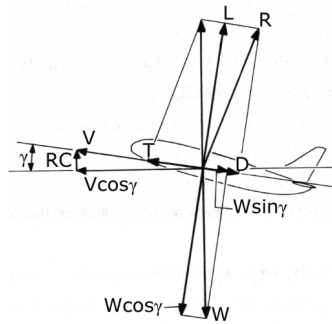


Figure 3.6: Airplane in Symmetric Flight [32].

3.6 Noise Model

The model where the awakenings cost and noise-Jacobian are established that are needed for the gradient-based optimization is the noise model. The noise model calculates the generated aircraft noise with an implemented noise model. Furthermore, the noise is combined with the data that contains the information of a populated area. By adding an awakening model, the noise impact on populated areas in the form of awakening is obtained. The following section discuss these models in detail.

3.6.1 Integrated Noise Model

The noise that is generated by the aircraft during the HeNAP is calculated by the *Integrated Noise Model* (INM). The INM was developed by the *Federal Aviation Administration* (FAA) [33] and it outputs the noise contribution of an individual aircraft flyover in terms of the outdoor SEL at preselected locations.

3.6.2 Implementation of the Noise Contribution

The states of the optimal control problem are used as input in INM in order to calculate the noise in the form of SEL. In addition to SEL, the partial derivatives of the states are also calculated with respects to SEL, which is needed for the gradient-based optimization. INM also uses a *Noise Power Distance* (NPD) table, where the SEL at all distances to the aircraft is stored for specific engine types. This table contains values that are under the reference conditions and thus corrections are needed and applied to the SEL that is derived from the NPD [9]. These correction are:

1. Noise fraction adjustment, this is needed as the SEL values defined in the NPD are valid for segments of infinite length, whereas in reality the segments have a finite length.
2. Speed adjustment, the NPD is based on a reference speed of 160 kts TAS. Therefore, for every speed above or below this reference value a correction is required.
3. Lateral attenuation adjustment, this correction compensates grid points that are not directly below the flight path for ground reflection and refraction, airplane shielding and other ground and aircraft effects.

The exact calculations for these corrections can be found in [33].

The resulting trajectories of the HeNAP optimization tool are actually segmented flight paths, where the user defines the amount of nodes. So with the *Sound Exposure Ratio* (SER), the segment to the observer grid points in the underlying grid is calculated:

$$SER_{seg} = 10^{[L_{AE,NPD} + NF + SA + LA]/10} \quad (3.29)$$

In this equation SER_{seg} is the SER in the segment under consideration and is dimensionless. $L_{AE,NPD}$ is the interpolated SEL derived from the NPD data. Furthermore the noise fraction NF , speed adjustment SA and lateral attenuation LA corrections are included in the calculation and expressed in dB. By taking the sum of the SERs of all segments the total SER of the flight becomes:

$$SER_{flt} = \sum_{i=1}^{n_{seg}} [SER_{seg}]_i \quad (3.30)$$

The corrected total SEL of the flight at the observer point can be calculated from the SER_{flt} and is expressed in dBA:

$$L_{AE,flt} = 10 \log_{10} [SER_{flt}] \quad (3.31)$$

By using the newly found value of the SEL, the amount of awakenings can be calculate with the Awakenings Model.

3.7 Awakenings Model

By combining the generated aircraft noise and the data about the populated area, we get the awakenings model. This allows the number of awakenings to be calculated by using the sleep disturbance dose-response relationship and eventually used as a cost parameter for the optimization process.

3.7.1 Geographic Information System

The *Geographic Information System* (GIS) is a set of data that contains all of the information of a populated area. This data is obtained from the Dutch *Centraal Bureau voor de Statistieken* (CBS) and provides the following information:

- Population distribution
- Population density

By means of this information, it is possible to avoid all the densely populated areas during an arrival or departure. Figure 3.7 shows a density map that is used within the optimization tool. This figure shows the inhabited areas around AAS clearly.

The INM only used the inhabited areas as this reduces the computation time of the tool considerably. Once the SEL and noise Jacobian are obtained, the GIS calculates the number of awakenings. This is done by using only the areas where the noise levels surpass a certain level.

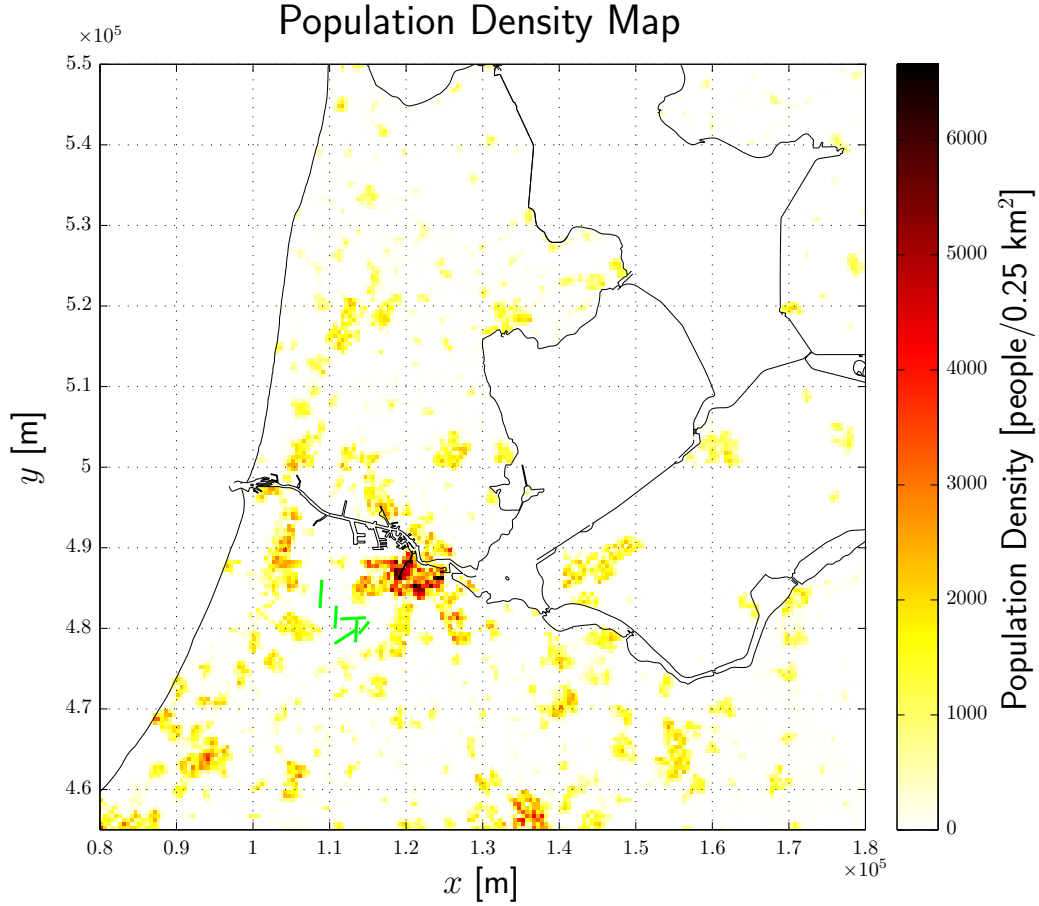


Figure 3.7: Population Density Map of the AAS Area [10].

3.7.2 Implementation of the Awakenings Cost Parameter

As was said before, the awakenings model calculates the number of awakenings with the sleep disturbance dose response relationship, Equation (2.8). However, this relationship is based on indoor SEL and thus results in a subtraction of 20.5 dB from the calculated $L_{AE,flt}$ of Equation (3.31). Since the number of awakenings is needed instead of the percentage, Equation (2.8) is transformed into:

$$Awakenings = 0.000087 \times (L_{AE,flt} - 50.5)^{1.79} \cdot pop \quad (3.32)$$

Where pop is the number of inhabitants at the underlying observer grid point. The total number of awakenings A for n inhabited observer grid points is calculated as:

$$A = \sum_{i=1}^n [Awakenings_i] = \sum_{i=1}^n [0.000087 \times (L_{AE,flt,i} - 50.5)^{1.79} \cdot pop_i] \quad (3.33)$$

3.8 Inequality Path Constraints

Section 3.1 mentions that for the optimization tool some constraints are needed and implemented. In this case, the constraint that is needed is one that makes sure that the aircraft performs only continuous descents. This inequality path constraint C in Equation (3.6) is implemented:

- Because of regulations, a $V_{CAS,max}$ of 250 kts (128.6 m/s) constraint is set and calculated with *Calibrated Airspeed* (CAS) below an altitude of 10,000 ft.
- A \dot{V}_{CAS} constraint such that the aircraft is not allowed to accelerate anymore. Only deceleration or constant CAS is allowed, this way the aircraft is forced to make a continuous descent. However, the aircraft can still hold its altitude with constant speed by using the throttle setting control variable Γ .

The choice behind the usage of CAS instead of the basic *Equivalent Airspeed* (EAS), is due to the fact that most of the simulations happen to start at a cruise altitude. At this altitude, the airspeed is usually higher than Mach 0.3 and needs to be adapted for compressible aerodynamic effects, which is true for the CAS. The EAS holds only for low subsonic airspeeds by assuming that the measured pressure difference is related to the airspeed by Bernoulli's equation for incompressible isentropic flow [32].

By using the function for $V_{TAS}(V_{CAS})$ as derived in [32], the inequality path constraint for maximum CAS is as follows:

$$V_{TAS,max}(V_{CAS,max}) - V_{TAS} \geq 0 \quad (3.34)$$

$$\sqrt{\frac{2\gamma}{\gamma-1} \frac{p}{\rho} \left[\left[1 + \frac{p_0}{p} \left[\left(1 + \frac{\gamma-1}{2\gamma} \frac{\rho_0}{\rho} V_{CAS,max}^2 \right)^{\frac{\gamma}{\gamma-1}} - 1 \right] \right]^{\frac{\gamma-1}{\gamma}} - 1 \right]} - V_{TAS} \geq 0$$

with $V_{CAS,max} = 250$ kts

V_{TAS} in Equation (3.34) is obtained from the state V of Equation (3.7). The second inequality path constraint \dot{V}_{CAS} can be written as:

$$\dot{V}_{CAS} \leq 0 \quad (3.35)$$

To derive \dot{V}_{CAS} first $V_{TAS}(V_{CAS})$ is rewritten to obtain $V_{CAS}(V_{TAS})$:

$$V_{CAS} = \sqrt{\frac{2\gamma}{\gamma-1} \frac{p_0}{\rho_0} \left[\frac{p}{p_0} \left[\left(V_{TAS}^2 \frac{\gamma-1}{2\gamma} \frac{\rho}{p} + 1 \right)^{\frac{\gamma}{\gamma-1}} - 1 \right] + 1 \right]^{\frac{\gamma-1}{\gamma}} - 1} \quad (3.36)$$

Now the time derivative of the CAS can be derived as follows in Equation (3.37):

3.9 Cost Function

Equation (3.3) shows that the cost function exists out of two parts, one being the Mayer part Φ and the other is the Lagrange part \mathcal{L} . The Mayer cost is calculated at the end of each optimization iteration and is added to the total performance index. Within the Lagrange part, the time derivatives of the cost parameters are calculated and integrated over time. To obtain a single optimal solution, the cost function consists of a single aggregate objective function. The method used to achieve this is by adding weights for the different objectives and minimizing the combined single linearly weighted sum of the objectives. So, by changing the weight factors of the different objectives it is possible to give importance to these objectives.

In order to find an optimal solution for the optimal control problem, the following cost function is used in the optimization tool:

$$J = k_{fuel} \cdot m_f(t_f) + k_A \cdot A + k_t \quad (3.40)$$

$m_f(t_f)$ is the fuel used at $t = t_f$ and k_{fuel} is the associated weight of this objective. Moreover, t_f is the end time and k_t is the associated weight. Additionally, the number of awakenings during the HeNAP trajectory can be included; this allows the noise abatement to be added to the minimum fuel problem of the HeNAP. Thus the A in Equation (3.40) stands for the total number of awakenings and k_A is its corresponding weight factor. However, now the noise Jacobians $\mathbf{J}_{A,states}$ and $\mathbf{J}_{A,controls}$ need to be included into the optimal control problem.

To solve the minimum fuel problem without the noise abatement part, k_A and k_t need to be set to zero. The same goes if minimum time problem with free end time needs to be solved, for this the k_{fuel} needs to set to zero. While, when adding the noise abatement part, the awakening weight k_A equals 0.1.

Chapter 4

Case Study

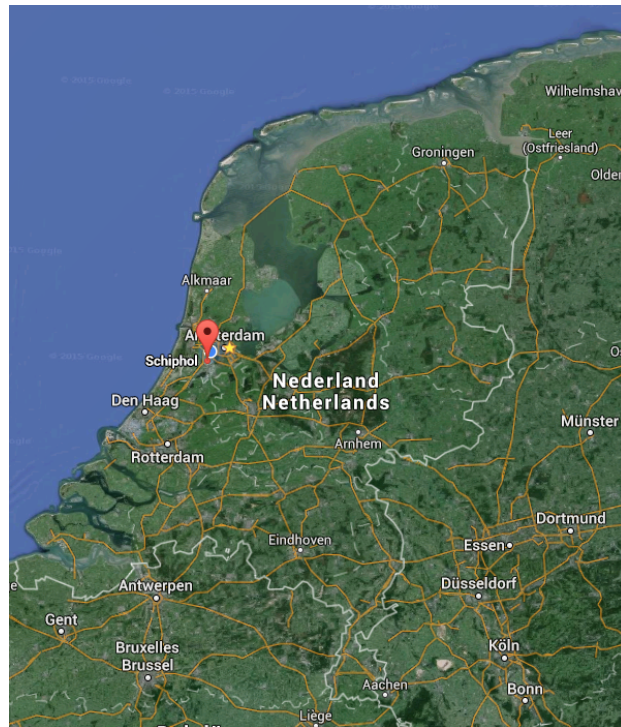
As the title suggests, this chapter provides a description of the case study performed regarding the HeNAP and the optimization of it. Recall the research objectives defined in Section 1.2:

- Develop a code for optimizing the HeNAP trajectories within GPOPS .
- Assess the influence of changing multiple variables on the environmental optimization of HeNAP's with respect to noise impact, fuel usage and time, such as:
 - The altitude
 - The helical radius
 - The number of spirals performed before landing

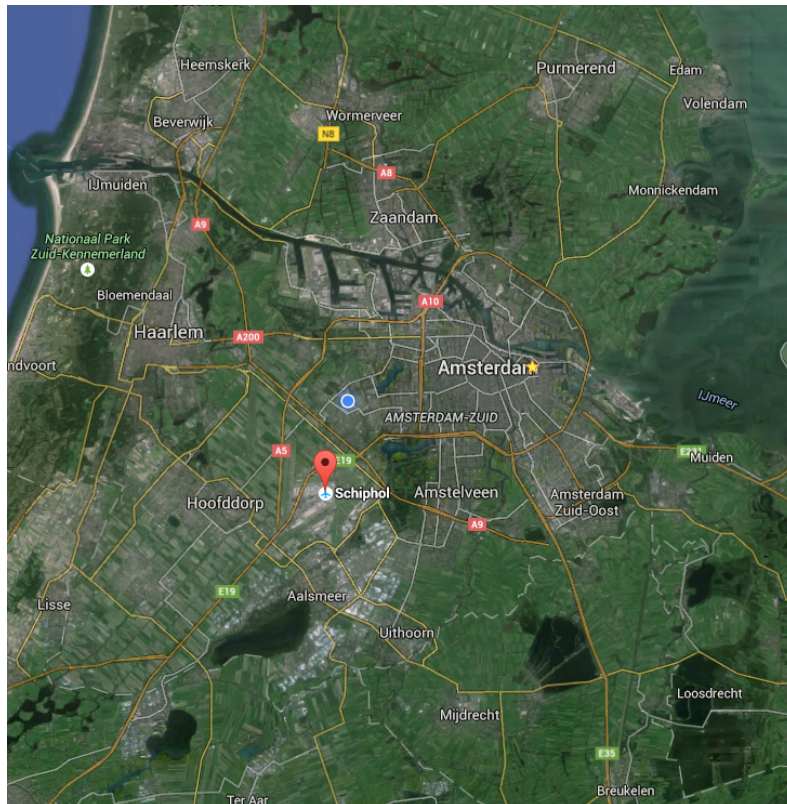
The case study environment used for this assessment is the AAS, which is illustrated in the following section. By adhering the regulations and guidelines of AAS, a realistic assessment of the HeNAP is achieved. Furthermore, the problem setup in GPOPS is briefly mentioned and describes the corresponding boundary conditions, cost functions and other settings that are necessary to simulate the HeNAP.

4.1 Amsterdam Airport Schiphol

AAS is a multi-modal transport hub, making it one of the busiest commercial traffic airports in the world. This is due to the vast number of passenger that transfers here for connecting flights. It is also located underneath one of the hectic skies in the world all due to the numerous traffic above Amsterdam, Frankfurt, London and Paris. This complicates the job of the *Air Traffic Management* (ATM) to avoid aircraft delays. AAS is also placed in the most populated area of the Netherlands namely the Randstad, which consists of the four largest cities of the country: Amsterdam, Rotterdam, The Hague and Utrecht.



(a) Location of AAS in The Netherlands.



(b) Location of AAS, 15 km south-west of Amsterdam.

Figure 4.1: Location of AAS in The Netherlands and Surrounding Cities.

From Figure 4.1¹, it is clear that AAS has to deal with a number of surrounding cities and towns. This is influential concerning the growth of both the cities and the airport. Moreover, as mentioned before in Section 1.1, noise is one of the limiting factors of growth for an airport, due to the regulations set by both the Dutch government and the European Union [34]. This makes the research on NAPs such as HeNAP lucrative.

4.1.1 Runways

Figure 4.2² reveals that AAS consists of six runways, where the usage of these runways depends on the weather condition, mostly wind related, and the peak hour waves. As mentioned before, AAS is one of the busiest airports in the world and knows eight peak hour waves throughout the day where up to 100 flights per hour are handled. This is also depended on wind conditions, mostly due to the fact that AAS is located near the North-Sea. This results in a variety of wind directions, which in turn dictate which of the runways are going to be used.

Between 06.00h and 23.00h, this is considered the daytime period, three of the six runways are used. This is often true for peak hours, while outside these hours just two of the six runways are used. Depending on the amount of traffic and weather conditions, the runways are either used just for arrivals/departures or a combination of the two, thus in either segregated or mixed mode.



Figure 4.2: AAS Runways

¹<https://www.google.com/maps/>

²<http://www.schiphol.nl/B2B/RouteDevelopment/AirportFacts2.htm>

Figure 4.3³ shows the usage of the runways during a period of a month. It is clear that the runways commonly used are the:

- Kaagbaan 24 for departures
- Polderbaan 18R for arrivals

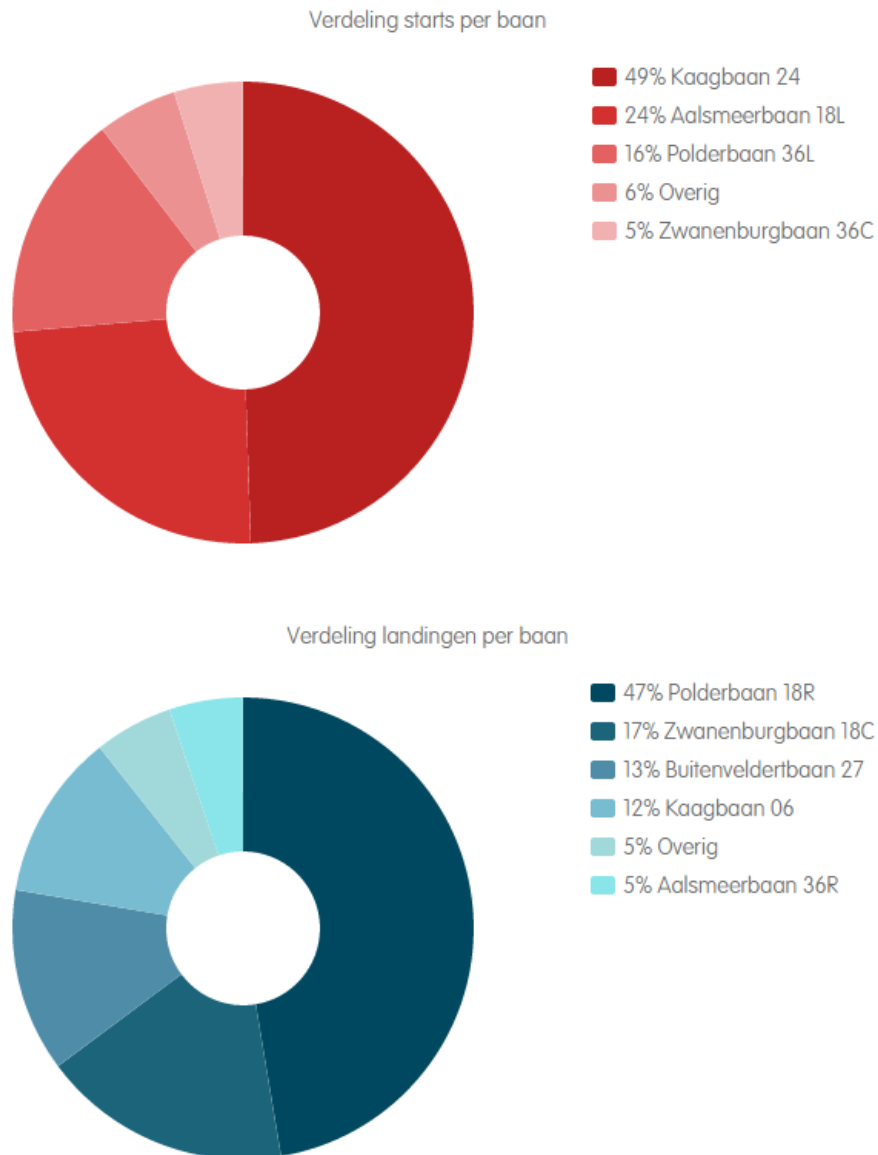


Figure 4.3: Runway Usage over a Period of One Month at AAS

Even though the Polderbaan (18R) and Zwannenburgbaan (18C) are the most commonly used runways by AAS, for this thesis work the HeNAP is going to be based at the Buitenveldertbaan (27). The reason for this is because the best approach for the HeNAP is from the east and the Buitenveldertbaan is ideally located in that direction.

³<http://noiselab.casper.aero/ams/>

4.2 Regulations and Guidelines

As in any working sector, the aviation has its own set of regulations and guidelines to safely regulate all type of flights. In order to produce a realistic and reliable optimization tool these guidelines and regulations are taken into account.

4.2.1 Airspace Domains

An airport differentiates between the airspace above it. This is because of both horizontal and vertical boundaries that are set by countries, laws and radar ranges. During an arrival of an aircraft, the aircraft encounters all of these separate airspaces and radar systems. By knowing which ones are involved a set of constraints can be deduced and used within the optimization tool. An arrival encounters the following airspaces [35]

1. **Upper Area Control (UAC):** This is the first part of the airspace that is encountered and is intended for traffic at and above FL 245 (24,500 ft std. Atmosphere). Eurocontrol in Maastricht in The Netherlands controls it. An UAC map of The Netherlands can be found in the Appendix.
2. **Area Control Centre (ACC):** This is the second part of the airspace that is encountered and is intended for traffic below FL 245 (24,500 ft) and above FL 095 (9,500 ft) around AAS. Within this airspace, air traffic services are provided for controlled flights in control areas under the jurisdiction of an airport. These flights are considered en-route traffic. The ACC controls the *Instrument Flight Rules* (IFR) air traffic in its *Flight Information Region* (FIR). The Amsterdam FIR map is also found in the Appendix.
3. **Terminal Control Area (TMA):** This is the final airspace encountered and is intended for traffic below FL 095 (9,500 ft). This airspace is intended for approaching and departing traffic that is traveling between the En-route phase and Control Zone (CTR's).

During this thesis work, the HeNAP is performed within both the ACC and TMA spaces.

4.2.2 Lateral Freedom

Each aircraft that enters the previously mentioned airspaces has to follow fixed route that is defined by beacons and waypoints. This allows the aircraft to be easily tracked and guided to correct runway by the parties involved in the airspace. However, due to the lack of lateral freedom the capacity of the runway is affected due to the delays created by this limitation. Nevertheless, during this thesis the HeNAP has all the lateral freedom, which allows the HeNAP path to be adjusted according to the best optimization.

4.2.3 Standard Terminal Arrival Routes

As mentioned in the previous section, an aircraft that enters the airspaces follows a predefined path by the means of waypoints and beacons, this is called a *Standard Terminal Arrival Route* (STAR). The locations of these waypoints and airspeed used are fixed. A map of these so-called STARs can be found in the Appendix. As can be seen from this map, there are three main STARs used to enter AAS, namely:

- ARTIP located North-East
- SUGOL located West
- RIVER located South-West

These STARs are used to enter the TMA airspace however, during this thesis none of these will be used as two of these are located in the wrong direction necessary to perform the HeNAP at Runway 27 and the one that is possible is less suitable than the waypoint ANDIK that will be used.

4.3 HeNAP Routes Setup

As mentioned at the end of the previous section, this study case uses the waypoint ANDIK as a starting point of the simulation. There are a number of simulations that will be carried out:

1. Case 1: is a CDA that will be used as a reference for the HeNAP trade-off
2. Cases 2 through 4: are HeNAPs with different flight levels, radiuses and number of spirals performed.

Figure 4.4 shows an example of the route used during the CDA and HeNAP, where the red line represents the CDA while the green line is the representation of the HeNAP.

These routes are plotted in the GPOPS framework as a single phase problem, where the following values are used as standards: L1, L2 and R respectively, Figure 4.4. These three values are used in order to plot the landing trajectory. Both the L2 and R are used as variables in the GPOPS framework, while L1 is the result of R and the initial starting coordinates.

Two altitude restrictions are in affect at the ANDIK waypoint, there is a maximum of FL 100 and a minimum FL 70, 10,000 ft and 7000 ft respectively. Both of these will be used during the cases to see the effect of altitude changes on the HeNAP optimization. The speed limit at and below FL 100 is equal to 250 kts, which is used within the optimization tool as the initial speed, while the landing speed used for all cases equals 140 kts.

Another restriction used, is one on the bank angle μ , which does not allow the aircraft to exceed the maximum of 25° . This results in the spirals being performed with a constant bank angle that is a result of the velocity, as is seen from Equation (3.27).

4.3.1 Case 1: CDA

This reference case starts at ANDIK with the minimum flight level of 7,000 ft and initial speed of 250 kts. From that point, the aircraft starts its continuous descent, where it is free to choose its speed and altitude. After flying a certain distance the aircraft makes a right turn where it is free to choose the radius of this turn in order to line up with the runway. From the standard approach map, located in the Appendix, it can be seen that the first ILS beacon is located at a distance of 6.2 nm from the runway, which is adhered during this case. From this point it is a straight line to the runway and when reached the final approach speed is kept at 140 kts. The trajectory described here can be seen in Figure 4.4. The following table gives the locations of the waypoints and beacons used as well as the starting point of Runway 27:

Table 4.1: Beacons, Waypoints and Runway 27 coordinates

Name	Coordinates		Restrictions
	WGS 84: lat lon [° ' "]	RD: x y [m]	
ANDIK	52°44'21.6" N 05°16'13.8" E	147,118 528,004	$h \geq \text{FL } 070$
EH639	52°19'26.0" N 04°57'50.0" E	126,140 481,856	$h = 2000 \text{ ft}$
RW 27	52°19'06.0" N 04°47'49.0" E	114,754 481,317	-

4.3.2 Case 2: HeNAP

This is the first simulation of the HeNAP and it uses the same procedure as the one in the first case except for the fact that a spiral is performed halfway the trajectory. The spiral is performed above the water and before the first beacon is reached. The radius of the spiral is a variable and is chosen by the optimization tool. The trajectory of this approach can be seen in Figure 4.4 and it tries to avoid inhabited areas as much as possible.

4.3.3 Case 3 & Case 4: HeNAP

Case 3 knows the same procedure as case 2, however now instead of using FL 70 FL 100 is used. This way the effects of different altitudes on the environmental optimization's can be measured. Subsequently, case 4 continues where case 3 ends and instead of performing one spiral two are performed with a constant radius. In both cases the radius used comes forth from the optimization tool because of the fact that it is a variable, meaning that for case 3 a different radius can be used than the one for case 4. Furthermore, the same goal of case 3 where the effects on the environmental optimization are measured is true for case 4.

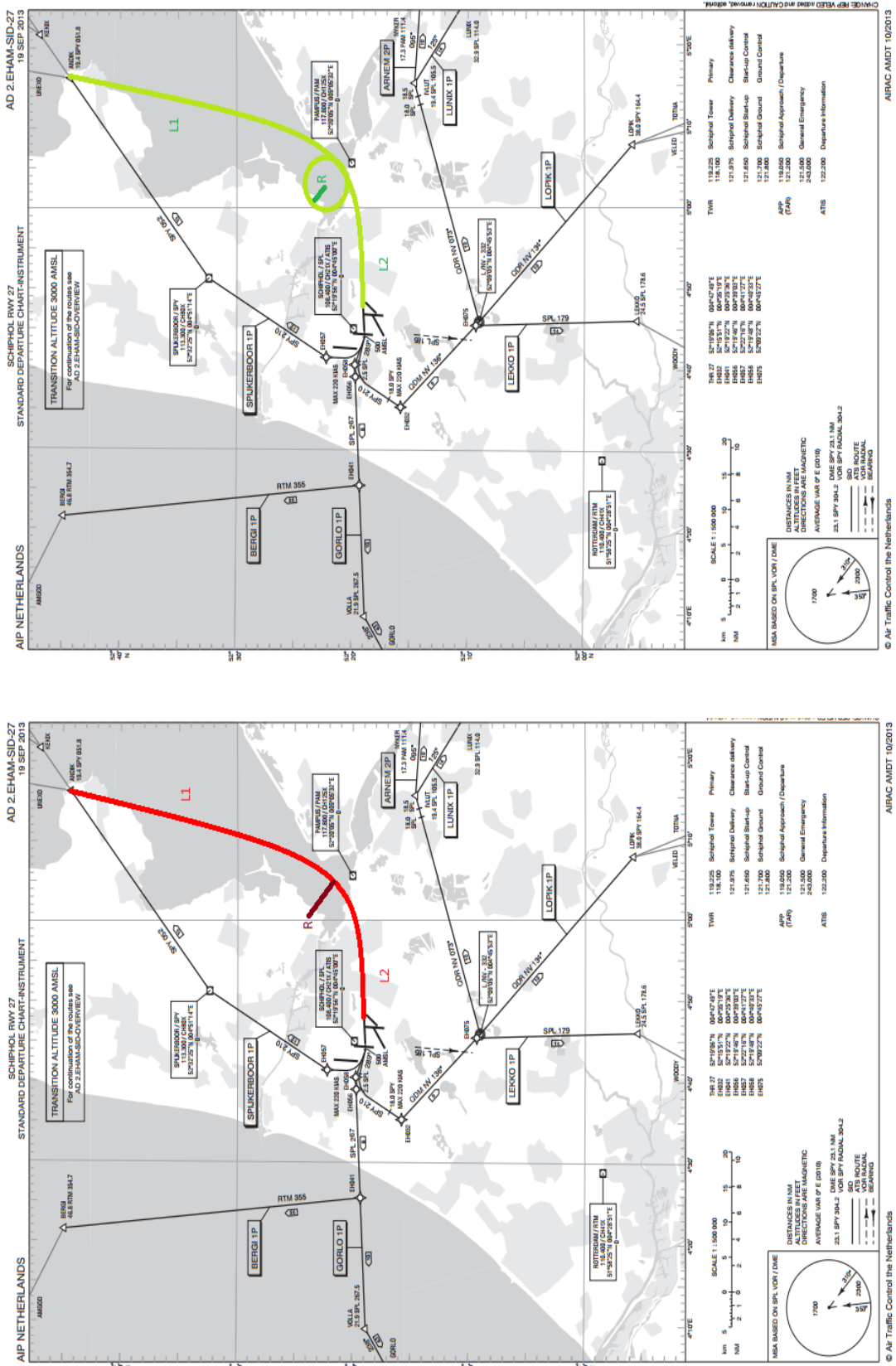


Figure 4.4: CDA (left) in red, HeNAP (right) in green

4.4 Case Study Strategy

Having defined the routes that will be used for this case study, it is important to define how the optimization tool is going to be used. This is done in order to reach the previously mentioned goals. By taking the following steps it is hoped to reach these goals:

1. First, simulations are run with the CDA route to get a feel for the numbers of awakenings, fuel consumed and time. These are necessary for the assessment of the HeNAP. This is done by solving the *minimum time optimization problem*, *minimum fuel optimization problem*, *minimum time and noise optimization problem* and finally *minimum fuel and noise optimization problem*.
2. Having run the simulations for case one and obtained the necessary numbers, the same is repeated to the remaining cases.
 - (a) During case 2 the first HeNAP simulation is run with an altitude of 7,000 ft and one spiral.
 - (b) Case 3 the altitude is changed to 10,000 ft.
 - (c) Case 4 the altitude of case 3 is still in effect and another spiral is added to the trajectory.
3. Finally, the results of all the solutions obtained from the optimization tool are compared and a conclusion is drawn.

Chapter 5

Results

The results obtained from the case study are analyzed and depicted in this chapter. As mentioned in the previous chapter, there are four cases, Case 1 through 4, that are solved for four set of optimal control problems, minimum time problems, minimum fuel problem, minimum awakenings and time problem and finally minimum awakening and fuel problem. The trajectory of the case study starts at the ANDIK waypoint and ends at the Buitenveldertbaan, aka Runway 27. This path is optimized within the optimization tool numerous times; this was a trial and error process that kept going until an optimal solution was found.

5.1 Minimum Time Problem Solutions

The optimization of this problem is done without noise abatement in order to get a reference on the fuel consumed, the path chosen, the time and the number of awakenings. The results are shown in the following table:

Table 5.1: Minimum Time Problem Solutions

Minimum Time Problem Optimization						
	Awakenings	Time [s]	Fuel Used [kg]	R [m]	L1 [m]	L2 [m]
Case 1	2168	478	160	3772	47146	11482
Case 2	5941	539	190	1230	55843	0
Case 3	5584	532	140	1228	55844	0
Case 4	5021	642	210	1317	55773	0

As can be seen from Table 5.1, the results of each case are given with respect to the number of awakenings, the time, the fuel used, the radius, the distance to the start of the radius or

L1 for short and L2 which is the distance from the exit of the radius till the runway. The radius and L2 are both variables within the optimization tool, and allow the tool to use any value to find the optimal solution. The radius, L1 and L2 are necessary for the definition of the trajectory flown. From Section 4.4 it can be seen what the conditions for each case are.

So, from Table 5.1 it can be seen that case 1 has the least travel time and the least number of awakenings. This was to be expected as flying a spiral adds in the duration of the flight time. However, it was not expected that the number of awakenings of the other cases would be so high. The only explanation for this the fact is that all the cases do not make use of the noise abatement and thus the effects of the HeNAP are not clear yet. In addition, another reason is the fact that all the HeNAP cases perform the spirals above and around the airport, which is highly populated, hence the zeros in L2 column in Table 5.1. All of the paths flown during the cases can be found in Figure 5.1.

From Figure 5.2, the altitude and velocity changes can be observed for each case. The remarkable thing is that for all the cases except case 1 the velocity is reduces before starting the spiral descent. The reason behind this is by reducing the velocity, the spiral radius, R , can be kept small. Which, in turn allows the area affected by the flyover to be kept small as well.

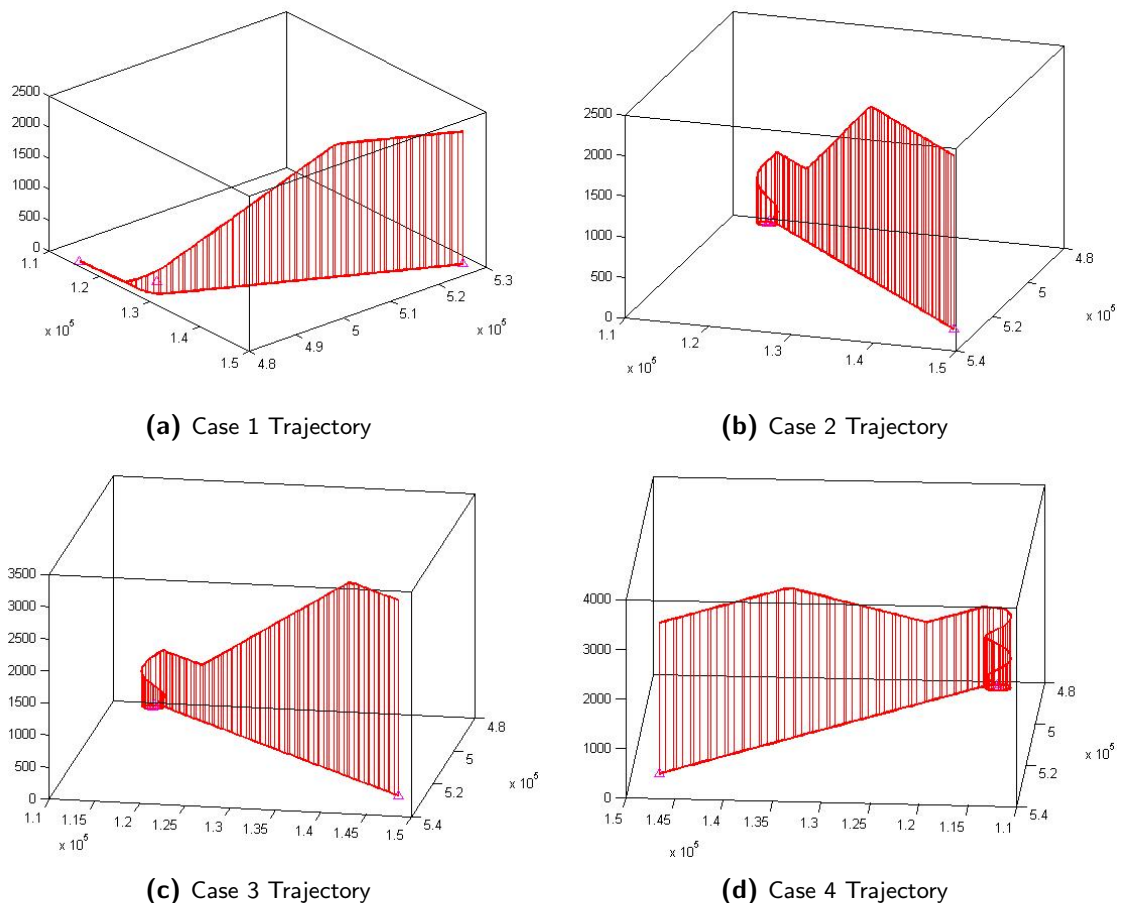
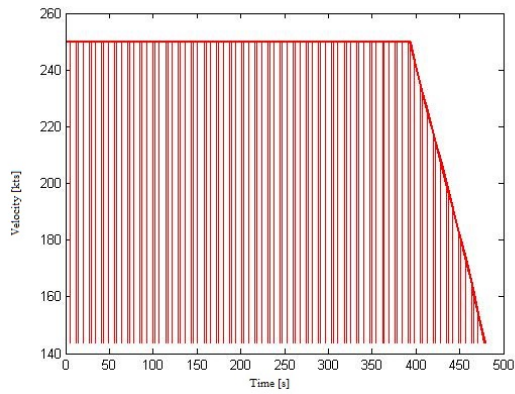
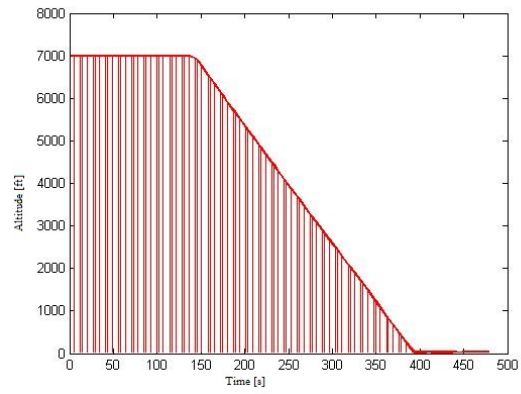


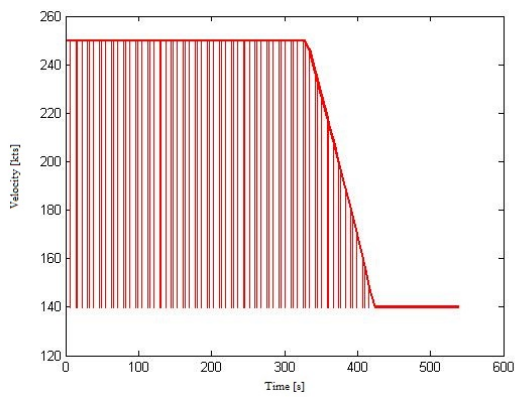
Figure 5.1: Trajectories of all the Minimum Time Problem Results Cases



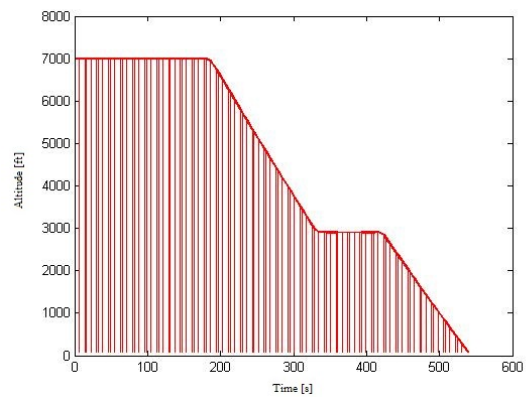
(a) Case 1 Speed



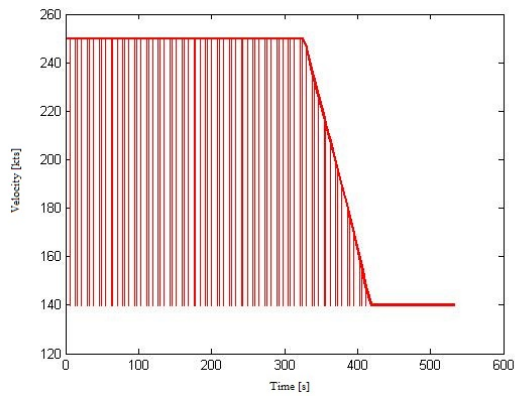
(b) Case 1 Height



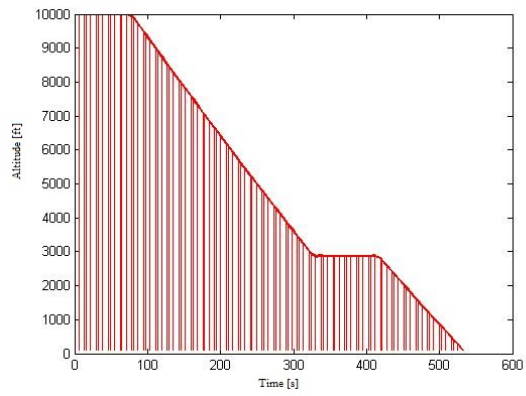
(c) Case 2 Speed



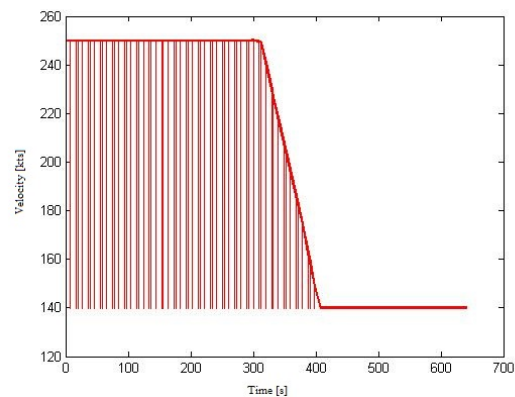
(d) Case 2 Height



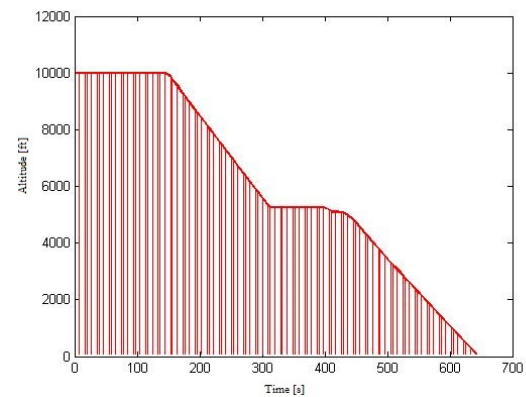
(e) Case 3 Speed



(f) Case 3 Height



(g) Case 4 Speed



(h) Case 4 Height

Figure 5.2: Velocities and Altitudes of all the Minimum Time Problem Results Cases

5.2 Minimum Fuel Problem Solutions

The optimization of this problem is also done without noise abatement for the same reason as in the previous section. The results are shown in the following table:

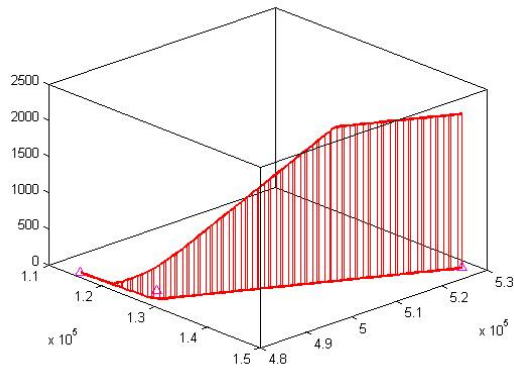
Table 5.2: Minimum Fuel Problem Solutions

Minimum Fuel Problem Optimization						
	Awakenings	Time [s]	Fuel Used [kg]	R [m]	L1 [m]	L2 [m]
Case 1	2302	501	160	3103	47779	11482
Case 2	5951	550	190	1255	55846	0
Case 3	5534	551	140	1239	55835	0
Case 4	4073	650	200	1344	55751	0

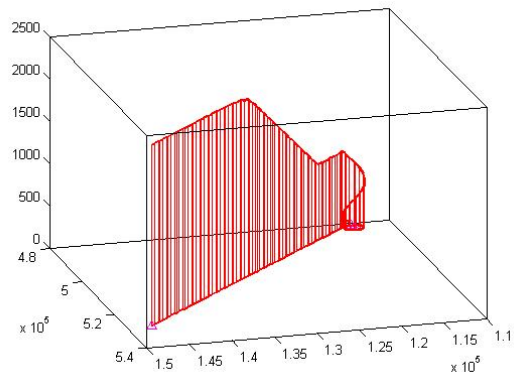
When comparing Table 5.1 and Table 5.2, it can be seen that there is not that big of difference in the numbers. The minimum fuel problem takes longer to land; this is because the distance traveled during these trajectories are longer than the ones traveled during the minimum time optimization problem. This is apparent from the R, L1 and L2 columns. Once more, cases 2 - 4 find the HeNAP performed directly above the airport and the spiral exit is directly at the beginning of the runway.

Another difference can be found when comparing Figure 5.4 with Figure 5.2. For all the cases, the velocity decreases from the initial 250 kts to 230 kts. The most likely reason behind this is to reduce the fuel consumption. However, due to the longer trajectories this effect is redundant, as can be seen from the fuel consumed, which has not changed except for case 4.

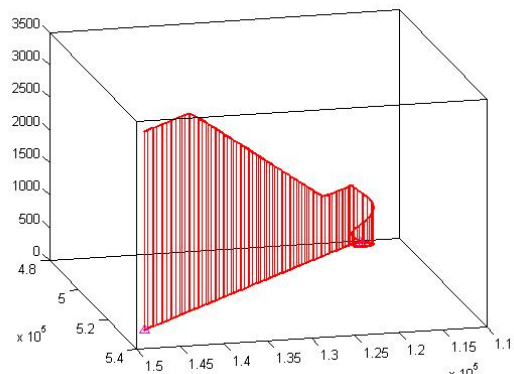
In turn, all of these differences result in a higher number of awakenings. The only exception to this rule is case 4, where the number of awakenings is significantly lower than the one at the minimum time optimization problem. The likely reason for this is apparent when comparing Figure 5.4h with Figure 5.2h. This shows that the section where the aircraft is at a constant altitude is higher than the one of the minimum time optimization problem. This, in combination with the lower velocity, results in lower noise production and thus fewer awakenings.



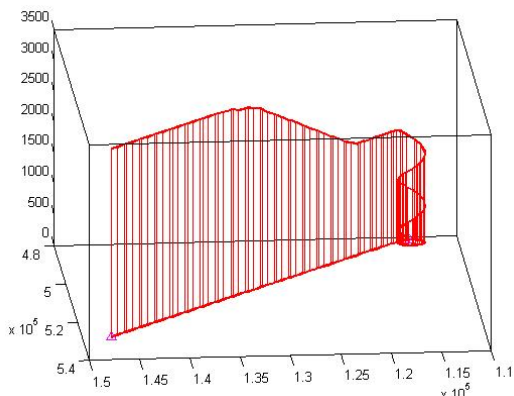
(a) Case 1 Trajectory



(b) Case 2 Trajectory

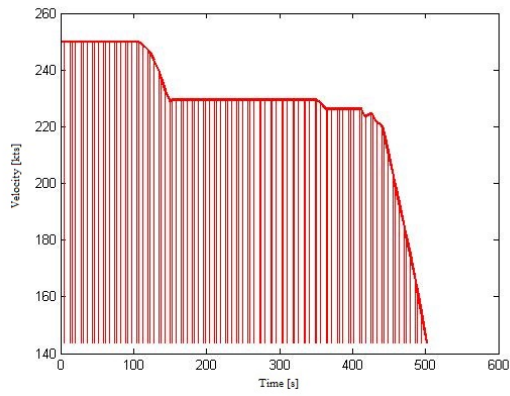


(c) Case 3 Trajectory

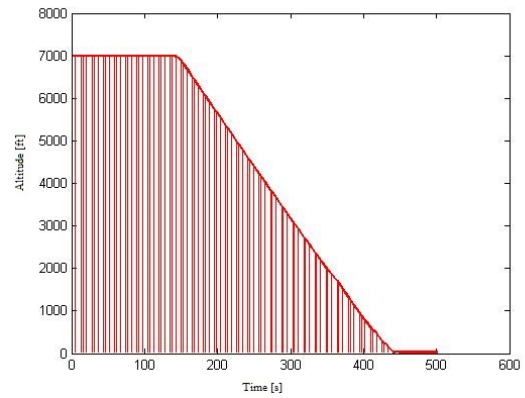


(d) Case 4 Trajectory

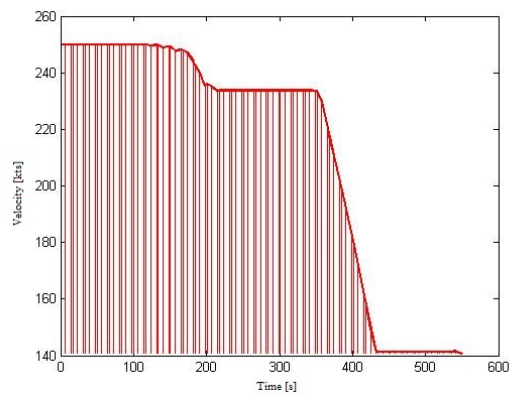
Figure 5.3: Trajectories of all the Minimum Fuel Problem Results Cases



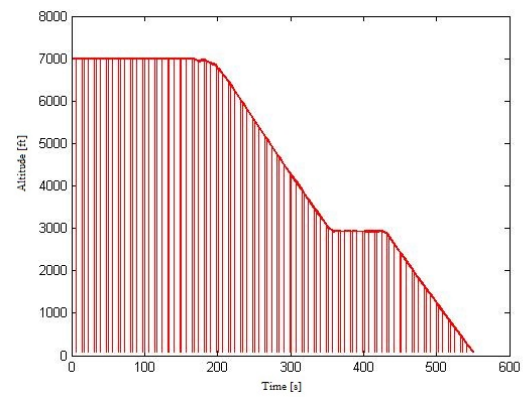
(a) Case 1 Speed



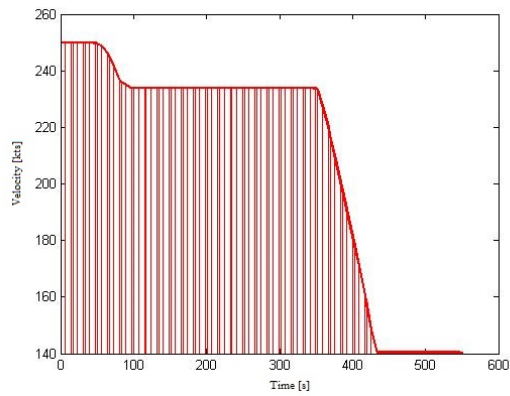
(b) Case 1 Height



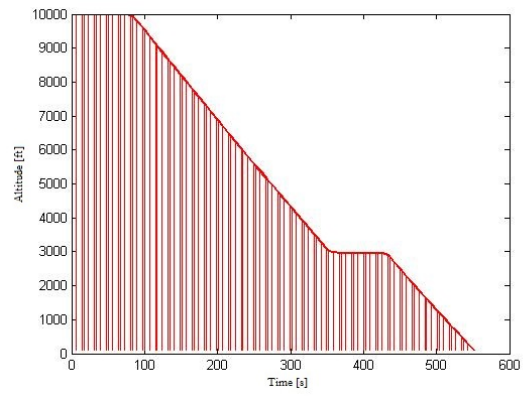
(c) Case 2 Speed



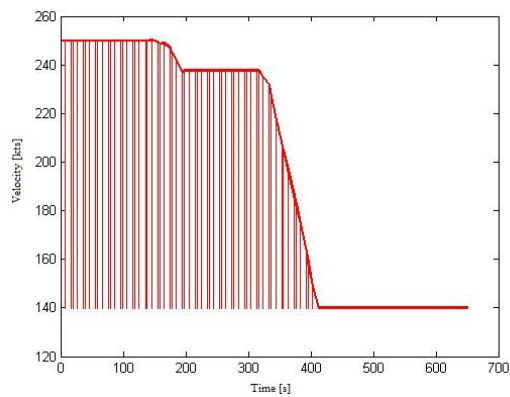
(d) Case 2 Height



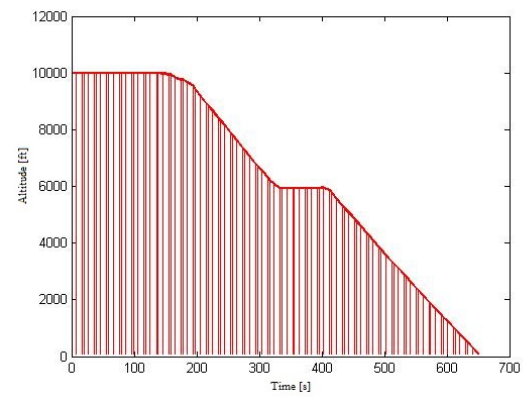
(e) Case 3 Speed



(f) Case 3 Height



(g) Case 4 Speed



(h) Case 4 Height

Figure 5.4: Velocities and Altitudes of all the Minimum Fuel Problem Results Cases

5.3 Minimum Time & Noise Problem Solutions

This section shows the results achieved during the optimization of the minimum time problem while including the noise abatement. Now it is expected that the numbers of the awakenings is lower than the ones of the minimum time problem without the noise abatement. Table 5.3 shows these results.

Table 5.3: Minimum Time & Noise Problem Solutions

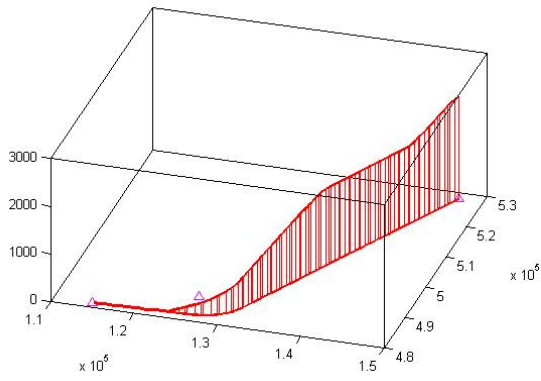
	Minimum Time Noise Abatement Problem Optimization					
	Awakenings	Time [s]	Fuel Used [kg]	R [m]	L1 [m]	L2 [m]
Case 1	1752	485	170	5768	45205	11482
Case 2	2115	695	300	3140	44630	18802
Case 3	1894	690	240	3304	44493	18723
Case 4	2311	839	330	2500	45223	18933

A quick comparison of Table 5.1 and Table 5.3 reveals that there is a significant change in numbers, which was expected. For all the cases the number of awakenings dropped drastically, some of the cases by almost two thirds. However, the fuel consumed and the time needed to perform the procedures has increased. Furthermore, it can be seen that the trajectories traveled are not the same anymore. This is an effect of the noise abatement procedure in order to avoid inhabited areas as much as possible. These paths can be seen in Figure 5.5. This figure also shows the noise patterns along the flown paths of all the cases in dBAs'.

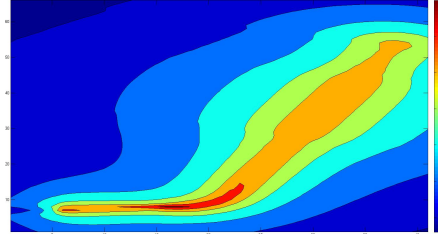
When taking a closer look at Figure 5.5, it is clear to see that there is not a big difference between case 1 and 2 noise wise except for the spiral. However, cases 3 and 4 seem to produce less noise in the beginning of the trajectory, during L1. The reason for this is due to the initial altitude. Nevertheless, case 4 still experiences a higher noise during the spiral procedure, this due to the number of spirals performed. While, during spiral of case 3 less noise is produced until the end of the spiral movement where the aircraft needs to use the throttle one more to stabilize for the straight part of the landing.

When making a case-by-case comparison of the simple time optimization problem and the time noise abatement optimization problem, it can be seen that there are significant differences between them. These differences can be seen when comparing Figure 5.2 and Figure 5.6.

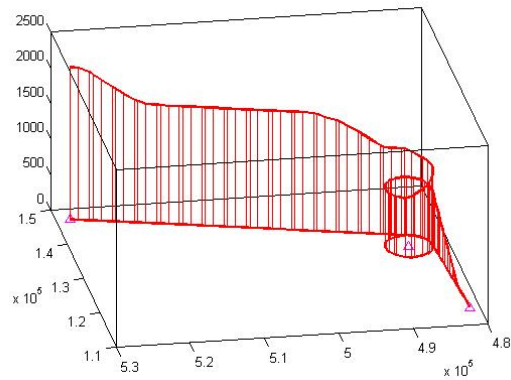
During case 1 nothing changes when considering the velocity, however there is an altitude change. This results in a decrease in number of awakenings as can be seen from the Table 5.3. In case 2 there are changes in both the velocity and altitude. The velocity drops to 220 kts instead of 140 kts at an earlier stage, and the descent of the minimum time optimal problem is smoother than the minimum time noise abatement optimization problem. Furthermore, the spiral is performed further in an open area, which results in a lower number of awakenings. The same is applicable to cases 3 and 4. Except during case 4 the velocity is changed to 200 kts instead of 220 kts and the altitude changes are steeper. All in all the results are clear in the number of awakenings, which have decreased drastically due to these changes.



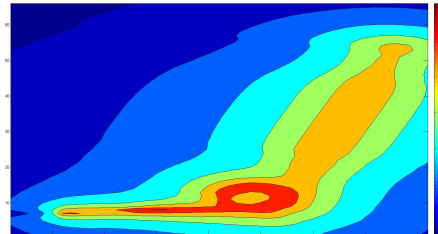
(a) Case 1 Trajectory



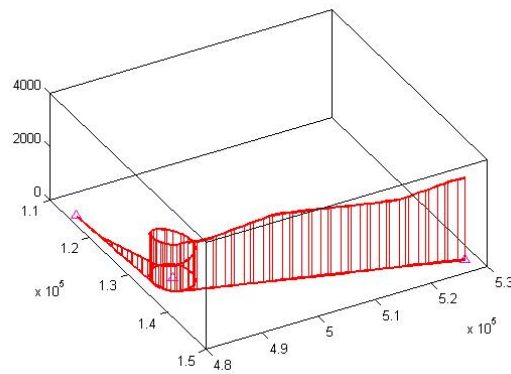
(b) Case 1 Noise Pattern



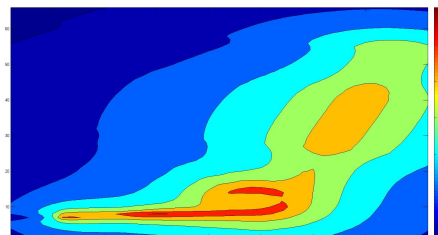
(c) Case 2 Trajectory



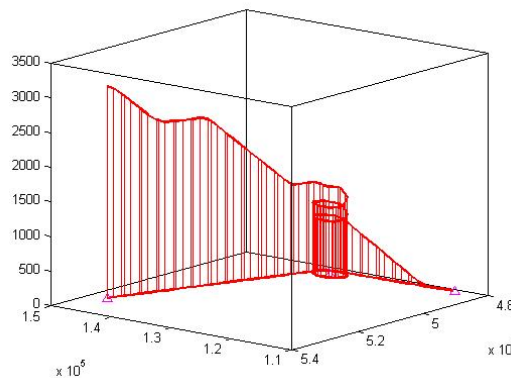
(d) Case 2 Noise Pattern



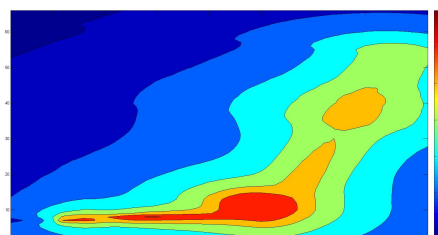
(e) Case 3 Trajectory



(f) Case 3 Noise Pattern

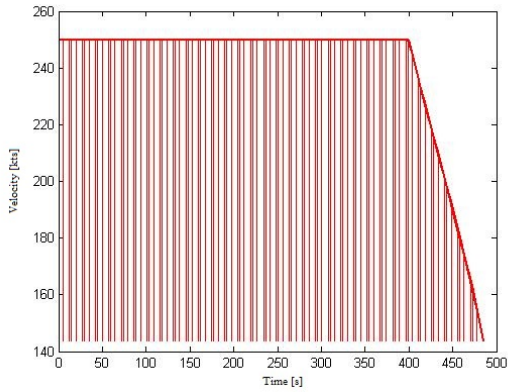


(g) Case 4 Trajectory

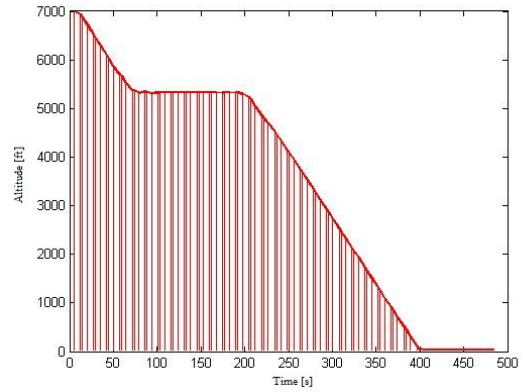


(h) Case 4 Noise Pattern

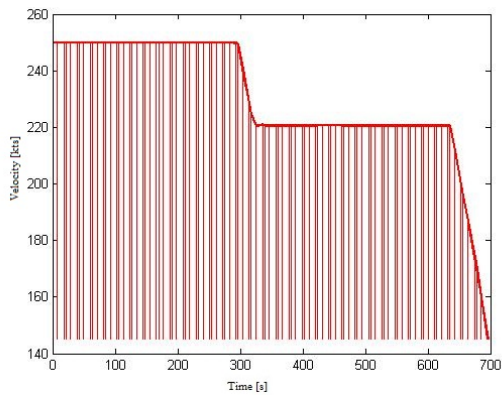
Figure 5.5: Trajectories and Sound Patterns of all the Minimum Time & Noise Problem Results Cases



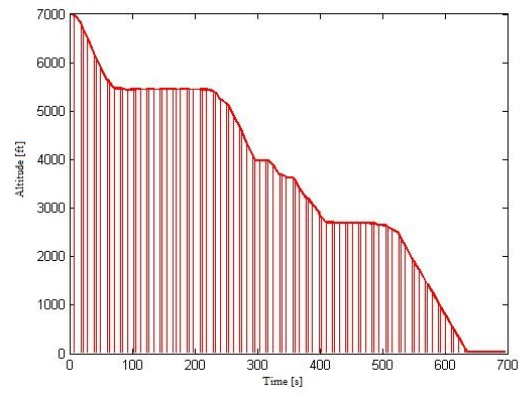
(a) Case 1 Speed



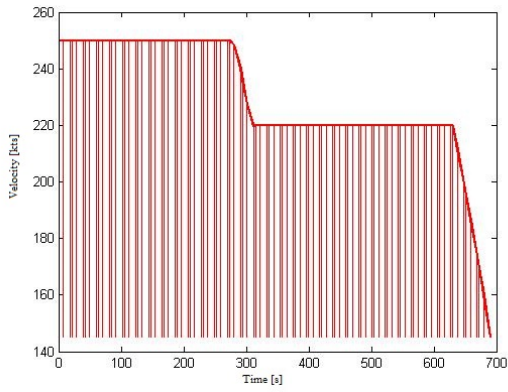
(b) Case 1 Height



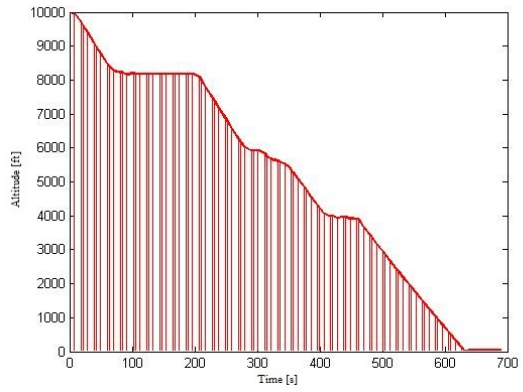
(c) Case 2 Speed



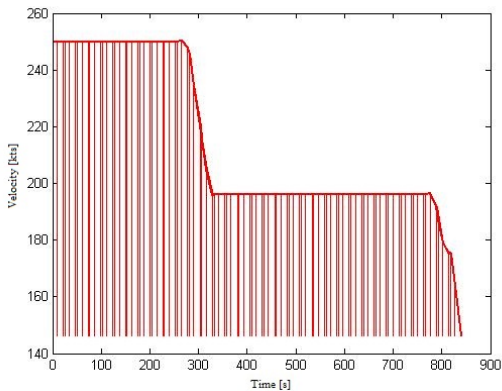
(d) Case 2 Height



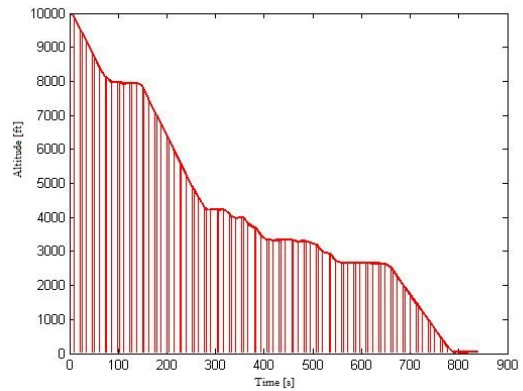
(e) Case 3 Speed



(f) Case 3 Height



(g) Case 4 Speed



(h) Case 4 Height

Figure 5.6: Velocities and Altitudes of all the Minimum Time & Noise Problem Results Cases

5.4 Minimum Fuel & Noise Problem Solutions

This section shows the results achieved during the optimization of the minimum fuel problem while including the noise abatement. The same expectations as in the previous section are still in effect. Table 5.4 shows these results.

Table 5.4: Minimum Fuel & Noise Problem Solutions

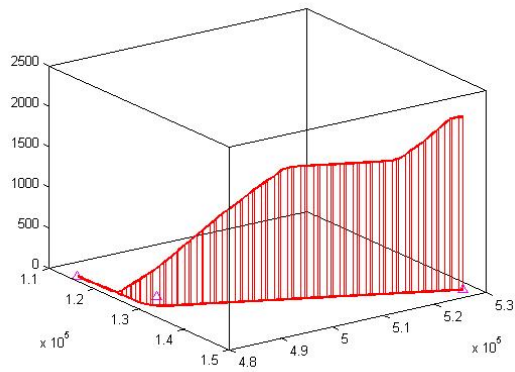
Minimum Fuel & Noise Problem Optimization						
	Awakenings	Time [s]	Fuel Used [kg]	R [m]	L1 [m]	L2 [m]
Case 1	1763	492	170	3709	46604	12727
Case 2	2130	702	290	2869	44901	18801
Case 3	1894	700	230	3400	44365	18807
Case 4	2178	861	320	2800	44900	19000

When comparing Table 5.2 and Table 5.4 it can be seen that the same effects that took place in the previous section are here as well. The number of awakenings dropped drastically, and once again in some of the cases by almost two thirds. Furthermore, the fuel usage and time increased due to the larger distance traveled during this problem, which can be seen from the values of R, L1 and L2. The trajectories and the noise patterns of this optimization problem can be seen in Figure 5.7.

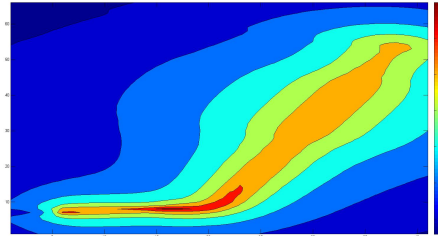
Again, from Figure 5.7 it can be seen that there is not a big difference between case 1 and 2 noise wise except for the spiral. The same thing goes for cases 3 and 4 where less noise is produced at L1. However, now that the minimum fuel problem is in effect it seems that during all of the spirals the engines are in idle resulting in less fuel usage and less noise production.

Making another case-by-case comparison, this time of the simple fuel optimization problem and the fuel noise abatement optimization problem, it can be seen that there are significant differences between the two problems. These differences can be seen when comparing Figure 5.4 and Figure 5.8.

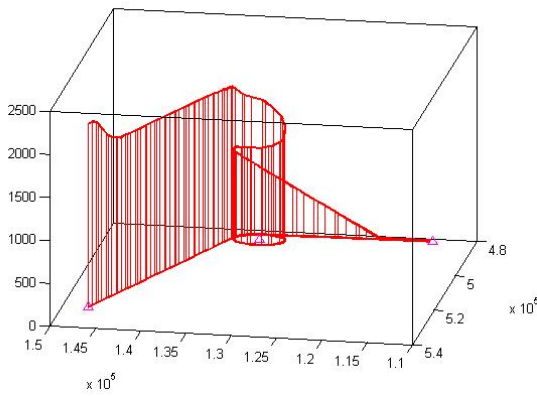
Case 1 knows a constant velocity during the noise abatement problem, and the same altitude changes found in the previous section are found here as well. In case 2 there are changes in both the velocity and altitude. The velocity drops to 210 kts instead of 140 kts halfway the trajectory, and the descent of the noise abatement optimal problem is almost continuous after the velocity drop. Furthermore, the spiral is performed again above an open area, which results in a lower number of awakenings. The same is applicable to cases 3 and 4. Except during case 3 the velocity is changed to 220 kts instead of 210 kts and case 4 it changes to 200 kts. All in all the results are clear in the number of awakenings, which have decreased drastically due to these changes.



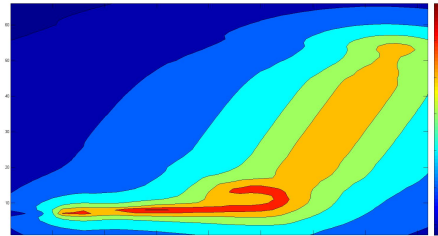
(a) Case 1 Trajectory



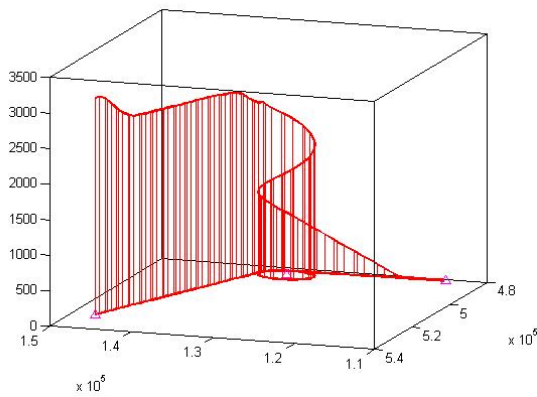
(b) Case 1 Noise Pattern



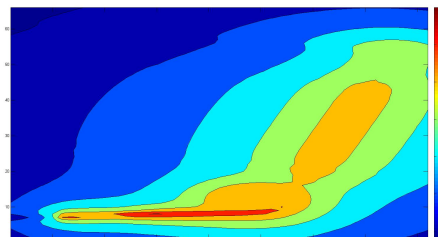
(c) Case 2 Trajectory



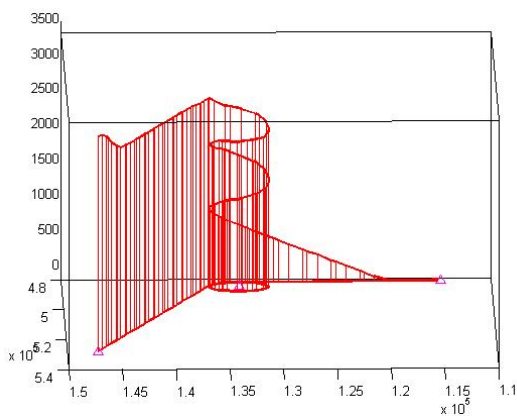
(d) Case 2 Noise Pattern



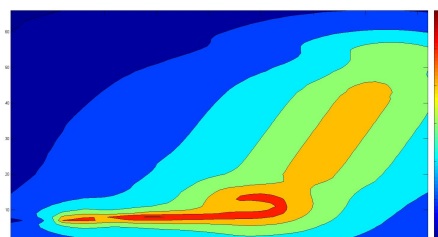
(e) Case 3 Trajectory



(f) Case 3 Noise Pattern

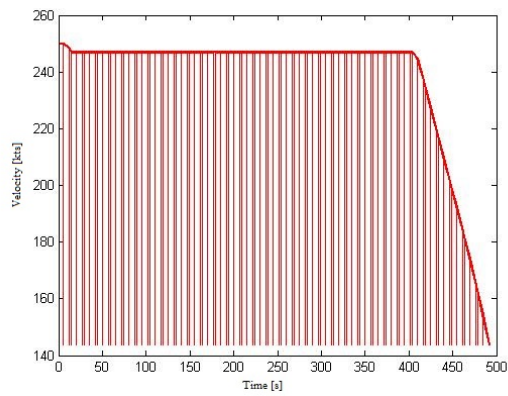


(g) Case 4 Trajectory

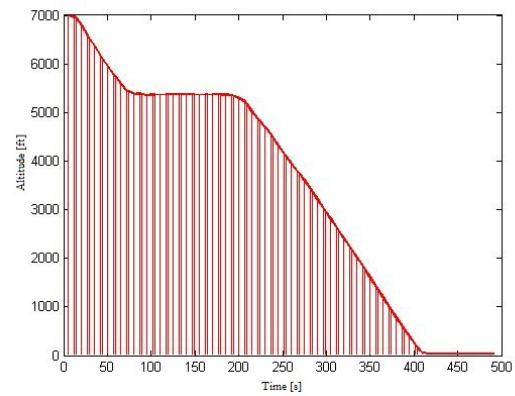


(h) Case 4 Noise Pattern

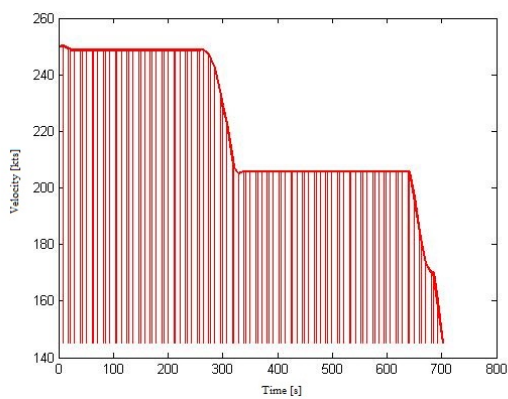
Figure 5.7: Trajectories and Sound Patterns of all the Minimum Fuel & Noise Problem Results Cases



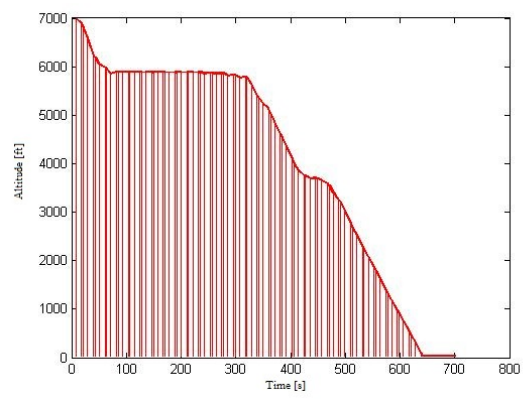
(a) Case 1 Speed



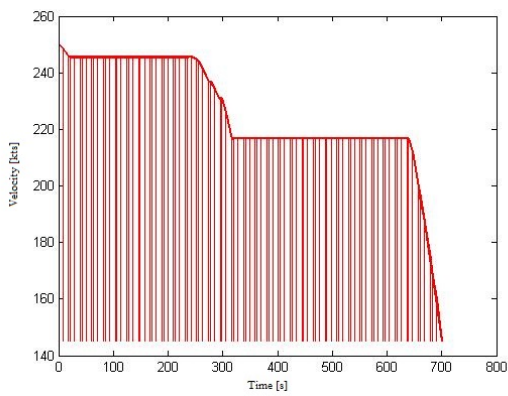
(b) Case 1 Height



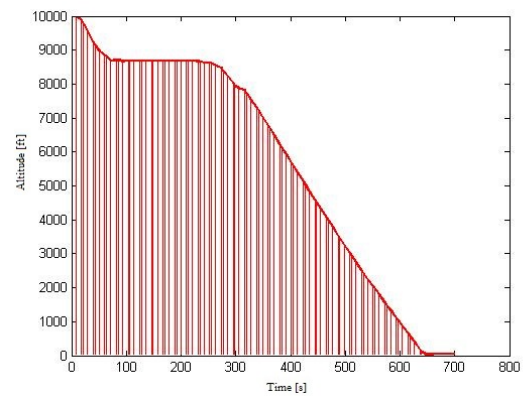
(c) Case 2 Speed



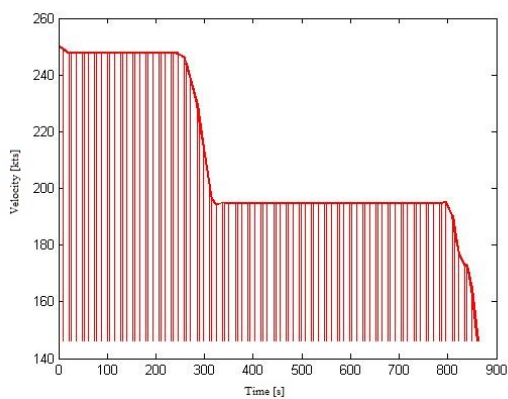
(d) Case 2 Height



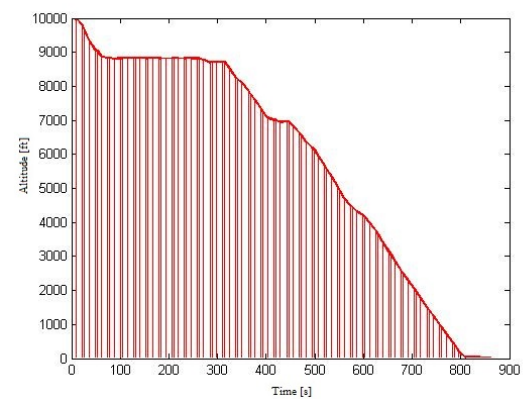
(e) Case 3 Speed



(f) Case 3 Height



(g) Case 4 Speed



(h) Case 4 Height

Figure 5.8: Velocities and Altitudes of all the Minimum Fuel & Noise Problem Results Cases

5.5 Trade-Off

By comparing Table 5.1, Table 5.2, Table 5.3 and Table 5.4, it is clear that within all the cases case 1 remains unsurpassed. The CDA is flown in this case and it shows the least amount of awakenings, time and fuel used. As a result, the HeNAP is less noise efficient than the CDA. The only HeNAP case that showed potential during the noise abatement optimization problems was case 3 where the initial altitude was 10,000 ft and had one spiral. The number of awakenings was comparable to case 1, while the fuel used and time are higher than case 1, which is an expected side effect of the HeNAP. The results of this comparison are disappointing with regards to the potential of the HeNAP.

In order to get an idea on the possible potential of the HeNAP, it has to be performed at an airport that is surrounded by inhabitants but with a small distance between the direct airport and the threshold of the cities. In the Netherlands, no such airports exist. However, should this be tried at these following airports it could reveal great potential, Figure 5.9. As can be seen, the area where the HeNAP might be performed is less inhabited for both airports. Thus making them ideal for the HeNAP.

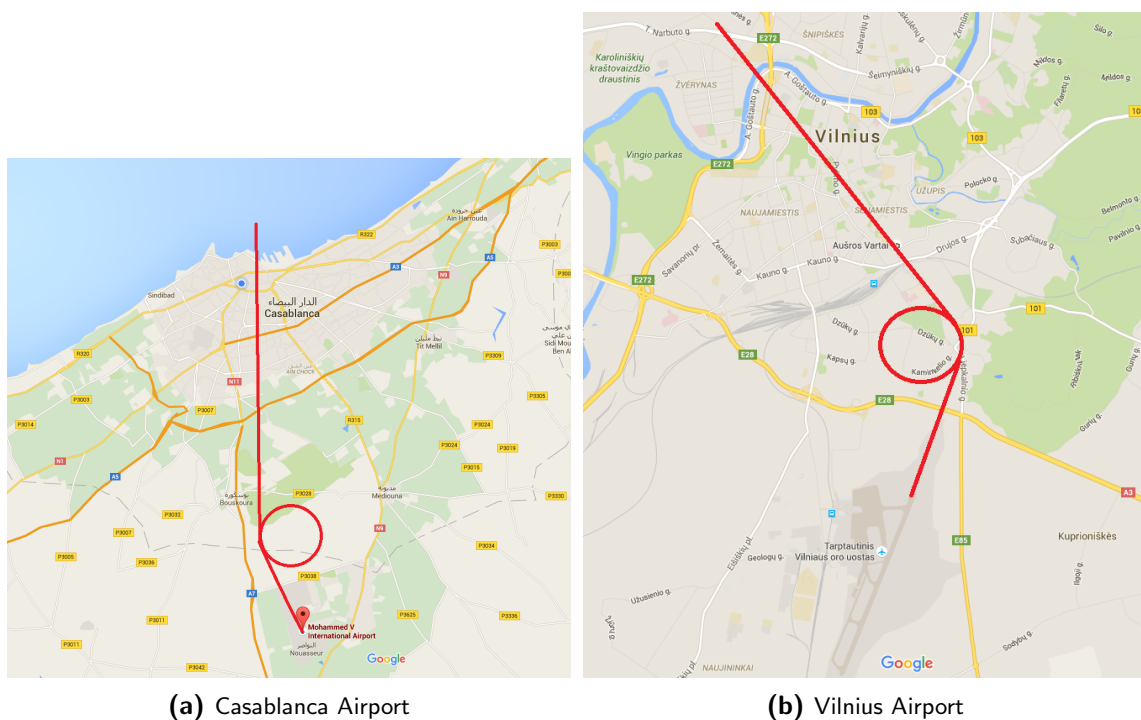


Figure 5.9: Possible Airports For HeNAP Procedure

In a last effort to show the potential of the HeNAP, an artificial population distribution around AAS is created. Within the following situation, the population underneath and around the approach path has been moved and redistributed around the initial part of the ground track, namely around L1. This is done in order to create the most suitable scenario for the HeNAP procedure. The minimum time noise abatement optimization problem and the minimum fuel noise abatement optimization problem are once more solved for all the cases. The following section will reveal the results of this new scenario.

5.5.1 Adjusted Population

As mentioned before, during this section the results of the new scenario are revealed, where the inhabitants underneath and around the glideslope are relocated underneath the initial part of the ground track.

Minimum Time & Noise Optimization Problem V 2.0

The results of the time noise abatement optimization problem for the new scenario are given in the following table including the previous results in order to allow a thorough comparison.

Table 5.5: Minimum Time & Noise Problem Solutions V2.0

Minimum Time & Noise Problem Optimization V2.0						
	Awakenings	Time [s]	Fuel Used [kg]	R [m]	L1 [m]	L2 [m]
Case 1	1752	485	170	5768	45205	11482
Case 2	2115	695	300	3140	44630	18802
Case 3	1894	690	240	3304	44493	18723
Case 4	2311	839	330	2500	45223	18933
Case 1*	1172	492	180	3230	47660	11482
Case 2*	1770	661	290	1665	48388	13050
Case 3*	928	654	220	1730	48323	13060
Case 4*	1316	831	350	2950	46006	15730

As can be seen from Table 5.5 the results are astonishing. By redistributing the population, the number of awakenings has decreased for all the cases. However, what is more astonishing is the fact that the HeNAP advantages have been proven. As can be seen, for the first time during this thesis work the number of awakenings for case 3 is lower than the one for case 1. Yet, this not true for cases 2 and 4, thus making a HeNAP procedure with an altitude of 10,000 ft and one spiral the optimal procedure to reduce noise and the number of awakenings around an airport. Nevertheless, this is only possible for airports such as the ones mentioned before in Section 5.5 and not the ones in the Netherlands.

Back to the results of Table 5.5, the number of awakenings and the time have both decreased significantly during the new scenario where the population is redistributed. This is partially true for the fuel consumption, though the increases in this criterion are not that large. As mentioned before, case 3 knows the largest reduction in number of awakenings followed by case 1, and thus proving the effectiveness of the HeNAP.

Figure 5.10 and Figure 5.11 both show the trajectory flown, the noise levels, velocity and altitude changes throughout the optimization.

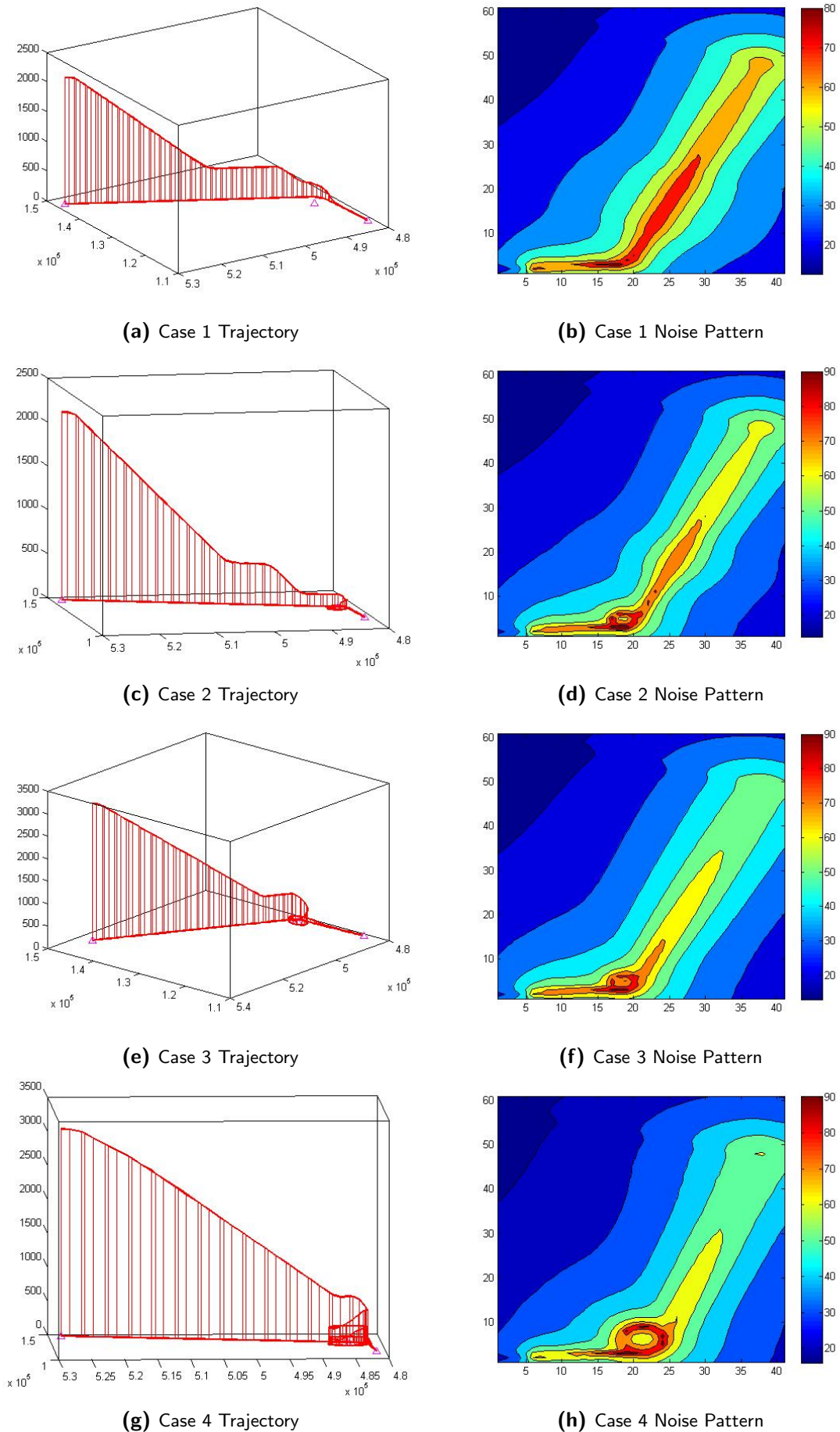
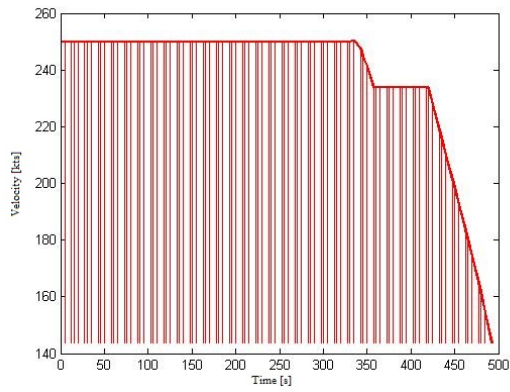
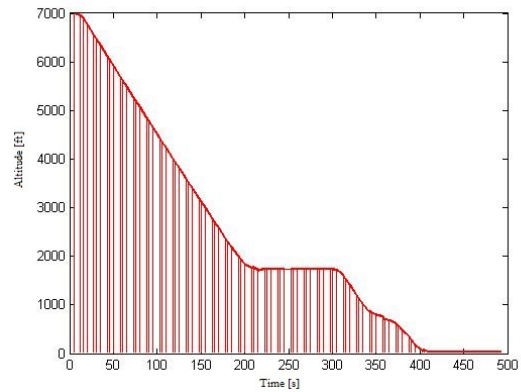


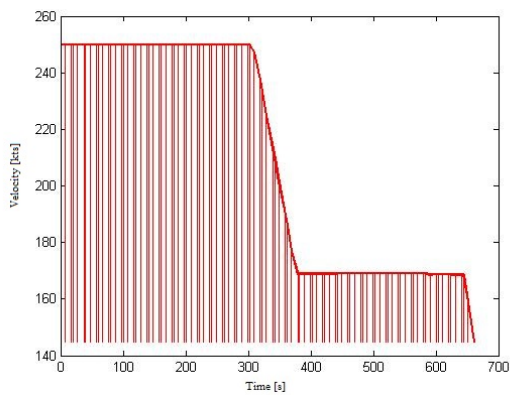
Figure 5.10: Trajectories and Sound Patterns of all the Minimum Time & Noise Problem Results Cases for the New Scenario



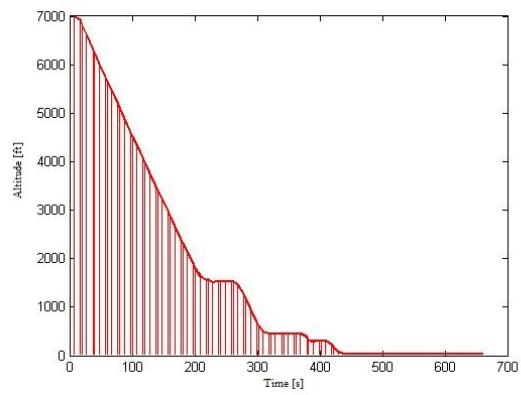
(a) Case 1 Speed



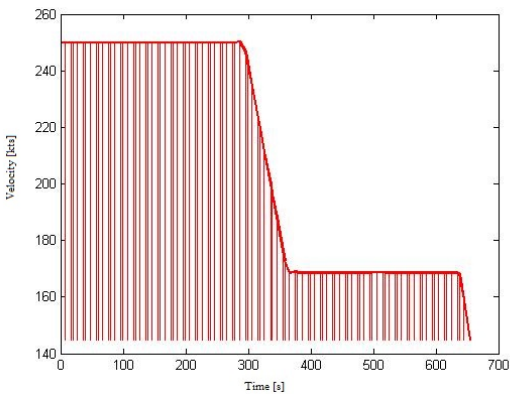
(b) Case 1 Height



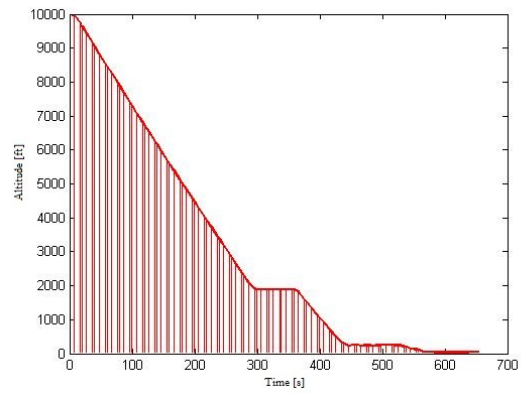
(c) Case 2 Speed



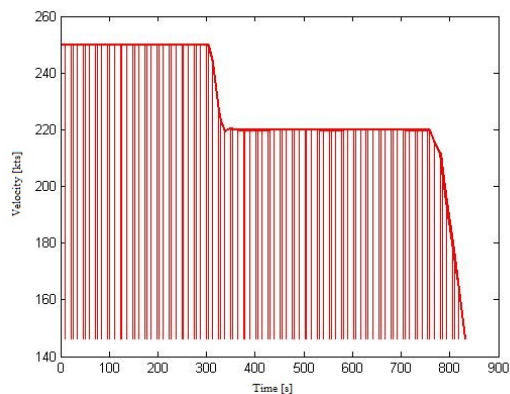
(d) Case 2 Height



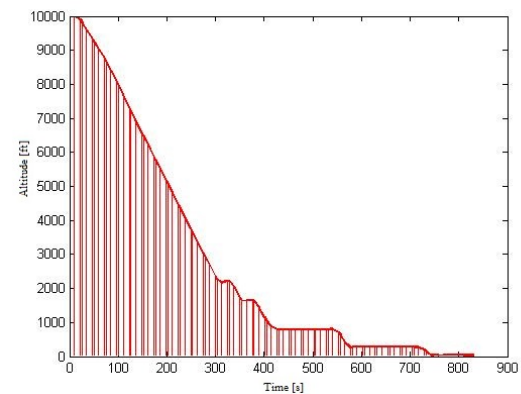
(e) Case 3 Speed



(f) Case 3 Height



(g) Case 4 Speed



(h) Case 4 Height

Figure 5.11: Velocities and Altitudes of all the Minimum Time & Noise Problem Results Cases for the New Scenario

Minimum Fuel & Noise Optimization Problem V 2.0

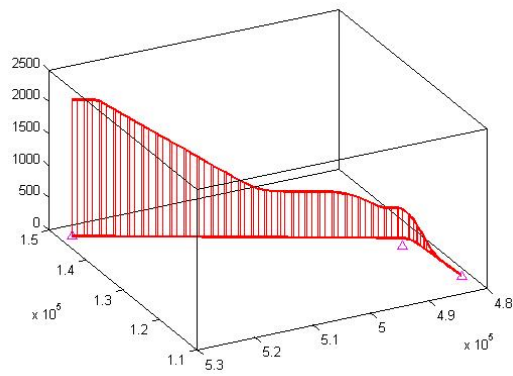
The results of the fuel noise abatement optimization problem for the new scenario are given in the following table including the previous results in order to do a thorough comparison.

Table 5.6: Minimum Fuel & Noise Problem Solutions V2.0

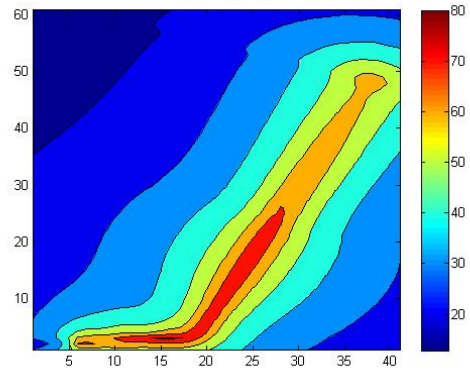
Minimum Time & Noise Problem Optimization V2.0						
	Awakenings	Time [s]	Fuel Used [kg]	R [m]	L1 [m]	L2 [m]
Case 1	1763	492	170	3709	46604	12727
Case 2	2130	702	290	2869	44901	18801
Case 3	1894	700	230	3400	44365	18807
Case 4	2178	861	320	2800	44900	19000
Case 1*	1087	526	170	2434	48404	11482
Case 2*	1710	678	280	1751	48308	13050
Case 3*	868	680	220	1786	48120	13397
Case 4*	1330	864	330	2940	46020	15720

As can be seen from Table 5.6 the results that are found for the minimum fuel noise abatement optimization problem are more or less the same as the ones found in the previous section. Again, the number of awakenings has decreased significantly for all the cases, and case 3 is yet again the most lucrative case. The time needed to perform the approach has also decreased, the same goes for the fuel consumed. The reason behind this is again the distance travelled is smaller than the one before, which can be observed from the values of R, L1 and L2.

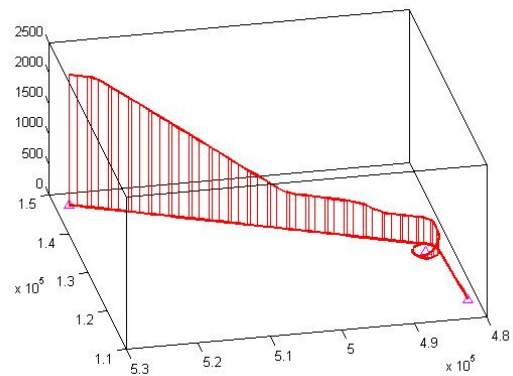
From Figure 5.12 and Figure 5.13 it can be seen what trajectories are flown and the noise levels that are reached during these flights.



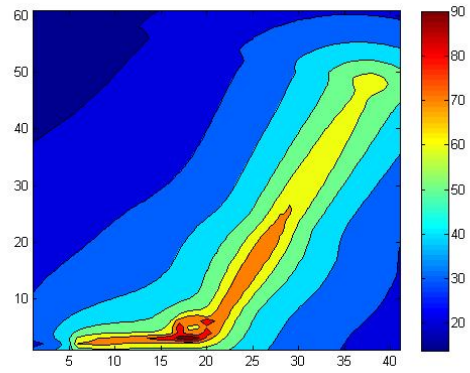
(a) Case 1 Trajectory



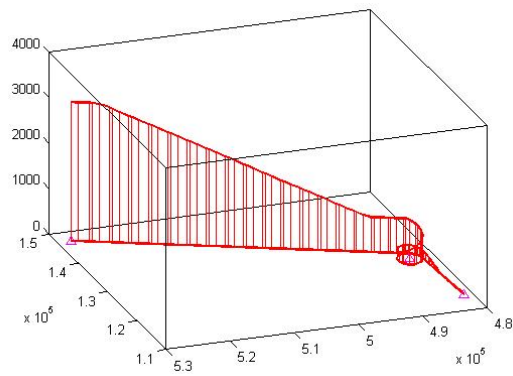
(b) Case 1 Noise Pattern



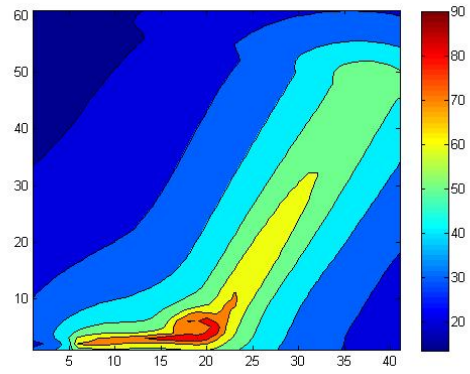
(c) Case 2 Trajectory



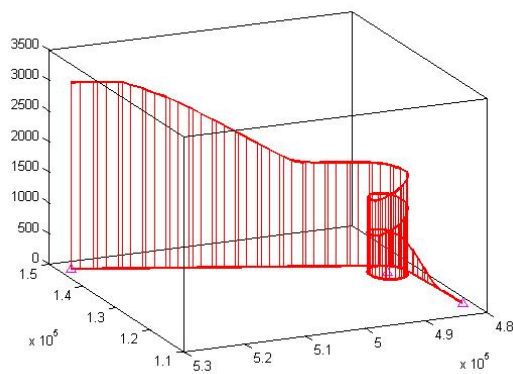
(d) Case 2 Noise Pattern



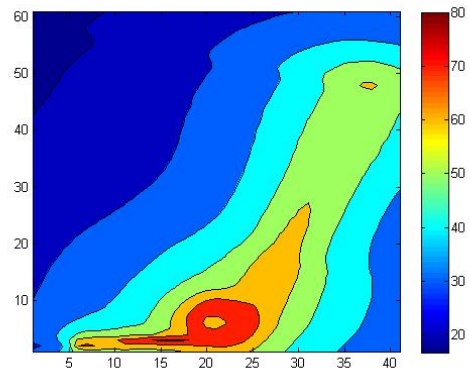
(e) Case 3 Trajectory



(f) Case 3 Noise Pattern

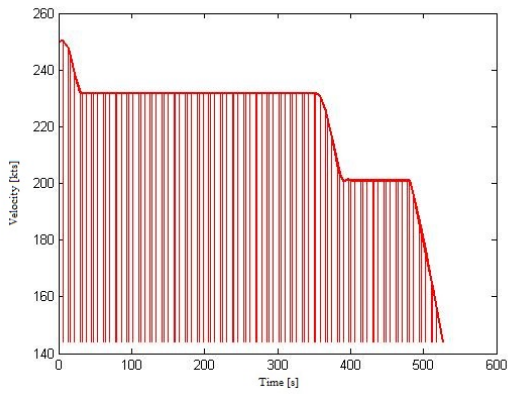


(g) Case 4 Trajectory

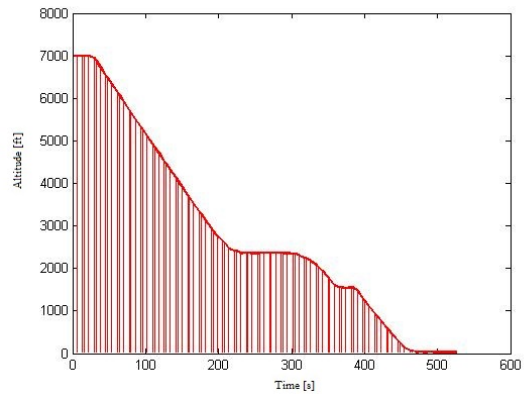


(h) Case 4 Noise Pattern

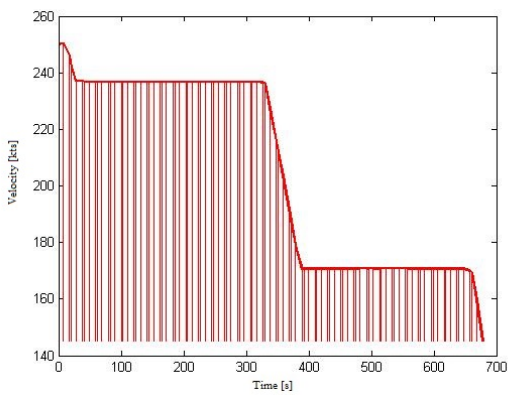
Figure 5.12: Trajectories and Sound Patterns of all the Minimum Fuel & Noise Problem Results Cases for the New Scenario



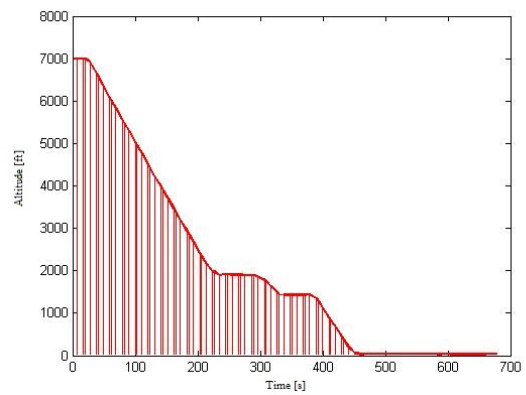
(a) Case 1 Speed



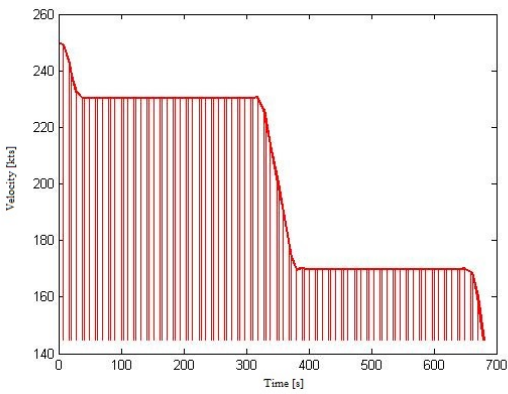
(b) Case 1 Height



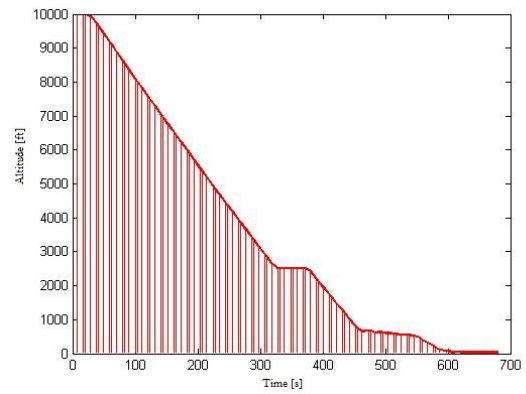
(c) Case 2 Speed



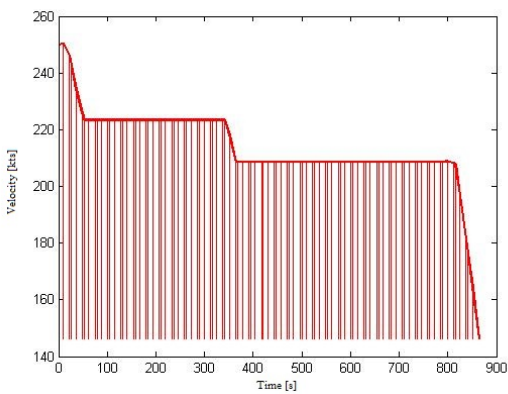
(d) Case 2 Height



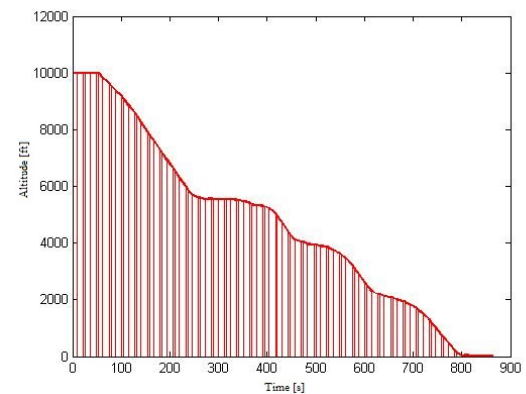
(e) Case 3 Speed



(f) Case 3 Height



(g) Case 4 Speed



(h) Case 4 Height

Figure 5.13: Velocities and Altitudes of all the Minimum Fuel & Noise Problem Results Cases for the New Scenario

5.5.2 Capacity

As was mentioned before, a capacity evaluation will be made should the HeNAP prove successful. From earlier results, such an evaluation would have been redundant. However, looking at the results revealed in the previous sections it would seem that such an evaluation is beneficial. This section explains this evaluation in a simplistic manner to reveal the capacity with respect to the HeNAP procedure.

RECAT Separation Matrix

		Follower					
		A	B	C	D	E	F
Leader	A	MRS	5.0	6.0	7.0	7.0	8.0
	B	MRS	3.0	4.0	5.0	5.0	7.0
	C	MRS	MRS	MRS	3.5	3.5	6.0
	D	MRS	MRS	MRS	MRS	MRS	5.0
	E	MRS	MRS	MRS	MRS	MRS	4.0
	F	MRS	MRS	MRS	MRS	MRS	MRS

Separation was increased for some or all aircraft pairs
 Separation remained the same for some or all aircraft pairs
 Separation was decreased for some or all aircraft pairs
 MRS Minimum Radar Separation (3NM, or 2.5 NM when existing requirements are met)

Figure 5.14: Wake Turbulence Related IFR Aircraft Separation Minima [36]

Figure 5.14 shows the minimum distance necessary for a safe approach between different types of aircraft. All aircraft are divided in different weight categories, namely A to F. Where:

- A is Super Heavy
- B is Upper Heavy
- C is Lower Heavy
- D is Upper Medium
- E is Lower Medium
- F is Light

A representation of the types of aircraft per category are found in Figure 5.15. So, when an aircraft of category B is leading and it is followed by an aircraft of category D, the *Minimum Radar Separation* MRS equals 5 NM. However, this is only applicable when the leading aircraft and the trailing aircraft are flying at an exact constant velocity. As can be seen from figures such as Figure 5.13, this is not always the case. In fact, in some cases there are multiple velocity changes. Thus, some adjustments are needed to make this evaluation more applicable to the HeNAP procedure. This depends on the type of situation represented by Figure 5.16.

A	B	C	D	E	F
A380	B744	MD11	B753	DH8C	E120
AN-225	A346	B763	B752	AT72	B190
	B773	A306	B739	RJ100	C650
	B772		B738	RJ85	H25B
	A343		B737	B463	C525
	A333		B736	B462	
	A332		A319	E170	
			A318	DH8B	
			A321	DH8A	
			A320	CRJ9	
			B722	AT45	
			MD83	AT43	
			MD82	GLF4	
			F50	CRJ7	
			B734	SF34	
			B733	CRJ2	
			B735	CRJ1	
			E190	E45X	
			B717	E145	
			GLF5	E135	
			DC95		
			DC93		
			DH8D		
			F100		

Figure 5.15: Aircraft Category Per Type Of Aircraft [36]

Figure 5.16 shows two situations, namely closing and opening. During the closing situation the leading aircraft travels at a constant speed and then lands, the trailing aircraft travels at the same speed or higher, however due to the fact that the leading aircraft lands, it is *closing in*. While during the opening situation, the leading aircraft travels at a higher speed than the trailing aircraft. However, this does not happen often, and for this evaluation only the closing case is considered.

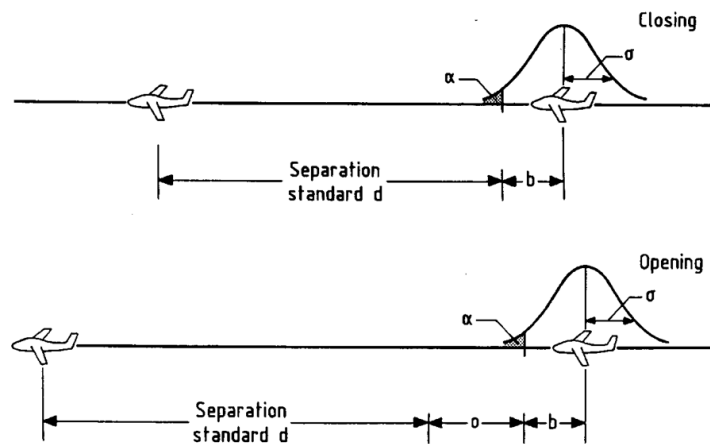


Figure 5.16: Adjusted Separation Distance [37]

Using the following equations, the capacity can be calculated:

$$T = \frac{d}{V_T} \quad (5.1)$$

$$E(t) = \sum P(T + b) \quad (5.2)$$

$$\mu = \frac{3600}{E(t)} \quad (5.3)$$

where,

- T is the time needed for standard separation distance
- $E(t)$ is the expected time between consecutive landings
- P is the probability of a given pair of aircraft weight categories (traffic mix)
- μ is the capacity

During this thesis work, all of the simulations were performed with a Boeing 737 or B737 for short. This is classified as a D-category aircraft. So for the first part of the evaluation, a homogeneous mix instead of a traffic mix will be used. This means the probability, P will be considered 1 and the separation distance will be 3 NM , as can be seen from Figure 5.14. As for the HeNAP part of the evaluation, only Case 3 will be considered, as it is the only one that has any promise. Thus, all of the values of this case will be used in the evaluation. The results are found by using the Equations (5.1), (5.2) and (5.3), and can be seen in the following table:

Table 5.7: Capacity Calculations Homogeneous Mix

	T [s]	b [s]	$E(t)$ [s]	μ [-]
CDA	77	18	95	38
HeNAP (Time)	152	18	170	21
HeNAP (Fuel)	157	18	175	21

As mentioned before, by using Equations (5.1), (5.2) and (5.3), these results are found. The values used for the CDA are, d is 3 NM , V_T is 140 kts and b is 0.7 NM , and they result in a capacity of 40 aircraft per hour. The values used for the HeNAP are based on the two minimum problems of fuel and time, hence the difference in the first column. The d is based on the circumference of the spirals, by using R found in Table 5.5 and Table 5.6, which are 1730 m and 1786 m respectively, this results in d of 5.9 NM and 6.1 NM respectively. This in combination with b results in a capacity of 21 aircraft per hour.

$$d = \frac{2 \cdot \pi \cdot 1730}{1852} = 5.9NM; \quad d = \frac{2 \cdot \pi \cdot 1786}{1852} = 6.1NM \quad (5.4)$$

However, this evaluation is not realistic enough, due to the fact that it only accounts for aircraft of the D-category. In conclusion, the capacity evaluation reveals that the capacity for the CDA is far higher than for the HeNAP.

Conclusions and Recommendations

This thesis had the objective of creating an optimization tool that researches the possibilities of the HeNAP concept. In order to validate the tool and assess the environmental impact of the HeNAP, a case study was set up and analyzed. The case study assessed the environmental impact of the HeNAP with respect to the fuel used, the number of awakenings and the time needed to perform the process within the AAS area. The reason behind the choice of AAS was its location within the Netherlands, which is heavily populated.

6.1 Conclusions

In order to reduce noise pollution at airports a new procedure was developed, the HeNAP. The HeNAP concept consists of an approach from a starting waypoint, followed by descending in a spiral formation and ending by exiting the spiral and landing. Previous research shows that by using this procedure the noise pollution can be concentrated on a desolated area instead of directly over the airport, which would result in less overall noise. However, the previous research did not optimize for an airport and instead it just showed the potential of the HeNAP. Hence, this thesis, where a case study is performed where the HeNAP is optimized.

Within the optimization tool a number of cases were optimized with respect to four optimization problems, *emph*minimum time problems, *minimum fuel problem*, *noise abatement time problem* and finally *noise abatement fuel problem*. The first case is used as a reference, in order to get a feel for the numbers that are expected from a CDA procedure. The initial altitude used for this case was 7,000 ft. The second case was the first HeNAP case, where the same initial altitude was used as the first case. The third case was the second HeNAP case. During this case, the effect of changing the initial altitude was assessed. The fourth and final case was the last HeNAP case, where the initial altitude of third case was still in effect and the number of spirals was changed.

Having performed the necessary simulations for all of the problems, the results were obtained. From these results, it was apparent that case 1 was the one that exceeded the others in almost every aspect. The number of awakenings, the fuel used and the performance time are far less

than the other cases. The second case that was supposed to test the HeNAP showed that when the HeNAP is performed with the initial altitude of 7,000 ft and one spiral, results in a higher number of awakenings than case 1. Case 3 was the only one that came near case 1 in performance. By changing the initial altitude from 7,000 ft to 10,000 ft while still using one spiral it showed that increasing the altitude results in a decrease in number of awakening. However, this is still not enough to surpass the first case. Therefore, in case 4 while still using the new altitude of 10,000 ft an extra spiral is performed to see its effects on the noise. This resulted in a higher number of awakenings than all the other cases, and thus coming to the conclusion that by adding a second spiral the reverse affect than was needed occurred and making an assessment of a fourth HeNAP where three spirals are performed redundant.

However, by moving the population around the airport to the first segment of the trajectory, it has yielded in different results. By doing so, the HeNAP advantages are realized and that is apparent from the results found. Case 3 proved superior over the CDA approach and thus concluding that the HeNAP procedure would be perfect for airports that are less densely populated.

In conclusion the HeNAP will not replace the current procedures at AAS but it might do so at other airports.

6.2 Recommendations

Due to the results that are obtained during this thesis, not a lot of recommendations can be made.

The first recommendation that can be given, is to use the results that are found within this thesis and use them as a basis for the same research but within another area that might be less inhabited than the area around AAS and where the night-curfew is also in effect.

Another recommendation that can be made is to add the wind and weather conditions to the GPOPS tool in order to get results that are more realistic and increase the reliability of the results and feasibility of the trajectories performed.

A final recommendation is to introduce better methods to avoid local minima within the GPOPS tool, this result in unnecessary delays.

Nevertheless, the research performed here shows the capabilities of the GPOPS tool even if the results were not the results wished.

Appendix A

Additional Theorem

During this chapter, the implementation of the awakenings gradients and the Multi-Phase Optimal Control Problem are discussed.

A.1 Implementation of the Awakenings Gradients

The optimization tool transforms the contribution of awakenings to the total cost Jacobian optimal control problem. Furthermore, the states are sent to the INM as is shown in Figure 3.2:

$$\mathbf{x}_{INM} = \begin{bmatrix} s \\ z \\ V \\ T \end{bmatrix} \quad (\text{A.1})$$

These states, (A.1), and the GIS are sent to the INM. The thrust T from Equation (A.1) is derived separately, as it is not a present state in Equation (3.17). This is also true for the partial derivative that constructs the thrust Jacobian \mathbf{J}_T , which is needed to calculate the partial derivatives of the awakenings.

The thrust is obtained from Equation (3.19) and is dependent on the states z and V according to the standard atmospheric relations in [32] and the control Γ according to Equation (3.19). The dependent states and control variables are described with a vector \mathbf{v} :

$$\mathbf{v} = [z \quad V \quad \Gamma] \quad (\text{A.2})$$

To find the partial derivatives of the thrust T to vector \mathbf{v} the following Jacobian can be constructed:

$$\mathbf{J}_T = \frac{\partial T}{\partial \mathbf{v}} = \begin{bmatrix} \frac{\partial T}{\partial z} & \frac{\partial T}{\partial V} & \frac{\partial T}{\partial \Gamma} \end{bmatrix} \quad (\text{A.3})$$

The partial derivatives of the dependent states and control variables to \mathbf{v} are:

$$\begin{aligned} \frac{\partial z}{\partial \mathbf{v}} &= \begin{bmatrix} \frac{\partial z}{\partial z} & \frac{\partial z}{\partial V} & \frac{\partial z}{\partial \Gamma} \end{bmatrix} = [1 \quad 0 \quad 0] \\ \frac{\partial V}{\partial \mathbf{v}} &= \begin{bmatrix} \frac{\partial V}{\partial z} & \frac{\partial V}{\partial V} & \frac{\partial V}{\partial \Gamma} \end{bmatrix} = [0 \quad 1 \quad 0] \\ \frac{\partial \Gamma}{\partial \mathbf{v}} &= \begin{bmatrix} \frac{\partial \Gamma}{\partial z} & \frac{\partial \Gamma}{\partial V} & \frac{\partial \Gamma}{\partial \Gamma} \end{bmatrix} = [0 \quad 0 \quad 1] \end{aligned} \quad (\text{A.4})$$

The following Jacobians have been derived by making use of implicit differentiation, the chain rule and the standard atmospheric relations in [32]:

$$\frac{\partial T}{\partial \mathbf{v}} = \lambda \frac{\partial z}{\partial \mathbf{v}} \quad (\text{A.5})$$

$$\frac{\partial \theta}{\partial \mathbf{v}} = \frac{1}{T_0} \frac{\partial T}{\partial \mathbf{v}} \quad (\text{A.6})$$

$$\frac{\partial p}{\partial \mathbf{v}} = -\frac{\rho g_0}{\lambda R \theta} \frac{\partial \theta}{\partial \mathbf{v}} \quad (\text{A.7})$$

$$\frac{\partial \delta}{\partial \mathbf{v}} = \frac{1}{p_0} \frac{\partial p}{\partial \mathbf{v}} \quad (\text{A.8})$$

$$\frac{\partial a}{\partial \mathbf{v}} = \frac{1}{2} \frac{\gamma R}{\sqrt{\gamma R T}} \frac{\partial T}{\partial \mathbf{v}} \quad (\text{A.9})$$

$$\frac{\partial M}{\partial \mathbf{v}} = \frac{\frac{\partial V}{\partial \mathbf{v}}}{a} - \frac{V}{a^2} \frac{\partial a}{\partial \mathbf{v}}, \quad (\text{A.10})$$

where:

- λ , The air temperature lapse rate with a value of -0.0065 K/m.
- T_0 , The air temperature at sea-level with a value of 288.15 K.
- ρ , The air density in kg/m³.
- R , The specific gas constant of air with a value of 287.05 m²/s²K.
- θ , The temperature ratio defined as T/T_0 and is dimensionless.
- δ , The pressure ratio defined as p/p_0 and is dimensionless.
- p_0 , The air pressure at sea-level with a value of 101,325 N/m².
- a , The speed of sound in m/s².
- γ , The ratio of the specific heats of air with a value of 1.4 and is dimensionless.
- T , The ambient temperature in K.
- M , The Mach number and is dimensionless.

From Equation (3.19) the following formula can be derived to calculate the thrust Jacobian \mathbf{J}_T :

$$\mathbf{J}_T = \frac{\partial \Gamma}{\partial \mathbf{v}} [T_{max} - T_{min}] + \Gamma \left[\frac{\partial T_{max}}{\partial \mathbf{v}} - \frac{\partial T_{min}}{\partial \mathbf{v}} \right] + \frac{\partial T_{min}}{\partial \mathbf{v}} \quad (\text{A.11})$$

Where $\frac{\partial T_{max}}{\partial \mathbf{v}} = f\left(\frac{\partial \delta}{\partial \mathbf{v}}, \frac{\partial z}{\partial \mathbf{v}}, \frac{\partial M}{\partial \mathbf{v}}\right)$ and $\frac{\partial T_{min}}{\partial \mathbf{v}} = f\left(\frac{\partial \delta}{\partial \mathbf{v}}, \frac{\partial M}{\partial \mathbf{v}}\right)$ are quite complex formulas with the engine characteristics included and have been derived and implemented as well.

By knowing the gradients of the thrust, the derivation of the awakenings gradients can start. By using Equation (3.30), the following noise Jacobian $\mathbf{J}_{noise, SER}$ for each observer grid point is obtained:

$$\mathbf{J}_{noise, SER} = \frac{\partial SER_{ft}}{\partial \mathbf{x}_{INM}} \quad (\text{A.12})$$

By making use of the chain rule the $\mathbf{J}_{noise, SER}$ can be rewritten as:

$$\mathbf{J}_{noise, SER} = \frac{\partial SER_{ft}}{\partial \mathbf{x}_{INM}} = \frac{\partial SER_{ft}}{\partial L_{AE, ft}} \frac{\partial L_{AE, ft}}{\partial \mathbf{x}_{INM}} \quad (\text{A.13})$$

Equation (3.31) is differentiated to get:

$$\frac{\partial L_{AE, ft}}{\partial SER_{ft}} = \frac{10}{SER_{ft} \ln(10)} \quad (\text{A.14})$$

By substituting Equation (A.14) into Equation (A.13) the SER Jacobian is transformed into a SEL Jacobian with:

$$\mathbf{J}_{noise, SEL} = \frac{\partial L_{AE, ft}}{\partial \mathbf{x}_{INM}} = \frac{\partial L_{AE, ft}}{\partial SER_{ft}} \frac{\partial SER_{ft}}{\partial \mathbf{x}_{INM}} = \frac{10}{SER_{ft} \ln(10)} \mathbf{J}_{noise, SER} \quad (\text{A.15})$$

By obtaining $\mathbf{J}_{noise, SEL}$, the awakenings Jacobian can be obtained:

$$\mathbf{J}_{Awakenings} = \frac{\partial Awakenings}{\partial \mathbf{x}_{INM}} = \frac{\partial Awakenings}{\partial L_{AE, ft}} \frac{\partial L_{AE, ft}}{\partial \mathbf{x}_{INM}}, \quad (\text{A.16})$$

with:

$$\frac{\partial Awakenings}{\partial L_{AE, ft}} = 0.000087 \cdot 1.79 (L_{AE, ft} - 50.5)^{0.79} \cdot pop \quad (\text{A.17})$$

Substituting Equation (A.17) into Equation (A.16) gives the awakenings Jacobian for each observer grid point:

$$\mathbf{J}_{Awakenings} = 0.000087 \cdot 1.79 (L_{AE, ft} - 50.5)^{0.79} \cdot pop \cdot \mathbf{J}_{noise, SEL} \quad (\text{A.18})$$

By knowing the contributions of the awakening for every single observer grid point, the total awakenings Jacobian can be calculated. This is done by taking the sum of all grid point contributions for every trajectory node. where $points$ is the total number of inhabited grid points:

$$\mathbf{J}_{A, states} = \begin{bmatrix} \frac{\partial A}{\partial s} & \frac{\partial A}{\partial z} & \frac{\partial A}{\partial V} & \frac{\partial A}{\partial T} \end{bmatrix} = \sum_{i=1}^{points} [\mathbf{J}_{Awakenings, i}] \quad (\text{A.19})$$

Finally, the thrust Jacobian \mathbf{J}_T of Equation (A.3) is included in $\mathbf{J}_{A,states}$. This is because the thrust Jacobian in Equation (A.3) and Equation (A.11) is depended on the states z , V and control Γ .

the partial derivatives of \mathbf{J}_T are included in $\mathbf{J}_{A,states}$ in the following way:

$$\left[\frac{\partial A}{\partial z} \right]_{new} = \left[\frac{\partial A}{\partial z} \right]_{old} + \frac{\partial A}{\partial T} \frac{\partial T}{\partial z} \quad (\text{A.20})$$

$$\left[\frac{\partial A}{\partial V} \right]_{new} = \left[\frac{\partial A}{\partial V} \right]_{old} + \frac{\partial A}{\partial T} \frac{\partial T}{\partial V} \quad (\text{A.21})$$

For the controls the Jacobian $\mathbf{J}_{A,controls}$ consists of:

$$\mathbf{J}_{A,controls} = \begin{bmatrix} \frac{\partial A}{\partial \Gamma} & \frac{\partial A}{\partial \gamma} & \frac{\partial A}{\partial \mu} \end{bmatrix} \quad (\text{A.22})$$

The thrust T influences $\mathbf{J}_{A,controls}$ only in the first column, where:

$$\frac{\partial A}{\partial \Gamma} = \frac{\partial A}{\partial T} \frac{\partial T}{\partial \Gamma} \quad (\text{A.23})$$

Finally, $\mathbf{J}_{A,states}$ of Equation (A.19) and $\mathbf{J}_{A,controls}$ of Equation (A.22) are added to the total optimal control problem derivatives.

A.2 Multi-Phase Optimal Control Problem

As is mentioned throughout this chapter, GPOPS has the ability to solve multi-phase optimal control problems. A multi-phase optimal control problem can be transformed from a normal single-phase optimal control problem, such is described in Section 3.1. The reason this is done is to deal with system discontinuities, such as path constraints, a change in aircraft characteristics or dynamic changes during flight. An optimal control problem that consists of multiple-phases has the following form, with a set of P phases, where $p = 1, \dots, P$, to minimize the cost functional:

$$J = \sum_{p=1}^P J^{(p)} = \sum_{p=1}^P \left[\Phi^{(p)} \left[\mathbf{x}^{(p)}(t_0^{(p)}), t_0^{(p)}, \mathbf{x}^{(p)}(t_f^{(p)}), t_f^{(p)}; \mathbf{q}^{(p)} \right] \right] + \sum_{p=1}^P \left[\int_{t_0^{(p)}}^{t_f^{(p)}} \mathcal{L}^{(p)} \left[\mathbf{x}^{(p)}(t^{(p)}), \mathbf{u}^{(p)}(t^{(p)}), t^{(p)}; \mathbf{q}^{(p)} \right] dt^{(p)} \right] \quad (\text{A.24})$$

Subject to the dynamic constraint:

$$\dot{\mathbf{x}}^{(p)} = \mathbf{f}^{(p)} \left[\mathbf{x}^{(p)}(t^{(p)}), \mathbf{u}^{(p)}(t^{(p)}), t^{(p)} \right], \quad [p = 1, \dots, P] \quad (\text{A.25})$$

The boundary conditions:

$$\phi_{min} \leq \phi^{(p)} \left[\mathbf{x}^{(p)}(t_0^{(p)}), t_0^{(p)}, \mathbf{x}^{(p)}(t_f^{(p)}), t_f^{(p)}; \mathbf{q}^{(p)} \right] \leq \phi_{max}, \quad [p = 1, \dots, P] \quad (\text{A.26})$$

The inequality path constraints:

$$\mathbf{C}^{(p)} \left[\mathbf{x}^{(p)}(t^{(p)}), \mathbf{u}^{(p)}(t^{(p)}), t^{(p)}; \mathbf{q}^{(p)} \right] \leq \mathbf{0}, \quad [p = 1, \dots, P] \quad (\text{A.27})$$

And the phase continuity (linkage) constraints:

$$\mathbf{P}^{(s)} \left[\mathbf{x}^{(p_l^s)}(t_f^{(p_l^s)}), t_f^{(p_l^s)}; \mathbf{q}^{(p_l^s)}, \mathbf{x}^{(p_u^s)}(t_0^{(p_u^s)}), t_0^{(p_u^s)}; \mathbf{q}^{(p_u^s)} \right] = \mathbf{0}, \quad (\text{A.28})$$

$[p_l, p_u \in [1, \dots, P], s = 1, \dots, L]$

Where $\mathbf{x}^{(p)}(t^{(p)}) \in \mathbb{R}^{n_p}$, $\mathbf{u}^{(p)}(t^{(p)}) \in \mathbb{R}^{m_p}$, $\mathbf{q}^{(p)} \in \mathbb{R}^{q_p}$, and $t^{(p)} \in \mathbb{R}$, are respectively, the state, control, static parameters, and time in phase $p \in [1, \dots, P]$, L is the number of phases to be linked, $p_l^s \in [1, \dots, P]$, ($s = 1, \dots, L$) are the “left” phase numbers, and $p_u^s \in [1, \dots, P]$, ($s = 1, \dots, L$) are the “right” phase numbers.

One of the notable things is that the phases do not need to be sequential in a multi-phase optimal control problem in order to be solved. Any two phases may be linked provided that the independent variable does not change direction (i.e., the independent variable moves in the same direction during each phase that is linked) [38]. An example of this is shown in Figure A.1, where the ends of phases 1, 2 and 3 are linked to the starts of phases 2, 3 and 4, respectively, while the end of phase 2 is linked also to the start of phase 5.

During each phase of the problem, a number of functions is written within MATLAB in order to specify the optimal control problem needed to be solved:

1. The cost functional
2. The right-hand side of the differential equations and the path constraints (i.e., the differential-algebraic equations)
3. The boundary conditions (i.e., event conditions)
4. The linkage constraints (i.e., how the phases are connected)

In addition, the lower and upper limits on every component of the following quantities need to be specified:

1. Initial and terminal time of the phase
2. The state at the following points in time:
 - At the beginning of the phase
 - During the phase
 - At the end of the phase
3. The control
4. The static parameters
5. The path constraints
6. The boundary conditions
7. The phase duration (i.e., total length of phase in time)
8. The linkage constraints (i.e., phase-connect conditions)

Having explained how a multi-phase optimal control problem works, mostly a single-phase optimal control problem is used during this thesis work. Nevertheless, it is always possible to transform it to a multi-phase optimal control problem, hence the explanation.

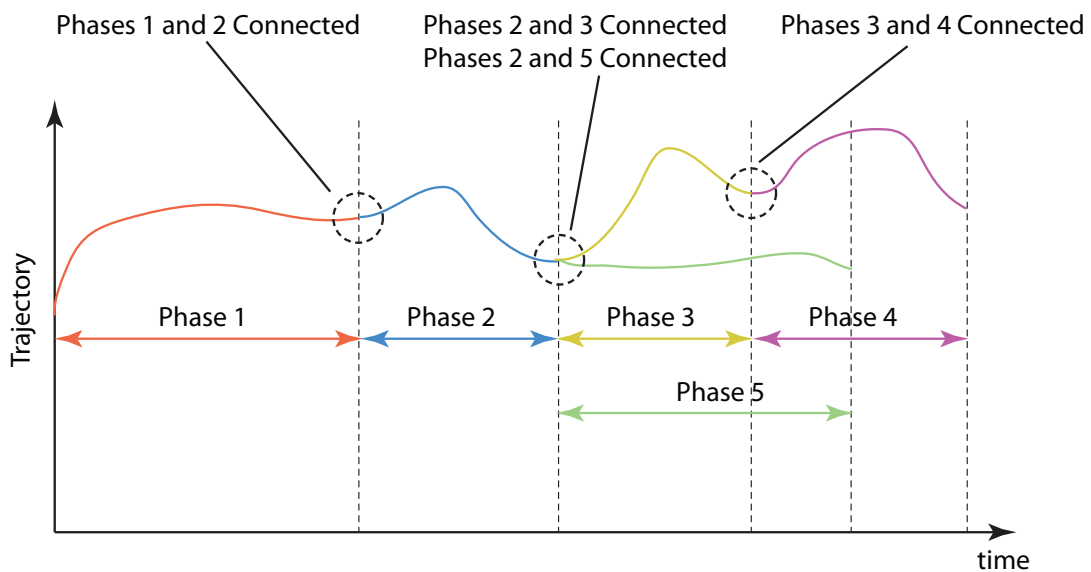


Figure A.1: Possible Linkages for a Multi-phase Optimal Control Problem [38].

Appendix B

Flight Charts

The coming pages show a number of flight charts that have been used throughout this thesis work.

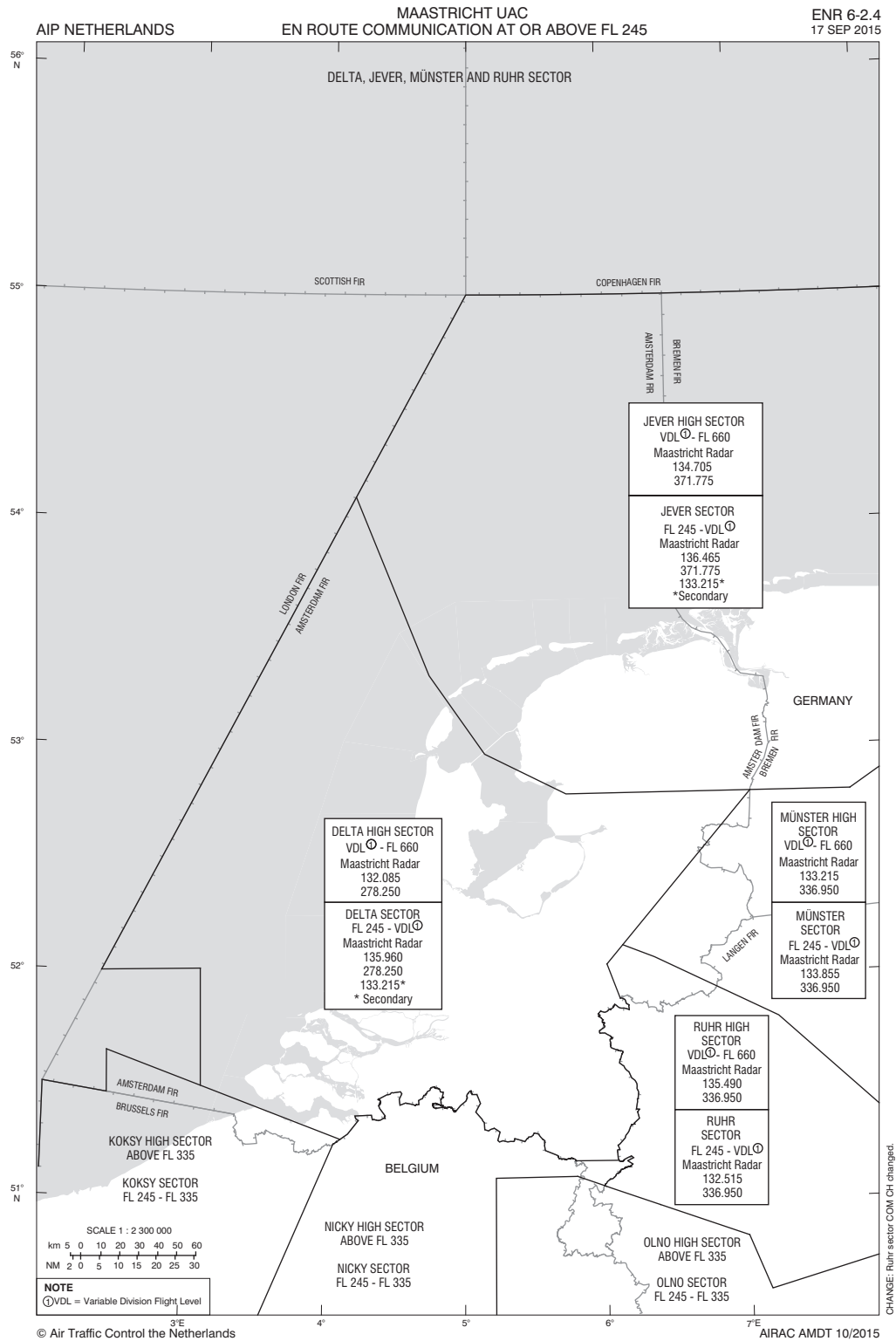


Figure B.1: Maastricht UAC En-route Communication at or above FL 245 [39].

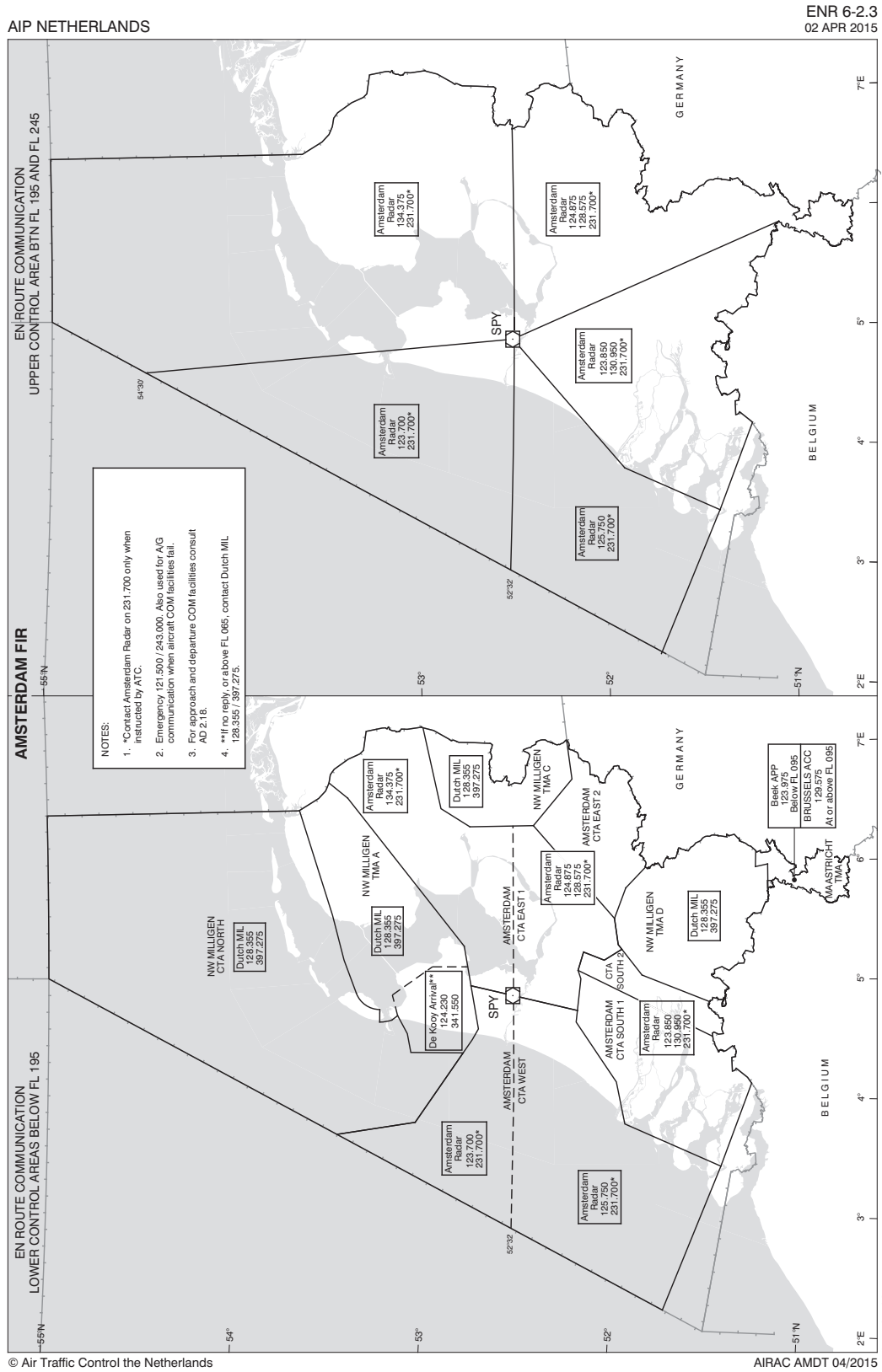


Figure B.2: Amsterdam FIR En-route Communication [39].

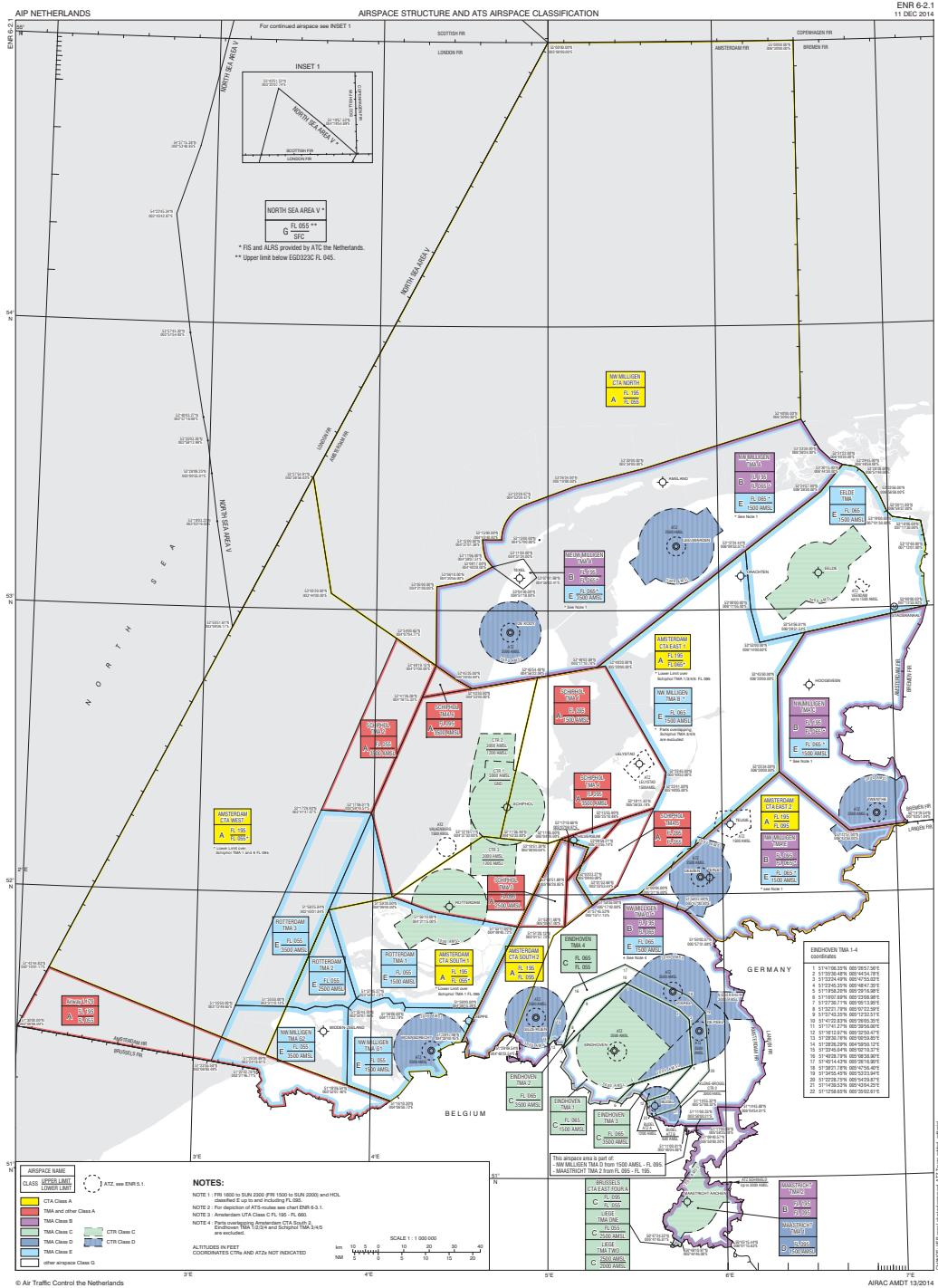


Figure B.3: Airspace Structure and ATS Airspace Classification [39].

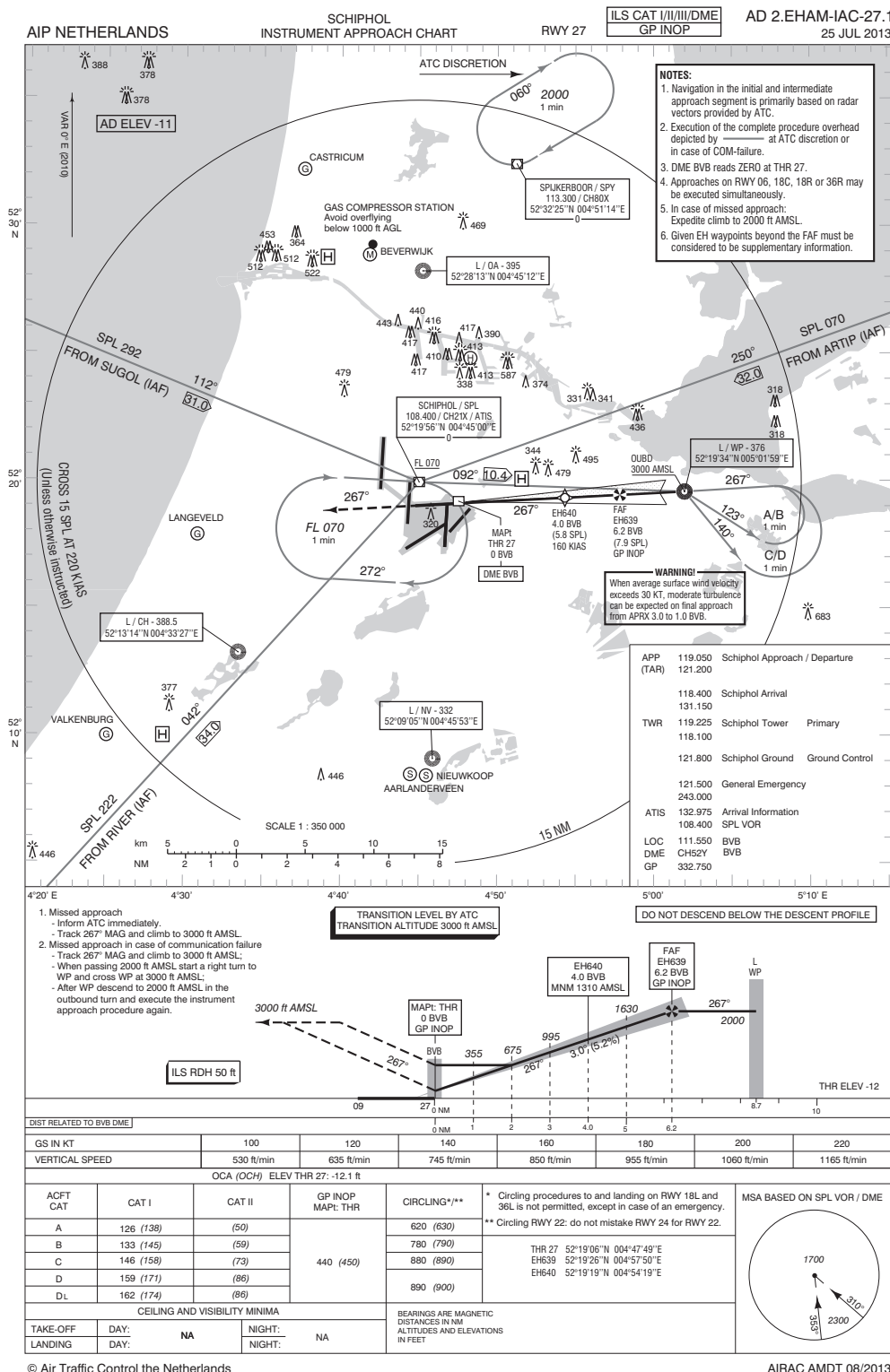
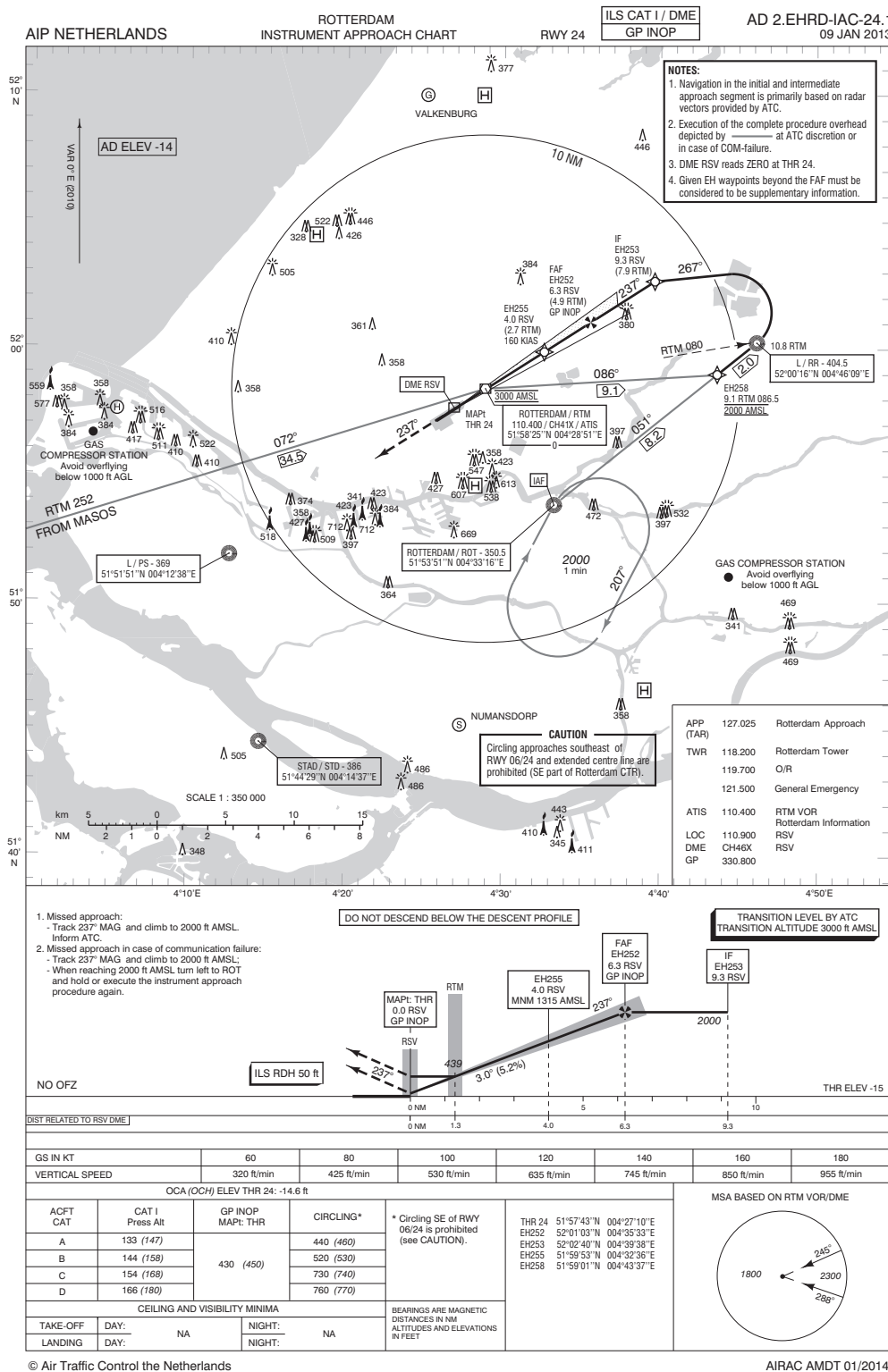


Figure B.4: Instrument Approach Chart For Amsterdam Runway 27 [39].



References

- [1] Mohamed, W., Curran, R., van der Zwan, F., and Roling, P., "Modeling the Effect of Night Time Penalties on Commercial and Business Flights for Regional Airport Noise and Economics: Rotterdam Airport Case Study," *AIAA*, 2009.
- [2] Dillingham, G., "Results From a Survey of the Nation's 50 Busiest Commercial Service Airports," Tech. rep., GAO, 2000.
- [3] Dobrzynski, W., "Almost 40 Years of Airframe Noise Research: What Did We Achieve?" *Journal of Aircraft*, 2010.
- [4] Bertsch, L. and Looye, G., "Flyover Noise Measurements Of A Spiraling Noise Abatement Approach Procedure," *AIAA*, 2009.
- [5] Wijnen, R. and Visser, H., "Optimal Departure Trajectories With Respect To Sleep Disturbance," *Elsevier*, 2003.
- [6] Visser, H. and Wijnen, R., "Optimization Of Noise Abatement Arrival Trajectories," *The Aeronautical Journal*, 2003.
- [7] Visser, H., "Generic And Site-specific Criteria In The Optimization Of Noise Abatement Trajectories," *Elsevier*, 2005.
- [8] Visser, H., "Environmentally Optimized Resolutions of In-Trail Separation Conflicts for Arrival Flights," *Journal of Aircraft*, 2008.
- [9] Hartjes, S., *Optimization Of RNAV Noise And Emission Abatement Departure Procedures*, Master's thesis, Delft University of Technology, 2008.
- [10] Spierings, M., *Optimizing Tailored Arrival Trajectories for Noise Abatement*, Master's thesis, Delft University of Technology, 2012.
- [11] Ruijgrok, G., *Elements Of Aviation Acoustics*, Delft University Press, 1993.
- [12] "Effects of Aviation Noise on Awakenings from Sleep," Tech. rep., Federal Interagency Committee on Aviation Noise, 1997.

- [13] Martens, S., "Jet Noise Reduction Technology Development At Ge Aircraft Engines," *ICAS*, 2002.
- [14] Erkelens, L., "Research Into New Noise Abatement Procedures For The 21st Century," *AIAA*, 2000.
- [15] Erkelens, L., "Advanced Noise Abatement Procedures For Approach And Departure," *AIAA*, 2002.
- [16] Ruigrok, R., Erkelens, L., Selier, M., Wubben, F., and de Jong, R., "Evaluation Of The Effect On Noise Reduction Of Increasing The ILS/MLS Glide Slope Angle To 3.2 Degrees," Tech. rep., NLR, 1998.
- [17] Erkelens, L., "Evaluation Of The Noise Effects Of Increasing The Final Approach Altitude From 2000ft To 3000ft," Tech. rep., NLR, 1998.
- [18] Ho, N. and Clarke, J., "Mitigating Operational Aircraft Noise Impact By Leveraging On Automation Capablity," *AIAA*, 2001.
- [19] Anderson, L. and Warren, A., "Evelopment Of An Advanced Continuous Descent Concept Based On A 737 Simulator," *Digital Avionics Systems Conference, 2002. Proceedings. The 21st*, 2002.
- [20] Clarke, J., *A Systems Analysis Methodology For Developing Single Event Noise Abatement Procedures*, Ph.D. thesis, Massachusetts Institute of Technology, 1997.
- [21] de Leege, A., in 't Veld, A., Mulder, M., and van Paassen, M., "Three-Degree Decelerating Approaches in High-Density Arrival Streams," *Journal Of Aircraft*, 2009.
- [22] Erkelens, L., "Research On Noise Abatement Procedures," Tech. rep., National Aerospace Laboratory, 1998.
- [23] Reynolds, T., "History, Development and Analysis of Noise Abatement Arrival Procedures for UK Airports," *AIAA*, 2005.
- [24] Wat, J., Follet, J., Mead, R., and Brown, J., "In Service Demonstration of Advanced Arrival Techniques at Schiphol Airport," *AIAA*, 2006.
- [25] Alam, S., Nguyen, M., Abbass, H., and Lokan, C., "Multi-Aircraft Dynamic Continuous Descent Approach Methodology for Low-Noise and Emission Guidance," *Journal Of Aircraft*, 2011.
- [26] Koeslag, M., "Advanced Continuous Descent Approaches An algorithm design for the Flight Management System," Tech. rep., NLR, 1999.
- [27] Bertsch, L., Looye, G., Anton, E., and Schwanke, S., "Flyover Noise Measurements of a Spiraling Noise Abatement Approach Procedure," *AIAA*, 2011.
- [28] Bertsch, L., Looye, G., Anton, E., and Schwanke, S., "Flyover Noise Measurements Of A Spiraling Noise Abatement Approach Procedure," Tech. rep., DLR, 2009.

- [29] Volovoi, V., Fraccone, G., Colon, A., Hedrick, M., and Kelley, R., "Agent-Based Simulation of Off-Nominal Conditions During a Spiral Descent (NextGen Vehicle NRA)," *AIAA*, 2009.
- [30] Visser, H., *Aircraft Performance Optimization*, Delft University of Technology - Faculty of Aerospace Engineering, 2010.
- [31] Garg, D., Patterson, M. A., Hager, W. W., Rao, A. V., Benson, D. A., and Huntington, G. T., "A Unified Framework for the Numerical Solution of Optimal Control Problems Using Pseudospectral Methods," *Elsevier*, 2010.
- [32] Ruijgrok, G. J. J., *Elements of Airplane Performance*, Delft University Press, 1996.
- [33] Office of Environment and Energy, *Integrated Noise Model (INM) Version 7.0 User's Guide*, 2007.
- [34] "Regeling Geluid Milieubeheer," 08 2015.
- [35] Borst, C. and Mulder, M., "Air Traffic Control & Air Traffic Management," Lecture Notes AE4393.
- [36] Express, F., "Recategorization of ICAO Wake Turbulence Standards "RECAT Phase I", "
- [37] Visser, D., "AE3502: Airport Planning, Design and Operation - Lecture : aircraft classification; airside capacity and delay issues," Lecture Slides, 11 2015.
- [38] Rao, A., Benson, D., Darby, C., and Huntington, G. T., *User's Manual for GPOPS Version 3.3*, 2010.
- [39] AIS The Netherlands, <http://www.ais-netherlands.nl/aim/2015-08-06-AIRAC/eAIP/html/index-en-GB.html>, [Online; accessed 06-10-2015].

